Heat Shock Factor 1 (HSF1) modulates Inflammation and Survival Post-Myocardial Infarction

By: Supriya Hota

Thesis is submitted to the University of Ottawa in partial Fulfillment of the requirements for the Master of Science degree in Cellular and Molecular Medicine

Department of Cellular and Molecular Medicine
Faculty of Medicine
University of Ottawa

Abstract

Introduction: Myocardial Infarction (MI) is the leading cause of premature death worldwide. During MI-induced ischemia, the release of heat shock proteins (HSPs), a classic damage-associated molecular pattern (DAMP), by severely injured cells leads to prolonged inflammation through their activation of innate pattern recognition receptors, fibrosis, and subsequent contractile dysfunction. The regulation of HSPs is orchestrated by its master transcription factor, Heat Shock Factor 1 (HSF1). However, it is unknown if HSF1 is a potential integrated functional target to improve MI outcomes. We addressed this question by asking if the coordinated modulation of HSPs via genetic deletion of *Hsf1* can be beneficial in MI.

Hypothesis: We hypothesized that genetic deletion of *Hsf1* can lead to improved survival and left ventricle (LV) remodeling through reduction of pro-inflammatory pathway activation in a murine model of MI-induced coronary artery ligation.

Methods and Results: Eleven to thirteen-week-old male *Hsf1*$^{-/-}$ mice and *Hsf1*$^{+/+}$ littermate controls were subjected to MI by left anterior descending (LAD) coronary artery ligation or sham operation. *Hsf1*$^{-/-}$ mice subjected to induced-MI had a significant higher survival rate (74%) at 28 days than WT mice post-MI in the same time frame (34%, $p<0.001$). Echocardiography at 3, 7, and 28 days post-MI; however, did not identify any difference in LV function between *Hsf1*$^{+/+}$ and *Hsf1*$^{-/-}$ mice. Masson Trichrome and Picro Sirius Red staining of heart tissue sections following 7 days of sham or MI-operation indicated that MI-operated *Hsf1*$^{-/-}$ hearts had a significant smaller infarct size than *Hsf1*$^{+/+}$ hearts at 19% compared to 32% ($p<0.05$), respectively; and less collagen deposition when compared to WT littermates. Cardiac expression of heat shock proteins was significantly lowered in the *Hsf1*$^{-/-}$ hearts compared to *Hsf1*$^{+/+}$ hearts following 3 and 7 days of MI. However, no significant difference was observed in number of immune cells, cardiac gene expression of pro-inflammatory cytokines and chemokines, cardiac protein expression of NF-κB and MAPK-ERK1/2 signaling proteins, and serum IL-6 concentration between *Hsf1*$^{+/+}$ and *Hsf1*$^{-/-}$ mice 3 days post-MI. Following 7 days of MI, there is a significant increase in the gene expression

of pro-inflammatory cytokines, such as *Il1b*, and chemokines, such as *Ccl2*, in *Hsf1*$^{-/-}$ hearts than *Hsf1*$^{+/+}$ hearts.

Conclusion & Future Directions: Overall, the loss of *Hsf1* improved survival and reduced infarct size following MI. However, its deletion did not affect inflammatory processes until 7 days post-MI or improved cardiac function in our specific murine MI model.

Statement of Contributions

My MSc thesis, which is titled “Heat Shock Factor (HSF) 1 modulates Inflammation and Survival Post-Myocardial Infarction”, was conceptualized by me under the supervision of Dr. Peter Liu. The execution of experiments, analysis and presentation of data, and preparation of the thesis including analysis and presentation of the data, were performed by me. I performed all the experimental protocols and analysis except for the following:

The Kaplan-Meier Survival chart in Section in 3.1 (Figure 8) and immunoblot result in Figure S7 were created by Philip Wood (a former PhD student of Dr. Peter Liu).

Animal Care Veterinary Services (ACVS) of University of Ottawa provided daily, pre-operation, and post-operation care to HSF1 animals (e.g. maintenance of animal cages, preparing animals for surgery, checking the health and wellness of the animals following surgery).

Vivian Franklin (Core Laboratory Technician of University of Ottawa Heart Institute (UOHI)) managed the generation of HSF1 mice colony. After HSF1 mice were weaned, she provided me with tail clips, from which I extracted genomic DNA and performed genotyping.

Rick Seymour (Technician in Dr. Darryl Davis’s Lab) performed sham or left anterior descending (LAD) coronary artery ligation (Myocardial Infarction/ MI) surgeries and echocardiography on the HSF1 animals. He also collected blood samples on my behalf.

Dr. David Smyth (Postdoctoral Fellow in Dr. Peter Liu’s Lab) performed the flow cytometry experiment and analysis, as described in Section 2.7, and represented in Section 3.7 (Figure 14).

Xiaoling Zhao (Technician of Core Histopathologist Lab at UOHI) processed my mouse tissues for paraffin embedding.

This MSc thesis was submitted to the Faculty of Graduate and Postdoctoral Studies after it was read and edited by Dr. Peter Liu.

Acknowledgments

First and foremost, I would like to thank my supervisor, Dr. Peter Liu, who welcomed me into his team as a fourth-year undergraduate student and has constantly provided me with invaluable expertise and challenges for me to learn and grow from. I am very grateful for his patience, support, and mentorship over the years. Moreover, I am always fascinated by his out-of-the-box scientific ideas and his passion to translate a hypothesis into life-changing research. This has inspired me to think critically and be determined and resilient towards my research.

I would also like to thank my thesis advisory committee members, Dr. Marc Ekker and Dr. Katey Rayner, for their scientific and research advice and for always being very approachable and incredibly supportive during my Masters.

I thank all my lab colleagues for being so kind and supportive, but a special note of thanks to Dr. Liyong Zhang, Dr. David Smyth, and Dr. Mo Al-Khalaf for their patience and mentorship. They have always gone the extra-mile with teaching new techniques, assisting with troubleshooting, and sharing ideas and opportunities for the advancement of my research and for me to grow as a scientist.

I would like to express my gratitude to the UOHI ACVS team, Rick Seymour and Vivian Franklin for their training and assistance with animal care, animal surgery and managing HSF1 mice colony, respectively. Also, I am extremely grateful to Xiaoling Zhao for her guidance and training with regards to histology experiments.

I thank the following past and present members of UOHI: Dr. Denuja Karunakaran, Sandrine Parent, Natasha Trzaskalski, Dr. Justina Pupkaite, Yena Oh, Dr. Veronika Sedlakova and Cagla Cimenci, for their guidance in various scientific experiments and their mentorship.

Lastly, I would like to send a big thank you to my Papa, Santosh, and my Ma, Prativa, for their patience and motivation, but most importantly, for having faith in my talent and hard work. Thank-you for always lifting my spirits and encouraging me to achieve my goals and fulfilling my dreams! This achievement and many more to come in the future are for both of you!

Table of Contents

List of Tables

List of Figures

List of Abbreviations

ACE	Angiotensin-converting enzyme
ACVS	Animal Care Veterinary Services
ANOVA	Analysis of variance
AP-1	Activator Protein-1
APC	Antigen Presenting Cell
ASSAIL-MI	Assessing the Effect of Anti-IL-6 Treatment in Myocardial Infarction
ATP	Adenosine Triphosphate
BSA	Bovine Serum Albumin
CANTOS	Canakinumab Anti-Inflammatory Thrombosis Outcomes
CCAC	Canadian Council of Animal Care
Ccl2	C-C motif Chemokine Ligand 2
cDNA	Complementary DNA
COLCOT	Colchicine Cardiovascular Outcome Trial
COX	Cyclooxygenase
CTGF	Connective Tissue Growth Factor
CVDs	Cardiovascular diseases
Cxcl1	C-X-C motif Chemokine Ligand 1
Cxcl10	C-X-C motif Chemokine Ligand 10
DAMPs	Danger Associated Molecular Patterns
DNA	Deoxyribonucleic acid
ECD	Ectodomain
ECG	Electrocardiogram
ERK	Extracellular-signal-regulated kinase
FS	Fractional Shortening
GAPDH	Glyceraldehyde 3-phosphate dehydrogenase
G-CSF	Granulocyte-colony stimulating factor
HE	Hematoxylin and Eosin Y

HFrEF	Heart Failure with Reduced Ejection Fraction
HIF-1α/*Hif1a*	Hypoxia Inducible Factor-1 α
HMGB1	High Mobility Group Box 1
Hprt1	Hypoxanthine-guanine phosphoribosyltransferase 1
HRP	Horseradish peroxidase
HSC	Hematopoietic Stem Cells
HSFs	Heat Shock Factors
HSF1	Heat Shock Factor 1
HSF2	Heat Shock Factor 2
HSP25	Heat Shock Protein 25
HSP70/ *Hsp70*	Heat Shock Protein 70
HSP90/ *Hsp90*	Heat Shock Protein 90
HSR	Heat Shock Response
HW	Heart Weight
IFN-α	Immune interferon alpha
IHD	Ischemic Heart Disease
IL-10	Interleukin-10
IL-1β/ Il1b	Interleukin-1 Beta
IL-6/ *Il6*	Interleukin-6
IRAK1	Interleukin-1 Receptor Associated Kinase 1
IRAK4	Interleukin-1 Receptor Associated Kinase 4
IRF3	Interferon Regulatory Transcription Factor 3
IRF5	Interferon Regulatory Transcription Factor 5
JAK	Janus kinase
KCl	Potassium chloride
LAD	Left Anterior Descending
LV	Left Ventricle
LVEF	Left Ventricle Ejection Fraction
LW	Lung Weight

MAPK	Mitogen-activated protein kinase
MCP-1/CCL2	Monocyte Chemoattractant Protein-1/ Chemokine (C-C motif) Ligand 2
MI	Myocardial Infarction
MLKL	Mixed lineage kinase domain-like pseudokinase
MMP	Matrix metallopeptidase
MPO	Myeloperoxidase
MTC	Masson trichrome
MYD88	Myeloid differentiation factor 88
NEMO	NF-κB essential modulator
NF-κB	Nuclear Factor kappa-light-chain-enhancer of activated B cells
NIH	National Institutes of Health
NSAID	Nonsteroidal anti-inflammatory drug
NSTEMI	Non-ST-Elevation-Myocardial Infarction
PAMPs	Pathogen Associated Molecular Patterns
PBS	Phosphate Buffered Saline
PBST	Phosphate Buffered Saline in Tween 20
PCI	Percutaneous Coronary Intervention
PRRs	Pattern Recognition Receptors
PSR	Picro Sirius Red
RIP1	Receptor-interacting protein kinase 1
RIP3	Receptor-interacting protein kinase 3
RNA	Ribonucleic acid
ROS	Reactive Oxygen Species
RPM	Rotations Per Minute
RT	Room Temperature
RT-qPCR	Quantitative reverse transcription polymerase chain reaction
SEM	Standard Error of Mean
siRNA	Silencer RNA
STAT	Signal Transducers and Activators of Transcription

STEMI	ST-Elevation-Myocardial Infarction
TBK1	TANK-binding kinase 1
TGFβ-1/*Tgfb1*	Transforming Growth Factor Beta-1
TIR	Toll IL-1 Receptor
TL	Tibia Length
TLR/ *Tlr*	Toll-like receptor
TNF-α/ Tnfa	Tumor necrosis factor alpha
TNK	Tenecteplase
tPA	Tissue plasminogen activator
TRAM	Translocating chain-associated membrane
TRIF	TIR-domain-containing adapter-inducing interferon-β
TUNEL	Terminal deoxynucleotidyl transferase dUTP nick end labeling
UOHI	University of Ottawa Heart Institute
VEGF	Vascular Endothelial Growth Factor

1.0 Introduction

1.1 Cardiovascular Diseases

Globally, cardiovascular diseases (CVDs) are the leading cause of premature mortality and account for more than 45% of non-communicable diseases. Cardiovascular diseases include ischemic heart disease, stroke, hypertension, atrial fibrillation, and myocarditis. In 2017, stroke and ischemic heart disease, which accounted for 85% of CVDs, were responsible for 17.8 million deaths worldwide but mostly in low and middle-income countries[1,2]. In Canada, CVDs are responsible for approximately 50, 000 deaths every year, becoming the second leading cause of premature mortality after cancer, despite the reduction in number of deaths since 2000[3,4]. Healthcare burden and lost work related to CVDs are also significant, costing the Canadian economy $21.2 billion every year[5,6]. If treatment options and quality of care do not improve, the cost for CVDs will increase to $293 billion a year by 2040[4].

1.1.1 Ischemic Heart Disease

Ischemic heart disease (IHD) accounts for most of the premature mortality caused by CVDs. IHD refers to heart problems caused by an interruption of the oxygenated blood supply to the heart muscle due to narrowing or blockage of coronary arteries. The narrowing of coronary arteries is caused by inflammation, and injury from risk factors or genetics, with gradual accumulation of lipid-rich plaque, which is termed atherosclerosis. Rupture or erosion of the lipid-rich plaque activates the platelet aggregation and clotting system, leading to the formation of blood clot on the surface of the plaque. The deprivation of oxygenated blood to the working heart muscle, leads to myocardial ischemia, which when prolonged leads to death of the myocardium or Myocardial Infarction (MI)[7].

1.1.1.1 Myocardial Infarction

1.1.1.1.1 Health Burned as a consequence of Myocardial Infarction

Myocardial Infarction (MI), also commonly known as heart attack, is a severe manifestation of IHD. In Canada, the incidence of MI is approximately 2/1000 individuals per year.

The incidence of MI had decreased by 17% between 2000-2001 and 2012-2013. However, the number of people living with IHD and a history of MI, or the prevalence, was approximately 578, 000 in 2012-2013 and it continues to increase over time, which reflects that more Canadians are surviving heart attacks. The prevalence was 2.1 times higher among Canadian men than women as recorded between 2000-2001 and 2012-2013. However, the gap between the sexes narrows with age. Consequently, Canadians with a history of MI are more likely to develop ischemic heart failure downstream and are 4 times more likely to die of any cause than those without MI[6].

1.1.1.1.2 Consequence of Myocardial Infarction – Ischemic Heart Failure

In the presence of myocardial ischemia, cellular function is disrupted due to lack of oxygen, in particular, oxidative metabolism ceases, forcing ischemic cardiomyocytes to use intracellular glycogen stores to perform anaerobic glycolysis as temporizing means to generate ATP. Unlike aerobic respiration, anaerobic respiration is inefficient at generating ATP, and produces lactic acid as a by-product that progressively leads to intracellular acidosis[8]. The presence of intracellular acidosis and unmet demand of ATP affects electrical conductivity in the ischemic heart, suppressing systolic and diastolic functions and predisposes to cardiomyocyte necrosis[9,10]. Therefore, restoration of blood flow in a timely manner is crucial to salvage the heart from cardiomyocyte necrosis as the mammalian heart does not have the regenerative capacity for lost myocytes. The necrotic myocardium or the infarct region, generate local inflammatory responses, and is later replaced by a non-contractile collagen-based scar. The peri-infarct region, which surrounds the necrotic myocardium, contains damaged cardiomyocytes that trigger an intense inflammatory response to mediate repair or replacement with scar. Non-infarct region is the area that contains functional cardiomyocytes and is also highly impacted by remote ischemia. Cardiomyocytes in the non-infarct region experience inflammation, hypertrophy, and myocardial fibrosis to compensate for loss in cardiac function in the infarct region[11]. Biological compensatory mechanisms, such as the sympathetic nervous system and renin-angiotensin-aldosterone system, are also activated to compensate for the loss in contractility, but the chronic activation of these pathways is maladaptive and leads to ischemic heart failure, more specifically Heart Failure with Reduced Ejection Fraction (HFrEF)[12]. Since IHD, especially MI, accounts for two-thirds

of HFrEF cases, the repair and remodelling of the ischemic heart is essential and progresses through three overlapping phases: Inflammatory phase (Stage 1), Proliferative phase (Stage 2), and Maturation phase (Stage 3)[13].

1.1.1.1.3 Stages of repair and remodeling post-MI

1.1.1.1.3.1 First Stage: Inflammatory Phase

Following the cardiac ischemic injury, the process of cardiac repair and remodeling begins with intense inflammation and immune cell infiltration in the infarct myocardium. This step is known as the inflammatory phase, which lasts 0-3 days in mice and 0-4 days in humans[14,15]. The sterile inflammation is initiated when injured or dead cells in the infarct myocardium release Damage Associated Molecular Patterns (DAMPs), such as High Mobility Group Box 1 (HMGB1), Heat Shock Proteins (HSPs), ATP and mitochondrial DNA, into the extracellular matrix. These "danger signals" or DAMPs are recognized by neighbouring cardiomyocytes, fibroblasts, and residential macrophages via their pattern recognition receptors (PRRs), triggering the innate immune response. Various PRRs, located on the surface of plasma membrane or in the cytoplasm, are known to identify DAMPs, but Toll-like receptors (TLRs) 2 and 4 are found abundantly in the mammalian heart[16]. After the recognition of DAMPs by neighbouring cells, downstream signaling pathways, such as the activation of Mitogen-Activated Protein Kinases (MAPKs), followed by activation of transcription factors, Nuclear Factor kappa-light-chain-enhancer of activated B cells (NF-κB) and Activator Protein-1 (AP-1), are initiated within the cell to upregulate and release a cascade of pro-inflammatory cytokines, such as Tumor necrosis factor-α (TNF-α) and Interleukin-6 (IL-6), and chemokines, such as Monocyte Chemoattractant Protein (MCP)-1/C-C motif chemokine ligand 2 (CCL2) and C-X-C motif chemokine ligand 1 (CXCL1)[17,18]. The burst of pro-inflammatory cytokines and chemokines initially recruit neutrophils into the infarct myocardium via sequential steps called extravasation. Neutrophils engulf dead cells and tissue debris and release reactive oxygen species (ROS), proteases that degrade extracellular matrix, and chemotactic factors, such as MCP-1/CCL2, that recruit pro-inflammatory $Ly6C^{high}$ monocytes. Even though the infiltration of neutrophils is necessary to clear up cellular debris, the release of ROS can actually further inflict injury, increasing necrosis in the area. The

Ly6C^{high} monocytes, which are the progeny of hematopoietic stem cells (HSCs) residing in the bone marrow, transition into pro-inflammatory M1 macrophages that engulf apoptotic neutrophils, remove dead cells and debris, and secrete pro-inflammatory cytokines[11,19,17] **(Figure 1)**. Therefore, continuous infiltration of neutrophils can lead to excessive cell death, which further amplifies the inflammatory process by promoting production of DAMPs and activating a cascade of inflammatory mediators. The prolongation of inflammation can lead to the rupture of LV wall[20]. Overall, targeting DAMPs, TLRs, NF-κB signaling pathways, pro-inflammatory cytokines and/ or neutrophils are known to be associated with smaller infarct size, less cardiac rupture rate, and, sometimes, better cardiac function[21–40]. Efficient clearance of debris and inflammation assist the heart to proceed to the next stage of cardiac repair and remodelling: the proliferative phase.

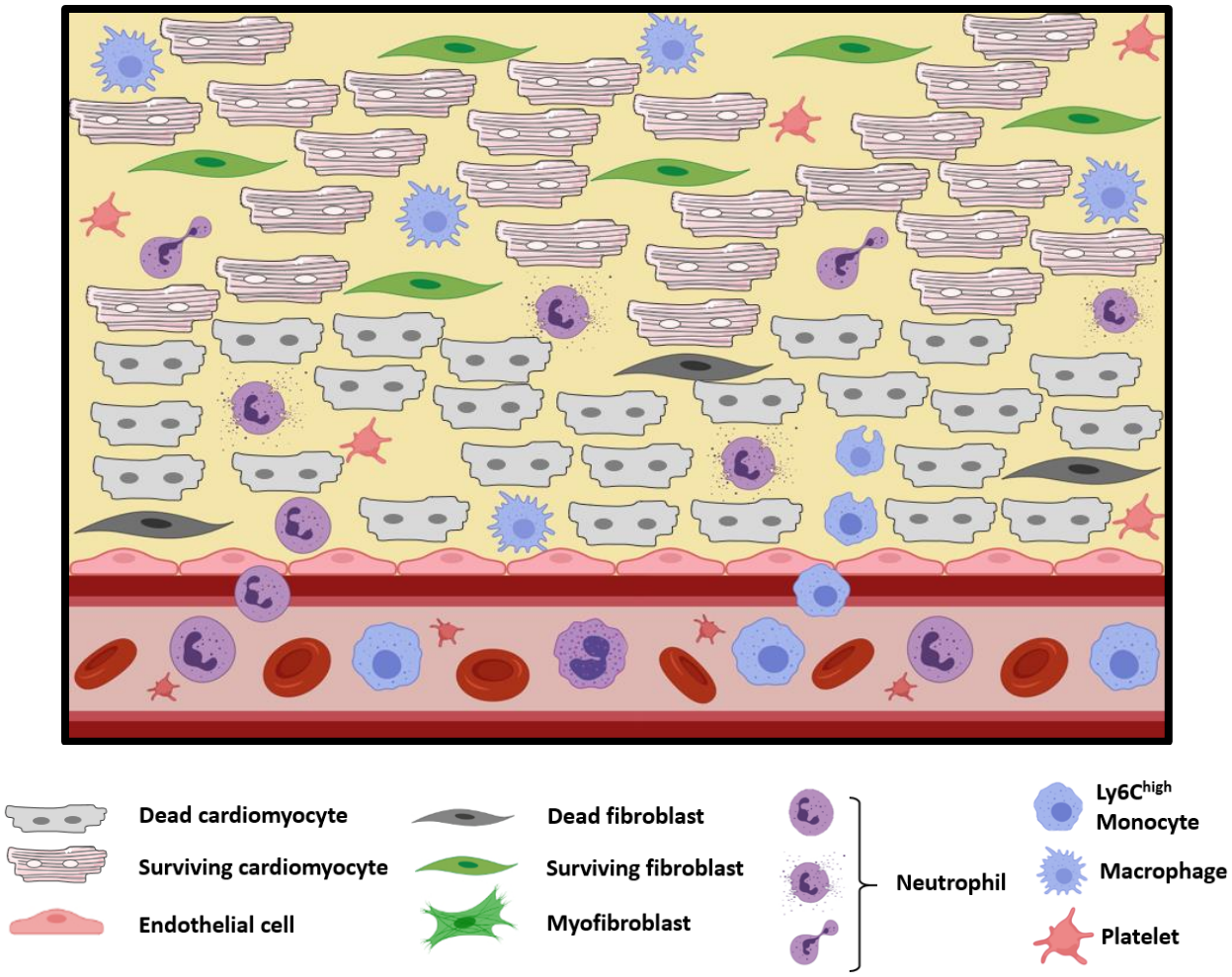

Figure 1. First Stage of Cardiac Repair: The Inflammatory Phase. Following MI, the release of DAMPs due to necrosis triggers the initiation of innate immune response. Neutrophils are the first immune cell to be recruited to the infarct region from the bone marrow to clear tissue debris. They engulf tissue debris and release ROS to clear up the infarct region. Neutrophils are followed by Ly6C^{high} monocytes, which transition into M1 macrophages and engulf apoptotic neutrophils and tissue debris. This phase lasts 0-3 days in mice and 0-4 days in humans.

1.1.1.1.3.2 Second Stage: Proliferative Phase

The proliferative phase initiates when the injury site is clear of dead cells, debris, and pro-inflammatory neutrophils. This phase lasts for 4-14 days in mice and 0-3 weeks in humans[14]. The clearance of cellular debris and immune cells leads to the activation of Ly6C^{low} monocytes, which transition into reparative M2 macrophages that secrete anti-inflammatory cytokines and pro-fibrotic and angiogenic factors, such as Interleukin-10 (IL-10), Transforming Growth Factor Beta-1 (TGFβ-1), and Vascular Endothelial Growth Factor (VEGF). Consequently, these factors lead to the suppression of pro-inflammatory processes and activation of reparative processes. One of the reparative processes is the activation of myofibroblasts, which are derived from cardiac fibroblasts[11,20,41]. In the infarct and peri-infarct regions, myofibroblasts produce interstitial collagen. Elevated levels of type III collagen are produced 2-3 days post-MI and their increased expression in the left ventricle (LV) tissues are sustained for 21 days; levels of type I collagen are elevated following 4 days of MI and are sustained for 90 days in LV tissue. Type III and type I collagen are also produced in the non-infarct region but by cardiac fibroblasts, not myofibroblasts. The deposition of collagen is followed by the production of extracellular and contractile proteins. Therefore, the cross-linkage of collagen and extracellular proteins brings strength and salvages the debris-free LV wall from intense pressure. Another reparative process that occurs is the angiogenic response. The generation of neovasculature, which is hyperpermeable and pro-inflammatory, is to provide oxygen and nutrients to the mesenchymal cells in the healing heart **(Figure 2)**. With the activation of reparative processes, collagen-based scar is formed, stabilizing the wound in the last phase of cardiac repair and remodeling - the maturation phase[11].

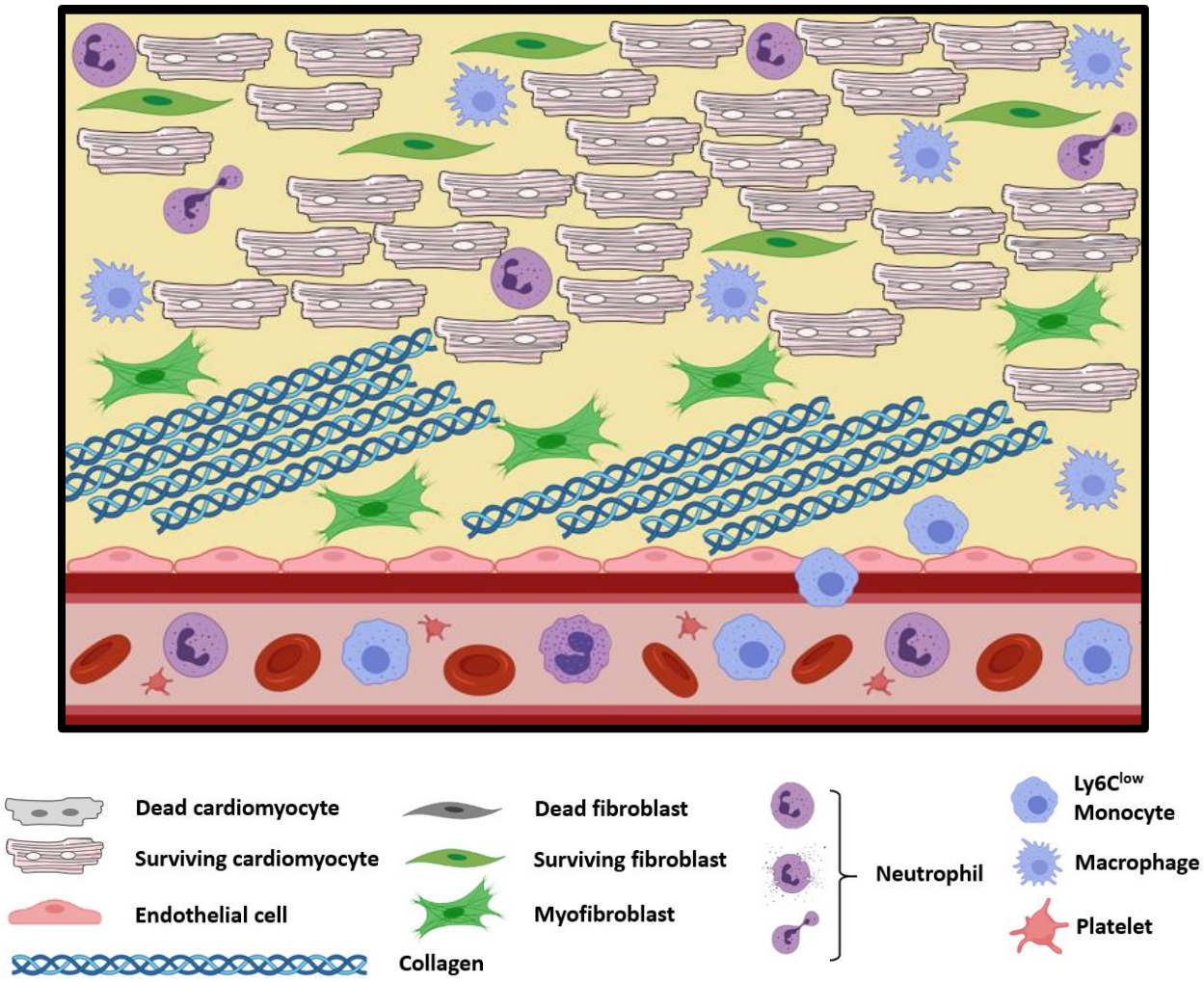

Figure 2. Second Stage of Cardiac Repair: The Proliferative Phase. The clearance of tissue debris leads to the recruitment of Ly6C^{low} monocytes that transition into M2 macrophages. M2 macrophages release anti-inflammatory cytokines and pro-fibrotic and angiogenic factors. Myofibroblasts initiate secretion of interstitial collagen, which replace the cleared infarct region. This phase lasts 4-14 days in mice and 0-3 weeks in humans.

1.1.1.1.3.3 Third Stage: Maturation Phase

The initiation of maturation phase is marked by the deactivation of reparative cells and the deposition of extracellular matrix. To achieve this, anti-inflammatory signals, such as TGFβ-1 and IL-10, angiogenesis, activation of myofibroblasts and matricellular protein expression, occur in the infarct and peri-infarct regions. Following the maturation of the scar, the proliferating myofibroblasts transition into a non-proliferating phenotype, called matrifibrocytes[42]. While reparative processes are progressing, the extracellular matrix and the collagen become cross linked via the assistance of enzymes, such as lysyl-oxidase. Therefore, defects in reparative processes can lead to overactive fibrotic response, which can worsen cardiac remodeling. Towards the end of the maturation phase, the healed heart consists of cross-linked interstitial collagen, macrophages, fibroblasts and matrifibrocytes, and blood vessels. The maturation phase takes 5-28 days in mice and 2-6 weeks in humans[11,14,15] **(Figure 3)**.

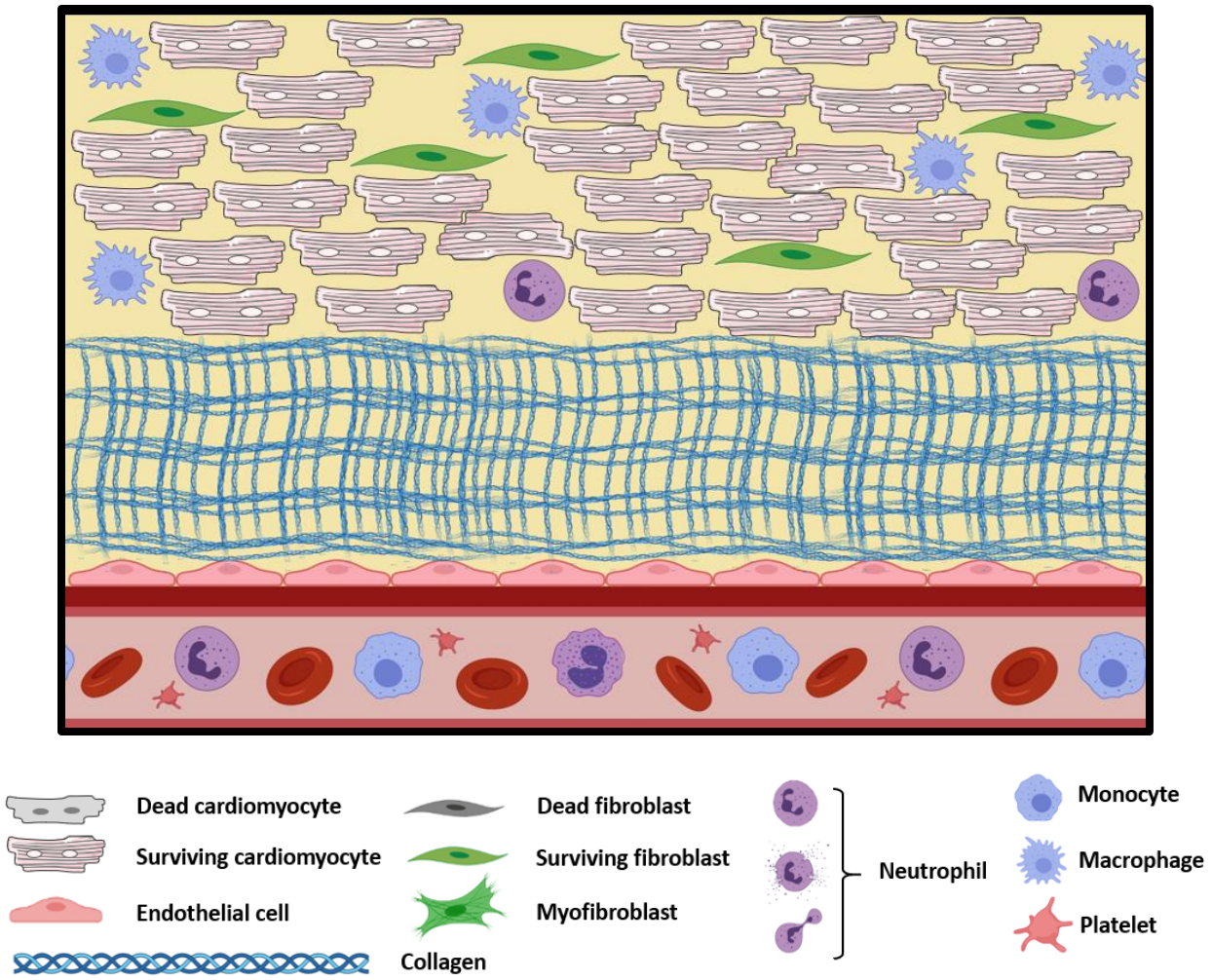

Figure 3. Third Stage of Cardiac Repair: The Maturation Phase. The anti-inflammatory signals and reparative processes are diminished. The infarct region is filled with collagen-based scar, new blood vessels, macrophages, fibroblasts and matrifibrocytes. This phase lasts up to 5-28 days in mice and 2-6 weeks in humans.

1.1.1.1.4 Current Therapies to mitigate downstream consequences of MI

One of the most severe consequences of MI, keeping in mind that the mammalian heart does not have the regenerative capacity, is cardiomyocyte necrosis. Therefore, the primary objective is to re-perfuse the ischemic heart in a timely manner to limit the infarct size and rescue the cardiac tissue from further ischemic damage. Both pharmacological interventions, such as thrombolytic agents (Tissue plasminogen activator (tPA) or Tenecteplase (TNK)), and Percutaneous Coronary Intervention (PCI)/ balloon angioplasty, are performed on the patient to restore perfusion. The application of these interventions depends on the following stages: pre-hospital care, hospital care, and post-discharge treatment[43].

Pre-hospital care refers to immediate medical support given by emergency medical personnel to patients experiencing angina while he or she is being transported to the hospital. At this stage, the patient is given an antiplatelet drug, such as aspirin, for dissolution of the thrombus and an analgesic, such as morphine, for pain management. At the same time, the electrical conductivity of the patient's heart is monitored using a single-lead electrocardiogram (ECG) to determine whether the patient is experiencing ST-elevation MI (STEMI) or Non-ST-elevation MI (NSTEMI). STEMI refers to MI that is caused by the complete blockage of the coronary artery due to thrombus, which can be detected by an elevation in the ST-segment on the ECG. NSTEMI patients are diagnosed by unstable ECG reading and elevated biomarker level, such as cardiac troponin[43]. If the patient is further away from a PCI centre, and is experiencing an ongoing STEMI, the patient may receive thrombolytic treatments in the transport vehicle.

At the hospital, the patient's treatment will depend on whether he or she is experiencing STEMI or NSTEMI. If the patient is experiencing STEMI, then either one of the following interventions are performed immediately to restore perfusion: PCI or fibrinolytic therapy. PCI is a cardiac catheterization procedure where a catheter balloon attached to stent is inserted via a blood vessel and localized to the site of blockage with the help of live x-ray and guided wire. At that occlusion site, the balloon inflates, expanding the narrowed artery and restoring blood flow. The inflation of the balloon puts the stent into place, preventing narrowing of the coronary artery[44]. For this procedure to be beneficial to the patient, it needs to be accomplished within 90

minutes following complete blockage of the coronary artery[45]. On the other hand, if PCI is not available or accessible, then fibrinolytic therapy, such as streptokinase, alteplase, and anti-coagulant proteases including tPA, is given to dissolve blood clots. The tPA in the fibrinolytic therapy cleaves circulating plasminogen to plasmin, which the latter leads to the lysis of fibrin clots. This intervention needs to be administered within 30 minutes of patient's arrival or if the 90-minutes goal of PCI cannot be met. PCI is the more preferred intervention than fibrinolytic therapy for STEMI patients because fibrinolytic therapy has limitations, such as intracranial bleeding, inability to re-establish flow, and high rates of recurrent ischemia and re-occlusion. NSTEMI patients are treated medically first, and then either revascularized with PCI or CABG, but PCI is the more preferred method[46].

After revascularization, both STEMI and NSTEMI patients are prescribed anti-platelets medications, beta-blockers, ACE inhibitors, and statins. They are also recommended to participate in cardiac rehabilitation and maintain a healthy diet post-hospital care[45,46].

1.2 Contributions of Innate Immunity and Inflammation to post-infarction remodeling

1.2.1 Inflammation and Myocardial Infarction

Inflammation and immune response are essential components for collagen-based scar formation following MI. Prolongation of myocardial ischemia causes necrosis in the myocardium, which leads to the release of "danger signals" or DAMPs, such as ATP, nucleic acids, HSPs, and HMGB1 by damaged cells. Detection of "danger signals" by neighbouring cells and resident immune cells via pattern recognition receptors (PRRs), such as members of the Toll-like receptor (TLR) family, leads to the activation of downstream MAPK and NF-κB signaling pathways, which produce and release pro-inflammatory cytokines and chemokines. The recruitment of immune cells into the infarcted myocardium by pro-inflammatory chemokines assists in the clearance of cellular debris, which later on is replaced by the synthesis of collagen-enriched scar tissue **(Figure 4)**. Hence, the activation of innate immune response mediates repair and recovery of the infarcted myocardium. However, excessive inflammation could prolong cardiomyocyte necrosis, leading to enhanced tissue loss, enzymatic imbalance favouring scar tissue breakdown,

myocardial wall thinning and cardiac rupture[11,20,41,47]. Greater understanding of the biological mechanism involved in the immune response following MI is important in developing new therapeutic approaches.

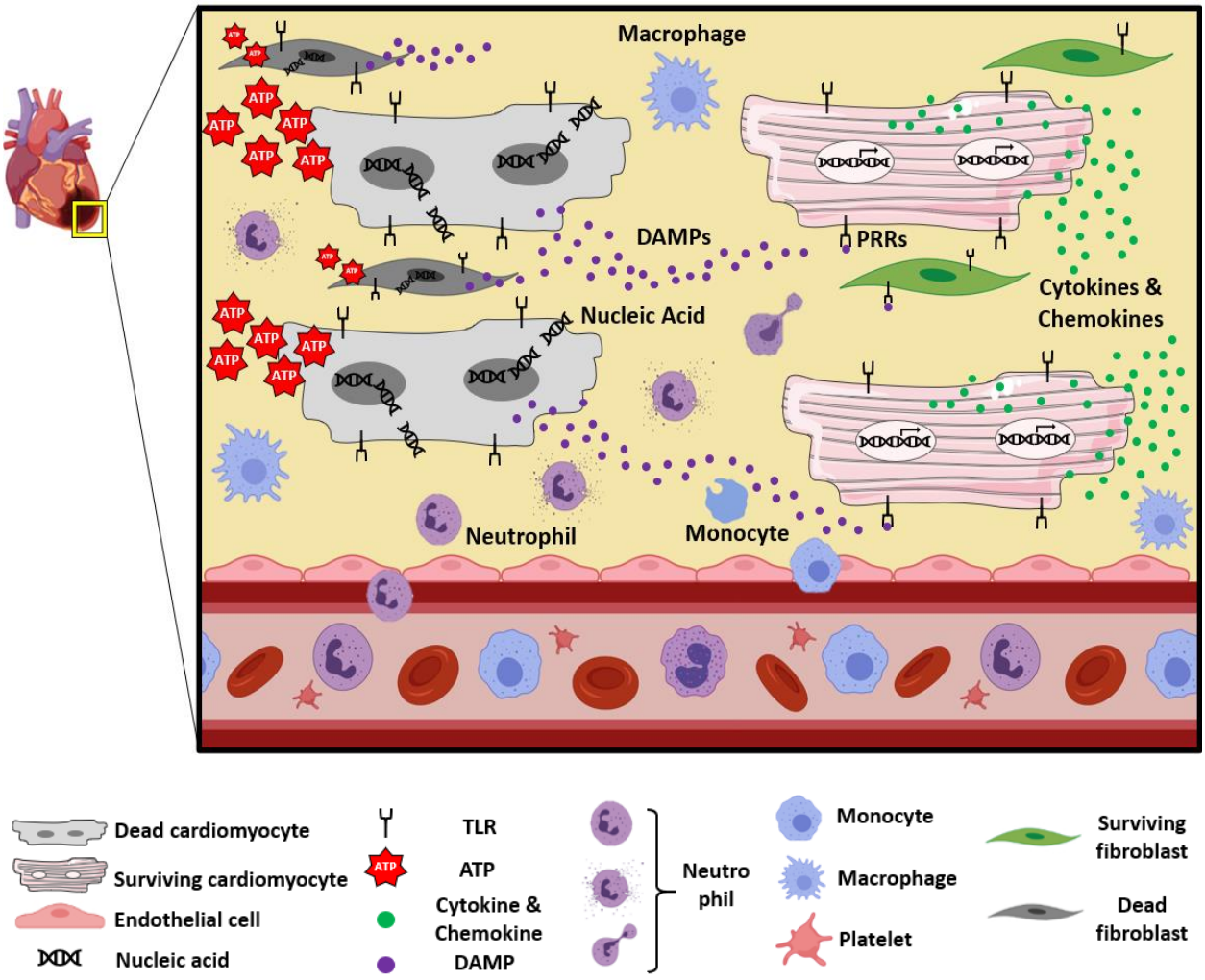

Figure 4. Ischemic injury releases danger signals to activate innate immune response. Following MI, necrotic cells in the infarct region release DAMPs, which are sensed by neighbouring cells via PRRs. Binding of DAMPs to PRRs activates downstream MAPK and NF-κB signaling pathways, which then release pro-inflammatory cytokines and chemokines for the recruitment of neutrophils and monocytes.

1.2.2 Danger Model Theory of Polly Matzinger in Immune System Activation

In the 1950s, an important principle that was accepted and followed in the field of immunology was the "self – non-self" theory, proposed by Nobel Prize winners Macfarlane Burnet and Frank Fenner. This simple model proposed that the immune system distinguishes between self and non-self, with the former being tolerated and latter not. The model also suggested that (i) "each lymphocyte expresses multiple copies of a single surface receptor (currently, known as the antibody) specific for a foreign entity", (ii) "signaling through this surface antibody initiates immune response", (iii) "the self-reactive lymphocytes are deleted early in life"[48,49]. Future scientific discoveries, such as Effector and Helper T cells and their role against foreign cells, strongly supported the "self – non-self" theory. However, the danger model, created by Polly Matzinger in 1990s, challenged the "self – non-self" theory because the latter could not explain why the immune system did not mount an attack on some non-self substances, such as silicone, foetuses, and tumours that express tumor-specific antigens[50]. The danger model proposed that Antigen Presenting Cells (APCs) are activated by "danger signals". These "danger signals" are endogenous substances that are produced and secreted by stressed or injured cells. Therefore, the model proposed that the immune system attacks when it detects "danger signals" rather than non-self or foreign substances[49,51]. Pradeu et al. indicated that the concept of "danger" is not well-defined. They argued that a logical name for Matzinger's model should be "damage theory", not "danger theory" because the general understanding of the term "danger" does not explain harmless antigens, such as allergens or food antigens. Even though the immune system recognizes those harmless antigens as "danger", they are not actually dangerous. In this case, the word "damage" would be more suitable because immune response is activated when a cell or tissue is damaged[52]. Therefore, the "danger" signals are referred to as Damage-Associated Molecular Patterns (DAMPs) in the scientific literature.

1.2.3 Role of Damage-Associated Molecular Patterns post-MI

Polly Matzinger's proposal of Danger Model caused many Damage-Associated Molecular Patterns (DAMPs) to be identified in various illnesses. DAMPs play a key role in the initiation of innate immune response following MI. They are endogenous molecules that are found either in

organelles or cytoplasm, such as HSPs, HMGB1, and mitochondrial DNA, or in extracellular matrix, such as Biglycan and Fibronectin-EDA, following cardiac injury. Moreover, they are either characterized as constitutive, such as mitochondrial DNA and Biglycan, or inducible, such as HSPs and HMGB1[53]. In order to differentiate DAMPs from biomarkers or inflammatory cytokines, the following criteria is considered: DAMPs must i) be released by nonprogrammed cell death, not apoptotic cells, ii) be produced and secreted as alarmins by immune cells, iii) have chemotactic effects on APCs and activate them, iv) restore homeostasis to promote reconstruction of the injured tissue, which are harmed due to direct insult or secondary effects of inflammation[54,55]. During an ischemic stress, DAMPs are known to be passively released by injured cells and are detected by PRRs, located on the surface of neighbouring cells, such as cardiomyocytes, fibroblasts, smooth muscle cells, and macrophages[56–59]. It is not understood why various DAMPs bind to the same PRRs, but it is known that co-receptors, such as CD24-Siglec-G/-10 or CD14/MD2, assist PRRs to distinguish between DAMPs and pathogen associated molecular patterns (PAMPs)[60]. Some of the well-studied DAMPs in MI are HMGB1, HSP60 and HSP70, which are known to activate inflammatory responses by binding to TLRs[56,57,61–63].

1.2.4 Toll-like Receptors are critical inflammation-promoting factors post-MI

Toll-like receptors (TLRs) are well-known to trigger the innate immune response by detecting various PAMPs and DAMPs during MI. TLRs are type I integral membrane proteins that are either found on the plasma membrane of the cell (TLR 1, 2, 4, 5, 6, 10 and 11) to survey the extracellular environment or on the membrane of the endosomal compartments (TLR 3, 7, 8, 9) of the cell to detect microbial or self-nucleic acids[64]. There are at least six TLRs (TLR 2, 3, 4, 5, 7, 9) in mice and at least 10 in humans[65]. The structure of a TLR consists of a highly glycosylated N-terminal ectodomain (ECD) for ligand recognition, a single transmembrane helix, and a C-terminal Toll IL-1 receptor (TIR) domain for signaling. Moreover, the N-terminal ECD consist of 22-29 residues long of leucine rich repeats that form a distinct horseshoe shape and recognize ligands via protein-protein interactions[66]. The interaction of DAMPs with the N-terminal ECD leads to the dimerization of C-terminal TIR domain which activates downstream kinases (i.e. IL-1 receptor-associated kinase 1 (IRAK1) and IRAK4) via either of the two adaptor proteins: Myeloid

differentiation primary response protein (MYD88) or TIR-domain-containing adapter-inducing interferon-β (TRIF). The activated C-terminal TIR domain of TLRs interacts with the TIR domain of the adaptors protein to activate further downstream kinases. Hence, TLR signaling, except for TLR3, is divided into two pathways: MYD88-dependent pathway or TRIF-dependent pathway (MYD88 independent pathway)[67]. The two most studied TLRs in the heart are TLR2 and TLR4[16]. Both TLR2 and TLR4 signaling occurs via MYD88 dependent pathway.TLR2 first dimerizes with TLR1 or TLR6 and then MYD88 is recruited to TLR2 via Mal protein. Consequently, IRAK1 and IRAK4 are activated to trigger the production of cytokine via upregulation of NF-κB. TLR4 signaling, unlike TLR2, can occur via MYD88 dependent or independent pathways. In MYD88 dependent pathway, TLR4 directly interacts with MYD88 via Mal protein to activate downstream IRAK1 and IRAK4, which consequently activates NF-κB and Interferon regulatory transcription factor 5 (IRF5) transcription factors to produce pro-inflammatory cytokines, such as TNF-α, IL-6, and IL-1β[67,68]. On the other hand, TLR4 can also activate NF-κB and IRF3 transcription factors via MYD88 independent pathway. Hence, dimerization of TLR4 leads to the interaction with TRIF protein via Translocating chain-associated membrane (TRAM) protein. As a result, TANK-binding kinase (TBK) 1 is activated to trigger the upregulation of NF-κB and IRF3, which consequently stimulate the production of Primary, or Type 1, interferons, such as Immune interferon-α (IFN-α) **(Figure 5)**. The activation of pro-inflammatory signaling pathways leads to myocardial inflammation and contractile dysfunction post-MI, which was reversed in *Tlr2* and *Tlr4* knockout mice post-MI[27,29,69]. Knocking out *Tlr2* gene in mice resulted in smaller infarct size, improved cardiac function, and attenuated myocardial inflammation post-MI[29]. Same results were observed when anti-TLR2 antibody was injected into wildtype mice post-MI[69]. At the same time, mice deficient of *Tlr4* demonstrated reduced myocardial inflammation compared to wildtype mice in an *in vivo* model of ischemia/reperfusion injury[27]. Therefore, TLRs play a significant role at mediating inflammation and are proven to be a potential therapeutic target post-MI.

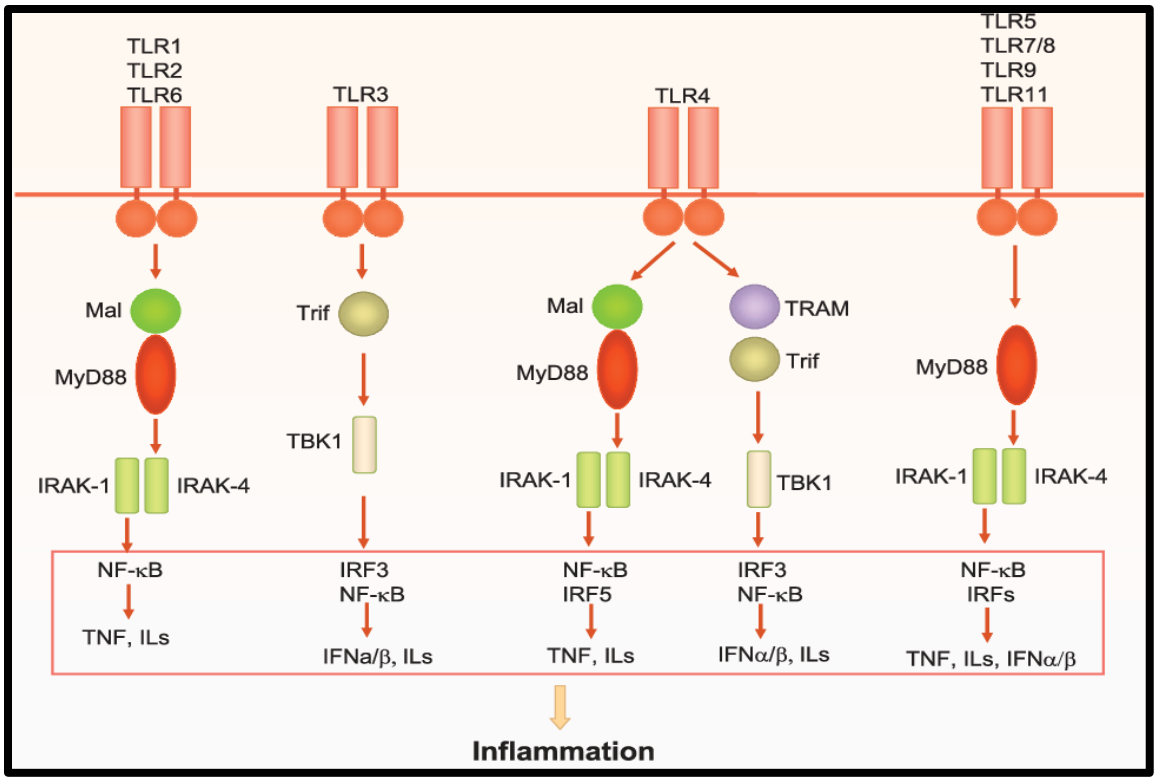

Figure 5. The Toll-Like Receptor (TLR) signaling in the ischemic heart[65]. TLRs play a significant role in activating innate immune response following MI. TLRs, located on the surface of the plasma membrane, are activated via MYD88 dependent or independent pathways. Eventually, transcription factors, such as NF-κB, IRF3 and/or IRF5, are activated to stimulate the production of pro-inflammatory cytokines.

1.2.5 NF-κB and MAPK-ERK Pathways stimulate inflammation and cardiac remodeling post-MI

NF-κB is a prominent and essential family of inducible transcriptions factors at mediating innate immune response following MI. It consists of five subunits which can assemble in various combinations to activate inflammation and survival-associated gene targets: p65 (RelA), RelB, c-Rel, p50, and p52. RelA/p65, c-Rel, and RelB subunits contain a transactivating domain, responsible for the transcriptional activity while p50 and p52 do not contain one and act as transcriptional repressors. In a resting cell, the transcriptional activity of NF-κB is inhibited when it is bound to IκBα. The activation of TLR2 or TLR4 and then its downstream targets IRAK1, IRAK4, and/or TBK1, leads to the phosphorylation of IκBα by IKK complex, which is recruited by NF-κB essential modulator (NEMO). As a result, NF-κB dissociates from IκBα and translocates to the nucleus while phosphorylated IκBα is polyubiquitinated and then degraded by the proteasome.

Nuclear translocation of NF-κB activates the transcription of genes including inflammatory cytokines, CXC and CC chemokines, and adhesion molecules **(Figure 6)**. Consequently, inflammatory response is amplified, and specific leukocyte population is recruited to the infarct region. NF-κB activation takes place within 24 hours following MI[70,71]. *In vivo* model of permanent occlusion and ischemia/reperfusion injury have demonstrated that NF-κB p65 or p50 or IKKβ inhibition ameliorates cardiac function and attenuates myocardial injury following MI[38,72,73].

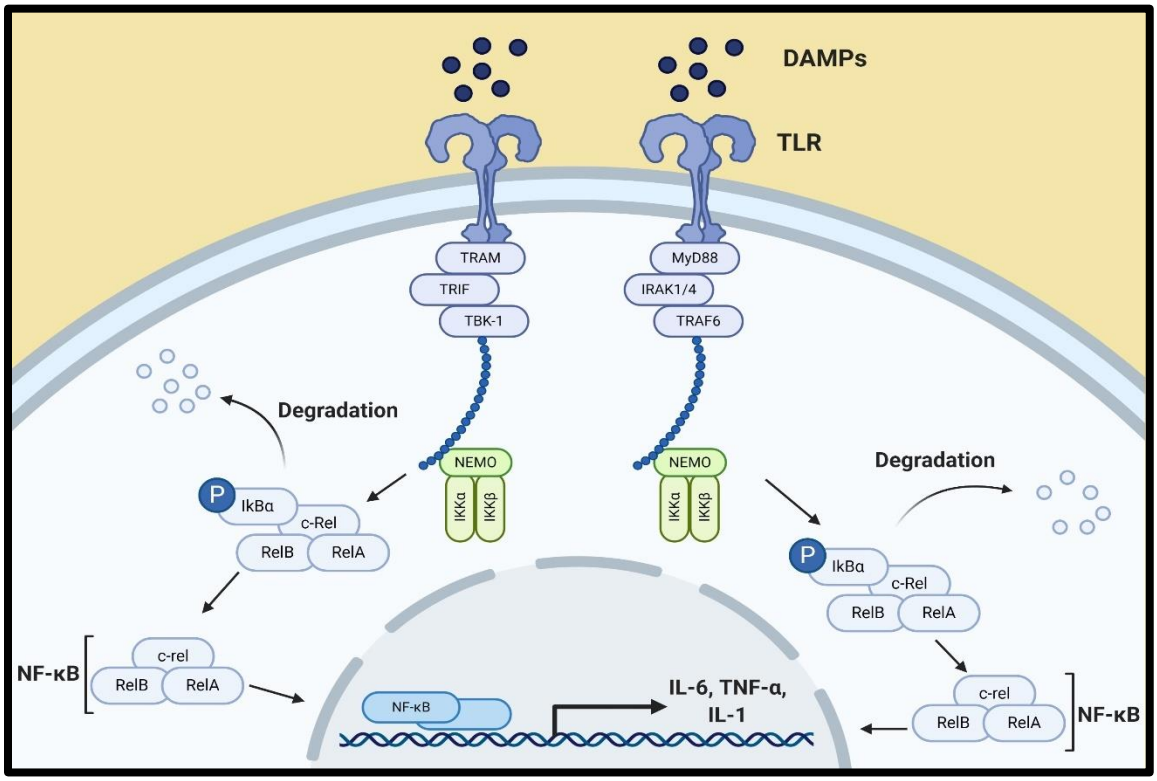

Figure 6. The NF-κB signaling pathway in the ischemic heart[65,74]**.** Following ischemia, DAMPs are sensed by TLRs, which leads to the recruitment and activation of their adaptor proteins. Consequently, the activation of IKK complex leads to the phosphorylation of IkBα, which is polyubiquitinated and then degraded. The NF-κB subunits (RelB, RelA, and c-Rel) then translocate to the nucleus for the transcription of pro-inflammatory cytokines and chemokines genes (Adapted from Kawai et al., 2007 and Chao et al., 2009).

The extracellular-signal-regulated kinase (ERK) signaling pathway is one of the major mechanisms of Mitogen-Activated Protein Kinase (MAPK) signaling pathways. The ERK signaling pathway can be activated by various biological substances, such as growth factors and hormones, or cellular stresses, such as hypertrophy and ischemia. This leads to the recruitment and

activation of Raf-1, B-Raf, and A-Raf protein kinases, which subsequently activates MEK1/2 kinases via phosphorylation and finally phosphorylates ERK1/2 protein kinases. ERK1 (p44) and ERK2 (p42) are isoforms of ERK. Phosphorylated ERK1/2 localize to the nucleus for the activation of downstream transcription factors. In the context of MI, the ERK1/2 signaling pathway is activated 30 minutes following MI[75,76]. Pre-clinical studies have demonstrated that the MEK1/2-ERK1/2 signaling pathway of the MAPK signaling pathway is cardioprotective despite of not improving cardiac function following MI[75]. Shimizu et al. showed that increased activation of MAPK following MI in rats leads to the activation of transcription factors NF-κB and AP-1, followed by increased expression of cytokines and chemokines[77].

1.2.6 Cytokines and Chemokines

Cytokines are an integral part of the innate immune response and play an important role in tissue injury and repair. They are small proteins that are released and act on various cell types. In the context of MI, some of the well-studied cytokines are TNF-α, IL-6, IL-1, IL-10. The expression of pro-inflammatory cytokines, such as TNF-α, IL-6, and IL-1, is upregulated (up to 50-fold) in the infarct region within the first few hours to days following MI. The expression of pro-inflammatory cytokines correlates with the size of the infarction. Therefore, if the infarction size is small, the expression of pro-inflammatory cytokines is remarkably similar to baseline[78,79]. Cytokines are sensed by other cardiac resident cells, such as fibroblasts, cardiomyocytes, and leukocytes, activating 3 major intra-cellular transduction pathways ((MAPK) and Janus kinase (JAK)/ signal transducers and activators of transcription (STAT) pathways), which then activate downstream transcription factors, such as NF-κB and AP-1, to produce and release more cytokines. This way, they have the ability to self-amplify[80]. Consequently, inflammatory cells, such as neutrophils, monocytes, and macrophages, are recruited to the injury site to clear up necrotic debris. Following a week of MI, the expression of pro-inflammatory cytokines decreases unless there are ongoing injury. Reduction in pro-inflammatory cytokines promotes inflammation resolution and may shift macrophage phenotype towards an anti-inflammatory profile including the release of IL-10. IL-10 inhibits the production of pro-inflammatory cytokines and chemokines, and promotes angiogenesis and extracellular matrix deposition[18,81]. Therefore, pre-clinical studies have

demonstrated that deficiency of pro-inflammatory cytokines, such as IL-6, TNF-α, IL-1, and excess of anti-inflammatory cytokines, such as IL-10, leads to improved survival rate and cardiac function, and reduces adverse remodeling following MI[22,30,37,57,82,83]. Promising results from the pre-clinical study of IL-1β led to the large clinical CANTOS (Canakinumab Anti-Inflammatory Thrombosis Outcomes) trial, where STEMI patients were either administered with monoclonal IL-1β antibody, called canakinumab, or placebo. The results showed that STEMI patients receiving canakinumab had significantly lower rate of recurrent cardiovascular events, independently of lipid lowering, but slightly higher incidence of fatal infection and sepsis in comparison to placebo-treated patients[22,84]. Clinical trial of Tocilizumab (IL-6 antibody) in STEMI patients, called ASSAIL-MI (Assessing the Effect of Anti-IL-6 Treatment in Myocardial Infarction), is currently ongoing[47,85].

Chemokines are another class of small extracellular released proteins that have chemotactic activities and are produced by various cells, such as cardiomyocytes, fibroblasts, macrophages, and endothelial cells. They are typically 8-10 kilodaltons in size and bind to G protein-coupled receptors on target cells. There are four classes of chemokines: CXC, CC, CX3C, and XC. Among the four groups, CXC and CC family of chemokines are the hallmark of inflammatory and reparative response post-MI[86]. CXC family of chemokines contain two cysteines that are separated by an amino acid while CC family of chemokines contain the first two residue of cysteines. CXC chemokines are subdivided into two groups: with or without ELR (Glu-Leu-Arg) motif in the N-terminal. CXC chemokines with ELR motif, such as CXCL8 and CXCL1, recruit neutrophils and monocytes. CXC chemokines without ELR motif, such as CXCL10, recruit and activate monocytes, T lymphocytes, and vascular smooth muscle cells[81,86]. Furthermore, CC chemokines, such as monocyte chemoattractant protein (MCP)-1/ CCL2, recruit monocytes, macrophages, T cells and NK cells into the infarct and peri-infarct regions[18,86,87]. Pre-clinical studies have demonstrated that deficiency of CXC and CC family of chemokines reduce inflammatory response and promote tissue repair following MI[25,31,32,88].

1.2.7 Neutrophils and Macrophages

Neutrophils, also known as polymorphonuclear granulocytes (10µm in diameter), are the first immune cells to massively infiltrate the infarcted myocardium following MI[89]. They are the most abundant type of leukocyte and are produced in the bone marrow[90]. Only the terminally differentiated neutrophils (~1-2%) circulate in the bloodstream; therefore, the body maintains a large bone marrow-located reservoir of these leukocytes to respond to infection or injury[91]. An increase in peripheral neutrophil count and neutrophil to lymphocyte ratio are prognosis of larger infarct size and cardiac dysfunction[92]. Following MI, cells in the infarcted myocardium, such as cardiomyocytes, fibroblasts, and resident immune cells, sense DAMPs in the cellular environment and in response, release neutrophil-attracting CXC chemokines, such as CXCL8 and CXCL1, to recruit circulating neutrophils into the infarct region. The neutrophils undergo a set of sequential steps, collectively known as extravasation, to reach the infarcted myocardium. This process is mediated by selectins, integrins, and intracellular and vascular cell adhesion molecules expressed by both endothelial cells and neutrophils. Once in the infarct region, neutrophils can also sense DAMPs or PAMPs via their PRRs, leading to the release of ROS and granule proteins, which can damage host tissue and cells. Neutrophils also engulf or 'phagocytose' dead cells and tissue debris to facilitate the clearance of infarct region. Following the onset of MI, infiltration of neutrophils into the infarct region occurs within hours and peaks at days 1-3. Then, at day 5 and onwards, the apoptotic neutrophils release "find me" signals (e.g. lipid mediators and nucleotides) and "eat me" signals (e.g. lysophosphatidylcholine) in order to be cleared by macrophages. The apoptotic neutrophils also release annexin 1, lactoferrin, and lipid mediators to stop the influx of neutrophils and promote monocyte migration to the infarct region[93,94]. Efficient clearance of debris and apoptotic neutrophils prevents cell death and further amplification of inflammation. The clearance of apoptotic neutrophils inhibits pro-inflammatory mediators, such as IL-6, IL-1, and TNF-α, and produces anti-inflammatory markers, such as IL-10 and TGFβ-1. Removal of apoptotic neutrophils is a hallmark of inflammation resolution and initiates the proliferative phase of MI[95,96].

Similar to neutrophils, macrophages and their precursors, monocytes, play a significant role in recognition and elimination of pathogens. Monocytes (~18μm diameter) and macrophages (~21μm diameter) exist as circulating and as tissue resident cells, respectively. Following MI, significant loss of resident cardiac macrophage is observed in the infarct region within 24 hours of ischemia. Consequently, monocyte-derived macrophages, which are produced in the spleen and bone marrow, are recruited from the circulation into the infarct and peri-infarct regions. The infiltration of monocyte-derived macrophages occurs via sequential steps called extravasation, which involves the interaction of MCP-1/CCR chemokines and endothelial adhesion molecules [96]. Once in the infarct region, macrophages can sense DAMPs via PRRs. They exhibit a pro-inflammatory phenotype within 1-3 days of MI and release pro-inflammatory cytokines, myeloperoxidase (MPO), matrix metalloproteinases (MMPs), and proteolytic mediators, such as cathepsins and urokinase, to facilitate the clearance of necrotic debris and drive inflammation. Macrophages with pro-inflammatory phenotype, also known as M1 macrophages, are derived from $Ly6C^{high}$ monocytes and dominate for 1-3 days following MI. Once the apoptotic neutrophils are clear, the pro-inflammatory macrophages transition into reparative macrophages, also known as M2 macrophages. These reparative macrophages are derived from $Ly6C^{low}$ monocytes and are the principle heart-constituent macrophage population for 5-7 days post-MI. They secrete high level of anti-inflammatory cytokines, such as IL-10 and TGFβ-1, and growth factors, such as VEGF, to mediate angiogenesis, collagen deposition, and myofibroblast accumulation[97]. The transition of the tissue environment from inflammatory (M1) to reparative (M2) macrophage-dominant is essential for the injured heart to initiate healing and salutary remodelling processes[98,99].

1.2.8 Therapeutic modulation of inflammation and immune system post-MI

The inflammatory response is essential to cardiac repair and remodeling following MI. However, excessive inflammation can prolong cardiomyocyte necrosis and cause cardiac rupture. Hence, an important therapeutic goal of MI is to develop pharmacological interventions to control the degree of inflammation in the infarcted myocardium. Many pre-clinical studies have identified therapeutic targets to lessen the degree of inflammation post-MI, but only few have

proven to be promising in STEMI and/or atherosclerotic patients following clinical trials. Therapeutic targets that have proven to be successful post-clinical trials reflect the necessity to reduce myocardial inflammation post-MI.

As discussed previously, acetylsalicylic acid, commonly known as Aspirin, is one of the well-known antiplatelet drugs administered to STEMI patients during the initiation of MI and post-revascularization. Aspirin is a nonsteroidal anti-inflammatory drug (NSAID) that reduces inflammation by inhibiting the rate limiting enzyme of prostaglandin synthesis, Cyclooxygenase (COX). There are two isoforms of COX: COX-1 and COX-2, that are induced by stress, inflammation, and ischemia. Aspirin irreversibly but non-competitively binds to COX-1, inhibiting platelet aggregation for the entire life of the platelet; thereby, reducing recurrent cardiovascular clotting events. For this reason, aspirin is administered to STEMI patients immediately after the onset of MI[81].

Inhibition of pro-inflammatory cytokines, such as IL-1, IL-6, and TNF-α, has protective effects in both *in vivo* models of permanent MI and myocardial ischemia/reperfusion. Among all the pro-inflammatory cytokines, blockage of IL-1 and associated signaling pathways were shown to be promising in pre-clinical and clinical studies. Abbate et al. used two independent strains of mice with genetic modifications to either enhance (*Il-1ra*$^{-/-}$) or repress (*Il-1r1*$^{-/-}$) IL-1 signaling pathway. They demonstrated that *Il-1r1*$^{-/-}$ mice had better survival rate, smaller infarct size, and less systolic dysfunction compared to *Il-1ra*$^{-/-}$ mice following permanent MI[21]. This conclusion was also supported by Bujak et al. who demonstrated that *Il-1r1* null mice exhibited reduced infiltration of neutrophils and macrophages and reduced expression of cytokines and chemokines in an *in vivo* model of myocardial ischemia/reperfusion[22]. Their pre-clinical study also showed that suppressed inflammation was followed by attenuated fibrotic response in the absence of IL-1 signaling. Hence, *Il-1r1* null mice had decreased myofibroblast infiltration and reduced collagen deposition in the infarcted myocardium. Toldo et al. took a step further and demonstrated that mice treated with IL-1β antibody significantly inhibited cardiomyocyte apoptosis, limited LV enlargement by 40% and improved systolic dysfunction by 17% following MI[30]. Consequently, early clinical studies showed the same promising result. The CANTOS study conducted a

randomized, double-blind trial of canakinumab with 10,061 patients with high-sensitivity C-reactive protein and previous MI. Canakinumab is a monoclonal antibody targeting IL-1β innate immune pathway. Administration of canakinumab at a dose of 150mg every 3 months resulted into a significantly lower rate of recurrent cardiovascular events, independently of lipid-lowering responses. However, investigators also reported a higher incidence of fatal infection and sepsis in comparison to placebo-treated patients[84]. Therefore, targeting IL-1β in STEMI patients is likely to be beneficial but with a cost.

Similar to the CANTOS trial, another anti-inflammatory candidate for the treatment of MI was colchicine. Akodad et al. demonstrated the administration of colchicine to mice following myocardial ischemia/reperfusion injury reduced infarct size, expressed lower levels of troponin, and decreased fibrosis[100]. These results were consistent with studies by Bakhta et al., who had found that colchicine treatment resulted in smaller infarct size. This outcome was associated with significantly increased levels of IL-10 and decreased levels of TGFβ-1. Moreover, their study demonstrated that colchicine, when administered alone, significantly reduced infarct size compared to colchicine and anti-IL-1β antibody combined treatment and anti-IL-1β antibody treatment alone[101]. Consequently, early clinical studies showed the same promising result. The COLCOT (Colchicine Cardiovascular Outcome Trial) study conducted a randomized, double-blind trial of colchicine, an anti-inflammatory medication for the treatment of gout and pericarditis, that was orally administered to patients. These patients were recruited within 30 days following MI and they were randomly assigned to receive either low-dose colchicine or placebo. At the end of the study, administration of 0.5mg of colchicine (low dose) to patients led to a significantly lower rate of ischemic cardiovascular event compared to placebo-treated patients[102].

Overall, current medications administered to STEMI patients, such as Aspirin, are effective at reducing inflammation following MI. Various pre-clinical studies have also shown that modulating inflammation by targeting DAMPs, TLRs, NF-κB, pro-inflammatory cytokines and chemokines, and immune cells have proven to be beneficial in the setting of MI[29,30,34,57,72]. However, only few inflammatory targets have proven to be promising at reducing inflammation

in STEMI patients, as learned from CANTOS and COLCOT clinical trials. Therefore, effective therapies are in-need to mitigate inflammation due to cardiomyocyte necrosis.

1.3 Heat Shock Proteins – Short Term Responses Post-Infarction

Recent pre-clinical and clinical research studies have identified extracellular heat shock proteins (HSPs), a classic DAMP, to be a prognostic marker for patients with MI and Heart Failure[103,104]. Intracellular HSPs, on the other hand, are a key factor in driving heat shock response (HSR) and cell stress responses[105].

1.3.1 Discovery of Heat Shock Proteins

Heat shock proteins (HSPs) were discovered by Italian scientist, Ferruccio Ritossa, in 1960s when he was studying nucleic acid synthesis in puffs of *Drosophila* salivary glands at the Genetics Institute in Pavia, Italy and the International Institute of Genetics and Biophysics in Naples, Italy. Ferruccio's experiment was accidently placed in the wrong incubator by one of his lab members[106]. When he examined those cells, he observed puffs in the polytene chromosomes of larval *Diptera*, which indicated a significant increase in the transcriptional activity. Intrigued by the outcome of the accident, Ritossa replicated the experiments, including the appropriate controls, and found that puffs in the polytene appeared again when placed in the 30°C incubator but disappeared when placed back in the 25°C incubator. He observed the same results when the cells were treated with various stress agents, such as sodium salicylate, ecdysterone, etc[107,108]. In 1973, Tissieres et al. demonstrated that the induction of puffs in polytene chromosomes corresponded with the production of small proteins, which today are known as heat shock proteins[109].

1.3.2 Acute Heat Shock Responses

Heat shock response (HSR), of which the family of mammalian heat shock factors (HSFs) and their downstream heat shock proteins are part of, is a conserved, adaptive mechanism that is found in all living organisms. HSR is significant because it maintains proteostasis and conserves cellular integrity in a stressful environment. Among the four HSFs, HSF1 is the master

transcriptional regulator that transactivates heat shock genes, which eventually encode for heat shock proteins (HSPs). HSPs are molecular chaperones that reduce misfolding and aggregation of cellular proteins via protein assembly and degradation in order to prevent proteotoxicity[110]. They bind to hydrophobic regions of non-native proteins, inhibiting protein aggregation and allowing folding via ATP consumption[111]. In a resting cell, HSF1 exists as a monomer and is bound to a multi-chaperone complex, which inhibits HSF1 activation. In the presence of cellular stress, HSPs sense proteotoxicity and release HSF1 to correct misfolded protein. Consequently, HSF1 oligomerizes to homotrimers and binds to heat shock elements (HSEs) to transcribe heat shock genes, which encode for heat shock proteins. Hence, HSPs restore proteostasis via *de novo* protein folding and protein degradation, leading to HSF1 inactivation and ceasing heat shock response. "Heat Shock" is a misnomer; HSR can be activated in the presence of any cellular stress in addition to heat, such as ischemia, oxidative stress, etc.[112] **(Figure 7)**.

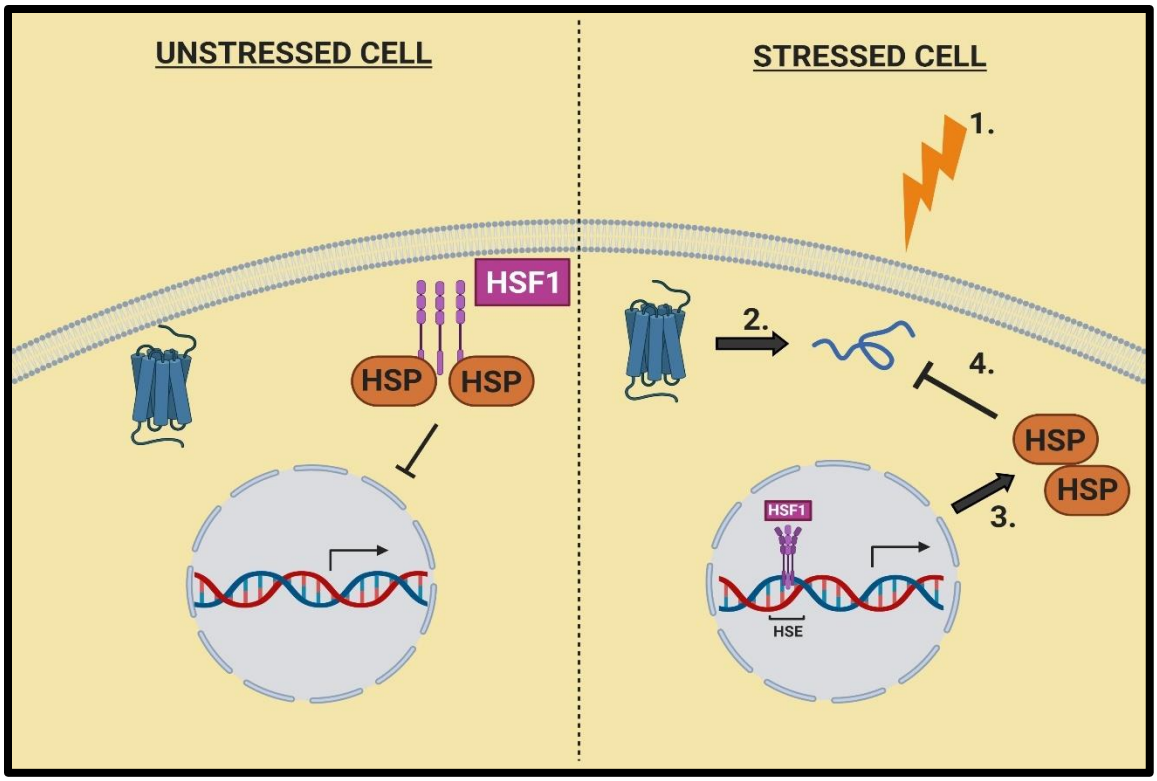

Figure 7. The Heat Shock Response. In a resting or unstressed cell, the monomers of HSF1 are attached to multi-chaperone complex, which inhibit the activation of HSF1 via a negative feedback loop. In the presence of cellular stress, such as ischemia, oxidative stress, etc., the gradual accumulation of unfolded protein causes proteotoxicity, which are sensed by HSPs bound to HSF1. As a result, the multi-chaperone complex releases HSF1, which trimerizes and localizes to the nucleus for the transcription of HSPs. Once the stress is eliminated, HSPs and post-translational modifications repress HSF1 activation.

1.3.3. Family of Heat Shock Proteins and their role in MI and Ischemia

Ischemia/reperfusion injury causes a wide range of damage to cardiomyocytes, including mitochondrial swelling, cytoskeleton damage, disruption of microtubules and mitotic spindle, inhibition of protein synthesis, and accumulation of protein aggregates, which if prolongs, leads to cardiac dysfunction. Cardiomyocytes are highly dependent on proteostasis because they are terminally differentiated, have a high metabolic demand, and use specialized molecular mechanisms for electrical conduction and contractility[113]. Hence, to maintain proteostasis, HSPs are constitutively expressed in different parts of the cell and are grouped into families according to their molecular weight, as indicated in **Table 1**[114,115]. However, upon prolongation of ischemia, heat shock proteins initiate inflammatory processes by acting as DAMPs. Nevertheless, there is a

growing number of pre-clinical and clinical evidence suggesting that extracellular heat shock proteins are detrimental in the setting of MI[56,62,116,117]. Whether HSPs is beneficial or detrimental in the setting of MI is controversial, and is context dependent, thus also known as the "heat shock paradox"[118].

Table 1 | **The main families of heat-shock proteins***

HSP family	Members	Intracellular location
Small HSPs	HSP10, GROES, HSP16, α-crystallin, HSP20, HSP25, HSP26, HSP27	Cytosol
HSP40	HSP40, DNAJ, SIS1	Cytosol
HSP47	HSP47	Endoplasmic reticulum
Calreticulin	Calreticulin, calnexin	Endoplasmic reticulum
HSP60	HSP60, HSP65, GROEL	Cytosol and mitochondria
HSP70‡	HSP72, HSC70 (HSP73), HSP110/SSE, DNAK SSC1, SSQ1, ECM10 GRP78 (BiP), GRP170	Cytosol Mitochondria Endoplasmic reticulum
HSP90	HSC84, HSP86, HTPG gp96 (GRP94, HSP108, endoplasmin)	Cytosol Endoplasmic reticulum
HSP100	HSP104, HSP110§ CLP proteins HSP78	Cytosol Cytosol Mitochondria

*The list is not all-inclusive. ‡Co-chaperones HIP (p48), HOP (p60), BAG-1, RAP46. §Distinct from the HSP70 member with the same name. HSP, heat-shock protein.

Table 1. Family of Heat Shock Proteins and their intracellular location[115].

1.3.3.1 Small HSPs

Small HSPs are highly expressed in the heart. HSPB1 (also known as HSP27 in humans and HSP25 in rodents), HSPB5 (α-crystallin B chain), HSPB6 (HSP30), HSPB7 (cardiovascular HSP) are small HSPs that are essential to cardiac morphogenesis and contractile function of the heart[113,114,119]. Both *in vitro* and *in vivo* models of ischemia/reperfusion injury have demonstrated that the overexpression of *Hspb1* leads to better cardiac function, reduction of infarct size, and attenuation of cardiomyocyte apoptosis[120,121]. Marunouchi et al. showed that the induction of HSPB1, HSPB5, and HSPB8 expression is crucial in salvaging the mitochondria in the failing heart[122]. Moreover, Li et al. observed that overexpressing *Hspa12b* gene in mice attenuated

cardiac dysfunction, cardiomyocyte apoptosis, and promoted myocardial angiogenesis via eNOS-dependent mechanism following ischemia/reperfusion injury[123]. On the other hand, extracellular HSP27 is known to induce inflammation by activating NF-κB signaling pathway[124]. While most studies indicated the induction of small HSPs to be necessary and beneficial in the setting of ischemia/reperfusion injury, extensive molecular studies, such as knock-out mice model, and clinical studies in STEMI patients are needed to validate the protective role of small HSPs in the setting of MI.

1.3.3.2 HSP60

HSP60 was primarily discovered in the mitochondria but is also found in the cytosol, where it promotes protein folding and trafficking in the mitochondrial matrix. Fan et al. demonstrated the significant role of HSP60 in cardiomyocytes by generating a cardiac-specific *Hsp60* conditional knock-out mouse model. They showed that cardiac-specific *Hsp60* conditional mice experienced altered mitochondrial complex activity, mitochondrial membrane potential, and ROS production, which led to dilated cardiomyopathy and lethality[125]. In the context of MI, the function of HSP60 has been linked to inflammation and the activation of innate immune response. Preclinical studies, mostly *in vitro*, have shown that extracellular HSP60 induces inflammation and cell death via TLR2 and TLR4[56,62]. Moreover, Zhang et al. conducted a clinical study where 1003 patients with coronary heart disease had higher levels of circulating HSP60[104]. Therefore, HSP60 can be a potential therapeutic target following MI, but experiments need to be replicated using a knockout mouse model to validate HSP60's detrimental role in MI.

1.3.3.3 HSP70

HSP70 is one of the well-studied HSP family in the context of MI. Most *in vivo* and *in vitro* models of ischemia/reperfusion injury have demonstrated that HSP70 has a protective role following MI[126]. Four *in vivo* studies have shown that overexpression of HSP70 via the usage of transgenic mice have improved cardiac function, reduced infarct size, attenuated cardiomyocyte apoptosis, and have lower levels of creatine kinase following MI[127–130]. Among the four preclinical studies, one study demonstrated that HSP70 protects the heart via the inhibition of p38 MAPK

signaling pathway[130]. On the other hand, knocking out HSP70 via a knock-out mouse model or injecting HSP70 inhibitor showed that absence of HSP70 leads to impaired contractility, cardiac hypertrophy, altered calcium handling and upregulation of JNK, p38, and ERK-MAPK signaling pathways[131,132]. Clinical studies were conducted to further validate the protective role of HSP70 in patients with coronary heart disease. It was learned from four clinical studies that elevated circulating levels of HSP70 predicted risk of acute coronary syndrome and heart failure[103,117,133–135]. Satoh et al. showed that extracellular HSP70 initiated inflammatory response via monocyte TLR signaling in patients with heart failure following MI. This scientific finding was replicated using primary and cell-line cardiomyocytes, which showed that exposure to HSP70 antibodies induced inflammation in both cell types via TLR2[117]. Furthermore, Liu et al. proved that targeting extracellular HSP70 ameliorates myocardial inflammation in doxorubicin-treated hearts, but no *in vivo* study has been conducted as of yet describing the role of extracellular HSP70 in the setting of MI[136]. Taken together, overexpression of HSP70 protects the heart and its resident cells from detrimental consequences following MI, but circulating HSP70 act as DAMPs to induce inflammation, worsening the consequences of MI.

In conclusion, various families of HSPs are essential to the function of the heart and its cells, especially cardiomyocytes. Overexpression of HSPs in the heart has shown to be protective because of their role in proteostasis, but exact mechanism still needs to be elucidated. However, circulating HSPs, which are released from injured cells, are known to act as pro-inflammatory activators because they induce inflammation by acting as DAMPs.

1.4 Heat Shock Factor 1 (HSF1)

1.4.1 Structure, Function, and Regulation of Heat Shock Factor 1

Heat Shock Factor 1 (HSF1), belonging to the HSF family, is a master transcription factor that orchestrates the synthesis of HSPs under stress. The main components of HSF1's structure are N-terminal helix-turn-helix DNA binding domain and the adjacent hydrophobic heptad repeats (HR A/B and HR C)[137]. In a non-stressful environment, the inactive HSF1 is found in the cytosol, bound to multi-chaperone complex of HSP90, co-chaperone p23, and immunophilin

FK506-binding protein 5[138]. Heptad repeat C allosterically inhibits trimerization of HSF1 by binding to the heptad repeat A/B. However, in the presence of stress, HSF1 is released by the multi-chaperone complex and is localized to the nucleus, where it binds to the DNA as a trimer. Trimerization is mediated by C-terminal heptad repeat (HR A/B) while the N-terminal helix-turn-helix DNA binding domain assists HSF1 to bind to the HSEs on heat shock genes, which are made of nGAAn pentamers[139]. HSF1 can be regulated in various ways. Even though it is unclear, current literature states that HSP90 and HSP70 or HSP70 and its co-chaperone, HSP40, can negatively regulate HSF1 via negative feedback loop. HSF1 can also be regulated via post-translational modifications, such as acetylation, sumolyation, and phosphorylation[140]. Moreover, pre-clinical studies have demonstrated that HSF1 can be regulated by various kinases and transcription factors, such as MAPK-ERK, GSK3β, SIRT-1, and HIF-1α[140–147]. The role of HSF1 in various disease models was further studied using *Hsf1*-knockout (*Hsf1*$^{-/-}$) mice.

1.4.2 Heat Shock Factor 1 function – insight from knockout mouse model

The creation of *Hsf1*-knockout (*Hsf1*$^{-/-}$) mice by McMillan et al. was a ground-breaking tool to study HSR in various *in vivo* disease models. Similar to other knockout animal models, there are phenotypes associated with the *Hsf1*-knockout mice model. First of all, *Hsf1*-knockout mice exhibit prenatal lethality, mostly between late mid-gestation to birth; hence, live *Hsf1*-knockout mice progeny is less than the predicted Mendelian distribution. *Hsf1*-knockout mice, that do not exhibit prenatal lethality, survive to adulthood. Interestingly, Xiao et al. demonstrated that *Hsf1*-knockout mice, generated from male 129-SvEv mouse and female 12-9SvJ mouse, significantly have lower percentage of survival in comparison to *Hsf1*-knockout mice generated from other targeted strains. Therefore, different genetic backgrounds affect the survival of *Hsf1*-knockout mice. Secondly, *Hsf1*-knockout female mice are sterile. Extensive molecular studies demonstrated that the spongiotrophoblast layer of the chorioallantoic placenta in *Hsf1*-knockout female mice is thinner than both wildtype and *Hsf1*-heterozygous mice and this observation was consistent between all *Hsf1*-knockout female mice of different genetic backgrounds. Thinner spongiotrophoblast interfered with the “normal architecture” of the embryo. Thirdly, *Hsf1*-knockout mice demonstrated postnatal growth retardation in comparison to wildtype and *Hsf1*-

heterozygous littermates, independent of sex. Finally, heat shock response is eliminated in *Hsf1*-knockout mice. Xiao et al. also showed that protein expression of HSP70, HSC70, HSP90α, HSP90β, HSP60, and HSP25 were abolished in *Hsf1*-knockout tissue (e.g. heart, brain, liver, and kidney) after heat shock but not in wildtype and *Hsf1*-heterozygous mice. Lastly but not the least, *Hsf1*-knockout mice are susceptible to endotoxin challenge, leading to significantly lower survival rate and higher TNF-α production than wildtype and *Hsf1*-heterozygous mice post-LPS administration[148,149].

1.4.3 Heat Shock Factor 1 and link with inflammation

The primary function of HSF1 is to maintain proteostasis. However, with the usage of *Hsf1*-knockout mice, ground-breaking scientific data suggested that HSF1 can modulate inflammation by controlling pro-inflammatory transcription factors and cytokines[148]. As explained in the previous section, *Hsf1*-knockout mice are susceptible to endotoxin, which led to an increase in TNF-α expression[149]. Further research revealed that promoter of TNF-α contains the binding site of HSF1, which represses its transcription. TNF-α can also inhibit the expression of HSF1 via TNF-R1 and activation of phosphatases, representing a negative feedback loop[150]. In relation, Wu et al. have shown that HSF1 attenuated cardiomyocyte death by repressing TNF-α via the suppression of NF-κB pathway[151]. In addition to TNF-α, HSF1 is found to block the transcription of IL-1β via the interaction with IL-6 transcription factor after LPS treatment[149,152]. Chen et al. have demonstrated that knocking down *Hsf1* in vascular smooth muscle cells induces inflammation via the activation of NF-κB and AP-1 transcription factors following angiotensin II treatment[153]. *Hsf1*-knockout mice have also shown to increase the activation of NF-κB via increased degradation of IkBα following endotoxin inhalation[154]. While the molecular connection between HSF1 and inflammation has been well-studied using various stress models, its role in MI is still unclear.

1.4.4 Remaining questions on the role of HSF1 in acute MI

The role of HSF1 has been extensively studied in cardiac hypertrophy but not in the setting of MI. Currently, there are three pre-clinical studies in the literature that have studied the role of

HSF1 in ischemia/reperfusion injury. The first study was by Zou et al., who demonstrated that transgenic mice overexpressing *Hsf1* had significantly better cardiac function, smaller infarct size and attenuation of cardiomyocyte apoptosis[155]. The result was further validated using primary cardiomyocytes conditioned with hyperthermia to increase HSF1 expression. It was observed that cells, preconditioned with hyperthermia, had a significant increased viability rate following oxidative stress. Yin et al., on the other hand, had shown that silencing *Hsf1* by injecting HSF1 silencer RNA (siRNA) in mice had significantly higher mortality rate due to thermal intolerance and larger infarct size following ischemia/ reperfusion injury[156]. Ma et al. took a step further to show that Granulocyte colony stimulating-factor (G-CSF) increased the association of STAT3 with HSF1, which resulted in cardioprotection post-ischemia/reperfusion injury. Moreover, Ma et al. used *Hsf1*-wildtype as their controls and considered *Hsf1*-heterozygote mice as their knockout mice[157]. Due to false assumptions and imprecise scientific tools used, there is a big gap in the understanding of HSF1's role following MI. In particular, false assumption refers to the idea that overexpression of *Hsf1* is beneficial, so *Hsf1*-knockout should be detrimental. Also, as we learned previously, the phenotype of *Hsf1*-heterozygote mice is very different than the *Hsf1*-knockout mice. Unlike previous pre-clinical studies, Vedam et al. used *Hsf1*-wildtype and *Hsf1*-knockout mice to show that *Hsf1*-knockout mice had lower mortality rate following doxorubicin treatment than *Hsf1*-wildtype mice because the accumulation of HSP25 in the *Hsf1*-wildtype mice led to the transactivation of p53, which further increased the expression of pro-apoptotic protein, Bax[158]. Therefore, there is no pre-clinical study that has used proper *Hsf1*-knockout mice to study the role of *Hsf1* and its downstream targets, HSPs, following MI injury.

1.5 Rationale, Hypothesis, and Objectives of Thesis

Inflammation response is essential to cardiac repair and remodeling following MI. However, excessive inflammation can accelerate cardiomyocyte necrosis, causing cardiac rupture. Therefore, controlling the degree of inflammation following MI is crucial to salvage the infarct heart. Emerging research indicates that extracellular HSPs are detrimental to injured heart following MI. Knowing that HSF1 controls the production of HSPs via heat shock response and there is a gap in the understanding of HSF1's role in inflammation following MI, we decided to

conduct a study using *Hsf1*-wildtype mice as controls and *Hsf1*-knockout mice to learn whether the presence of HSF1 and downstream target, HSPs, are beneficial in the setting of acute MI.

The hypothesis of the study is that genetic deletion of *Hsf1* will cause injured cells in the infarct and peri-infarct regions to release less heat shock proteins post-MI. This will lead to less activation of innate immune signaling; hence, less production of cytokines and chemokines by neighbouring cells. As a result, the presence of inflammation will be short, leading to attenuation of mortality, cardiac rupture rate, infarct size, and better cardiac function. This is balanced by the more short-term reduction in the levels of intracellular HSPs.

The following are the objectives of this study:

1. Does the deficiency of *Hsf1* improve cardiac function and reduce infarct size in the mice model of acute MI?
2. What is the effect of *Hsf1* deficiency on innate immune system in the mice model of acute MI?

2.0 Materials & Methods

2.1 Generation of *Hsf1*$^{+/+}$ and *Hsf1*$^{-/-}$ mice

Hsf1-heterozygous (*Hsf1*$^{+/-}$) female mice, with a mixed genetic background of FVB129/ C57Bl/6, were obtained from Dr. Ivor Benjamin's Lab (Medical College of Wisconsin). They were backcrossed with C57Bl/6 wildtype (*Hsf1*$^{+/+}$) mice for several generations to ensure C57Bl/6 background of *Hsf1*-knockout (*Hsf1*$^{-/-}$) mice. *Hsf1*$^{+/+}$ and *Hsf1*$^{-/-}$ mice were generated by using different breeding pairs as indicated in **Table 2**. *Hsf1*$^{-/-}$ females were not used for breeding because they were sterile. All animals were bred and handled in accordance with the animal ethics and protocols of Animal Care Veterinary Services (ACVS) of University of Ottawa (protocol# HI-1698) and the Canadian Council of Animal Care (CCAC) standards. Animals were housed in identical conditions and food and water were provided *ad libitum* at the ACVS, University of Ottawa Heart Institute (UOHI), Ottawa, ON, Canada. Tail clips were collected from mice after they were weaned. Genomic DNA was isolated from tail clips of newly weaned mice using the DNA Purification Kit (Thermo Fisher Scientific) and the presence of *Hsf1* was determined by polymerase chain reaction (using the forward and reverse primers listed in **Table 3**) and agarose gel electrophoresis.

	Female		**Male**
#1	*Hsf1*$^{+/-}$	**X**	*Hsf1*$^{-/-}$
#2			*Hsf1*$^{+/+}$
#3			*Hsf1*$^{+/-}$
#4	*Hsf1*$^{+/+}$		*Hsf1*$^{+/-}$

Table 2. Breeding pairs to generate *Hsf1*$^{+/+}$ and *Hsf1*$^{-/-}$ mice.

	Forward primer	**Reverse primer**
***Hsf1*$^{+/+}$**	5'-TCTCCTGTCCTGTGTGCCTAGC-3'	5'-CAGGTCAACTGCCTACACAGACC-3'
***Hsf1*$^{-/-}$**	5'-AGGACATAGCGTTGGCTACCCGTG-3'	5'-GCCTGCTATTGTCTTCCCAATCC-3'

Table 3. Primers for genotyping *Hsf1* mice.

2.2 *In Vivo* Myocardial Infarction Model

Eleven-to-thirteen-week-old male *Hsf1*$^{-/-}$ mice and their wildtype littermates were randomized to sham-operated or MI-operated groups. The animals were anesthetized using 2-3% isoflurane mixed with 100% oxygen. They were intubated using a small animal ventilator (Hugo Sachs Elektronik, MiniVent Ventilator for Mice - Model 845, Harvard Apparatus). A left thoracotomy was performed in the 5th intercostal space and the pericardium was opened. MI was induced by performing a permanent ligation on the left anterior descending (LAD) coronary artery, situated 1-1.5mm below the atrial appendage, using a 7-0 silk suture (protocol# HI-2466, approved by ACVS of University of Ottawa). For a sham operation, the left thoracotomy in the 5th intercostal space was performed but with no ligation. All the surgeries were performed by the same technician blinded to the study. However, the initial survival study was done with larger MI generation with ligature in LAD located higher[159], shown in Section 3.1 **(Figure 8)**. Subsequent studies were done with smaller MI to avoid survival bias in tissue harvesting and analysis. Animals were euthanized for sample collection and the body weight was measured. After euthanasia, the heart weight and lung weight were measured and normalized to tibia length. Tibia length is a good comparator than body weight because it is more consistent between mice[160]. The ratio of heart weight to tibia length and lung weight to tibia length are plotted in Section 3.2 **(Figure 9)**. Blood and following organs were collected as part of sample collection: heart, lung, liver, and spleen. Collected organs were washed in cold 1X Phosphate Buffered Saline (PBS), quickly dried on the paper towel, weighed, and then they were snap-frozen in liquid nitrogen. Hearts were divided into infarct, peri-infarct, and non-infarct regions before they were snap-frozen. The organs and serum were stored in -80°C for further molecular studies. Animals that died before the end-of-study (3, 7, and 28 days post-MI) were censored from the study. Following MI operation, 7 in 26 *Hsf1*$^{+/+}$ mice died (3 died due to cardiac rupture, 2 died due to fighting with cage mates, and 2 died to unknown reason) and one in 28 *Hsf1*$^{-/-}$ mice died (due to cardiac rupture) before the end-of-study.

2.3 Echocardiography

At the end of the study (3, 7, and 28 days post-MI), cardiac function parameters were assessed by echocardiography using Vevo Imaging system. Animals were anesthetized using 2-3% isoflurane mixed with 100% oxygen. Echocardiography was performed by both parasternal long-axis (EKV-mode) and short-axis (B-mode and M-mode) views of LV using Vevo 3100 system and its MX550D transducer scanhead probe (FUJIFILM Visual Sonics). Tracings were performed using the Vevo Lab software, supplied by the manufacturer. Left ventricle ejection fraction (LVEF) was determined using tracings of the parasternal long axis (EKV-mode) of LV while fractional shortening (FS) were determined using tracings generated from the short axis view of LV (M-mode). LVEF and FS are plotted in Section 3.3 **(Figure 10)**.

2.4 Cardiac Histology

Hearts collected at day 3 and 7 post-MI were processed to determine cardiac structure by histology. Hearts were first washed in cold 1X PBS to remove blood residues, quickly dried on the paper towel, and then weighed. The hearts were then placed in cold 1M KCl (Thermo Fisher Scientific) solution for 5 minutes to achieve uniform diastolic cardiac arrest. After 5 minutes, the hearts were quickly washed in 1X PBS (Thermo Fisher Scientific) solution and then fixed in neutral buffered 10% Formalin (Thermo Fisher Scientific) for 48 hours at 4°C and then washed with 1X PBS for 48 hours at 4°C, and finally washed in water for 48 hours at 4°C. The atria were separated from the ventricles and discarded before the ventricles were embedded in paraffin. The ventricles were sectioned (5µm) at the papillary muscle level and the slides were stored at room temperature (RT) for further experimentation. Immune cell recruitment was analyzed at day 3 and 7 post surgery using Hematoxylin and Eosin Y (HE) (Sigma-Aldrich) stain, as shown in **Supplementary Figures S2 & S3**, respectively. The blue-purple stained for nuclei and the pink stained for cytoplasm and extracellular matrix. Furthermore, Picro Sirius Red (PSR) stain (Picric acid – Sigma-Aldrich and Direct red 80 – Sigma-Aldrich) was used to assess collagen deposition and extent of fibrosis in the day 7 post-MI heart, as shown in **Figures 11C, 11D, & S4**. The yellow-orange dye of PSR stained for cytoplasm and the red dye stained for collagen. Infarct size was determined using Masson Trichrome (MTC) (Sigma-Aldrich) at day 7 post-MI, as shown in **Figures**

11A & S5. The red dye of MTC stained for muscle and cytoplasm while the blue dye stained for collagen. The stained sections were mounted in permount solution (Thermo Fisher Scientific), captured with Lecia Aperio Versa 8 (Leica Biosystems Imaging) and then analyzed using the Image Scope software (supplied by Leica).

2.4.1. Infarct Size Calculation

ImageJ software (National Institutes of Health) was used to trace and measure infarct length and circumference of LV sections stained with MTC. According to Takagawa et al., infarct size was calculated based on the following equation[161]:

$$Infarct\ size\ (\%) = \frac{Mid-line\ infarct\ length}{Mid-line\ circumference}\ x\ 100\%$$

The changes in infarct size between *Hsf1*$^{+/+}$ and *Hsf1*$^{-/-}$ mice post-MI is plotted in **Figure 11B**.

2.5 Quantitative Reverse Transcription Polymerase Chain Reaction (RT-qPCR)

Gene expression of heat shock proteins, pro-inflammatory cytokines (e.g. *Il6, Tnfa*, and *Il1b*) and chemokines (*Cxcl1, Ccl2, Cxcl10*) were determined from the RNA extracted from peri-infarct regions of *Hsf1*$^{+/+}$ and *Hsf1*$^{-/-}$ hearts 3 and 7 days post-MI using TRIzol (Thermo Fisher Scientific) according to the manufacturer's protocol. The concentration of the RNA was measured using NanoDrop Spectrophotometer (Thermo Fisher Scientific). 1000ng of RNA was reverse transcribed to produce cDNA using All-In-One 5X RT Master Mix (Abm). Target gene specific forward and reverse primers, that are indicated in **Table 4**, were designed using primer3 and BLAST tool (NCBI, USA). To minimize the effect of genomic DNA contamination, if possible, the designed primer pair are always separated by at least one intron on the corresponding genomic DNA. BrightGreen 2x qPCR MasterMix (Abm), qPCR primers, and diluted cDNA, were used to perform qPCR. qPCR was quantified using LightCycler96 (Roche Applied Science) and the software provided by the manufacturer. All reactions were run in triplicates. Gene expression was normalized to hypoxanthine-guanine phosphoribosyltransferase 1 (*Hprt1*) housekeeping gene and plotted in **Figures 12, 15, 18, & 20**.

	Forward primer	Reverse primer
Hsf1	5'-CCCTATGGACACAACCGGAG-3'	5'-GTCACCGAGGGGCTGAAC-3'
Hprt1	5'-CAAGCTTGCTGGTGAAAAGGA-3'	5'-TGAAGTACTCATTATAGTCAAGGGGATATC-3'
Hsp90	5'-GGAAACCCAGACCCAAGACC-3'	5'-GTCCGTCAGGCTCTCGTAAC-3'
Hsp70	5'-ACTGGATCGAAGGCGTAGAGA-3'	5'-CTGGTTCTTGGCAGCGTCT-3'
Il6	5'-CTGCAAGAGACTTCCATCCAG-3'	5'-AGTGGTATAGACAGGTCTGTTGG-3'
Tnfa	5'-CCCTCACACTCAGATCATCT-3'	5'-GCTACGACGTGGGCTACAG-3'
Il1b	5'-GAAATGCCACCTTTTGACAGTG-3'	5'-TGGATGCTCTCATCAGGACAC-3'
Cxcl1	5'-AGCCACCCGCTCGCTTCTCT-3'	5'-ACAGCGCAGCTCATTGGCGA-3'
Cxcl10	5'-GCGATGGATGGACAGCAGAGAGC-3'	5'-GACCACGGCTGGTCACCTTTCAG-3'
Ccl2	5'-GCTGGAGCATCCACGTGTTG-3'	5'-CTGCTGCTGGTGATCCTCTTGT-3'

Table 4. Primer sequences used for RT-qPCR.

2.6 Immunoblotting

Expression of proteins related to the HSR and signaling pathways was determined from the peri-infarct regions of *Hsf1*$^{+/+}$ and *Hsf1*$^{-/-}$ hearts 3 days post-MI using immunoblotting. The peri-infarct tissue was homogenized in the Pro-Prep protein extraction buffer (Intro Biotechnology). Bradford assay (Bio-Rad Laboratories) was performed according to manufacturer's protocol for protein quantification. Equal amount of protein (~10μg) was loaded on NuPAGE 4-12% Bis-Tris Mini Protein gel (Thermo Fisher Scientific) with BluElf Protein Ladder (Frogga Bio). The proteins were separated by electrophoresis using Mini Gel Tank apparatus and 1X NuPAGE MES SDS Running buffer (Thermo Fisher Scientific). After gel electrophoresis, the separated proteins on the gel were transferred onto the Immunoblot PVDF membrane (Bio-Rad Laboratories) using Mini Gel Tank apparatus and 1X Bolt Transfer Buffer (Thermo Fisher Scientific). The PVDF membrane was blocked with 1% BSA in PBST solution for at least 30 minutes at RT and then incubated in the following diluted primary antibodies (1:1000): HSF1 (Cell Signaling Technology), HSP90 (Abcam), HSP70 (Abcam), HSP25 (Enzo Life Sciences), phosphorylated p44/42 (ERK1/2) MAPK (Cell Signaling Technology) and total p44/42 (ERK1/2) MAPK (Cell Signaling Technology), phosphorylated NF-κB p65 (Cell Signaling Technology) and total NF-κB p65 (Cell Signaling Technology), GAPDH (Thermo Fisher Scientific) or vinculin (Sigma-Aldrich) at 4°C for 16 hours. The membrane was then washed with 1X PBST for three times at RT, each time for 10 minutes to remove unbound antibody and incubated with an appropriate

secondary antibody conjugated with horseradish peroxidase (HRP) for one hour at RT. Unbound secondary antibody was removed by washing the membrane with 1X PBST for three times at RT, each time for 10 minutes. Protein of interest was probed using a SuperSignal West Pico PLUS chemiluminescent substrate (Thermo Fisher Scientific) and detected using ChemiDoc XRS+ System and its Image Lab software (Bio-Rad Laboratories). The bands of the protein interest were quantified and analyzed using Image Lab and Microsoft Excel software. Protein expression from each membrane was normalized to loading control, which was either GAPDH or vinculin expression, on that same membrane and plotted on **Figures 13, 16, & 19**.

2.7 Flow Cytometry

Cells were suspended from the peri-infarct region of *Hsf1*$^{+/+}$ and *Hsf1*$^{-/-}$ hearts collected at day 3 post-MI. Heart tissues were collected in ice-cold 1X PBS, transferred to a digestion cocktail containing 100 units (U)/mL each of Collagenase Type I, Collagenase Type II and Collagenase D (Worthington Laboratories) supplemented with 25U/ mL DNase 1 (Thermo Fisher), 5nM EDTA, 2.5mM $MgCl_2$ and 2.5mM KCl buffered in 10mM sodium bicarbonate containing PBS. Tissue pieces were finely minced using fine-tipped scissors and the mixture was incubated at 37°C with constant shaking for an hour. Digested cells were filtered by gravity in 1X PBS through 40µm nylon strainers, a small aliquot (approximately 10µL) was reserved for cell counting by hemocytometer, and the remainder was centrifuged at 2000 RPM for 10 minutes at 4°C. Pelleted cells were washed in 1X PBS, and 2 million cells per isolated sample were transferred to 5mL round-bottomed polystyrene test tubes for flow cytometry staining. The cells were stained on ice and protected from light for 60 minutes with a cocktail of the following surface-targeted antibodies, diluted in PBS supplemented with 1% (volume to volume) bovine serum albumin, to characterize cell populations: phycoerithryn (PE)-conjugated anti-Ly6G (anti-neutrophil marker, 1:250 dilution, BD Biosciences); allophycocyanin (APC)-conjugated anti-F4/80 (anti-macrophage marker, 1:250 dilution, BD Biosciences); Brilliant Violet (BV) 421-conjugated anti-Ly6C (anti-monocyte marker, 1:250 dilution, BioLegend); Alexfluor-488-conjugated anti-CD45 (anti-hematopoietic (immune) marker, 1:250 dilution, BD Biosciences); and allophycocyanin/Cy-7 (APC-Cy7)-conjugated anti-CD11b (myeloid differentiation marker, 1:250 dilution, BD

Biosciences). At the conclusion of staining incubations, cells were washed with 1X PBS and centrifuged at 2000 RPM for 5 minutes. The supernatant was discarded, and the cell pellet was then resuspended in PBS supplemented with 1% BSA. Cell populations were resolved using a BD FACS Aria III cell sorter/cytometer (BD Biosciences), and data were analyzed using FACSDiva software (Version 8) (BD Biosciences), according to consensus phenotypic gating and cell identification protocols. Cell quantitation data presented in Section 3.7 **(Figure 14)** were plotted as neutrophils, macrophages, and Ly6C^{high} or Ly6C^{low} monocytes, respectively, per isolated left ventricular peri-infarcted tissue region.

2.8 Enzyme-linked Immunosorbent Assay (ELISA)

Blood samples were collected via cardiac puncture from mice 3 days post-sham and MI operation. The blood samples were then spun in 4°C centrifuge for 20 minutes at 1500 x g. Serum was collected and stored in -80°C. Serum samples were thawed, and IL-6 concentration was determined using IL-6 Mouse Simple Step ELISA kit (Abcam). Samples were diluted two-fold with sample diluent NS solution (provided in the kit) and IL-6 concentration was determined in accordance with manufacturer's instructions. IL-6 concentration was quantified by measuring absorbance at 450nm using Synergy Mx plate-reader (BioTek Instruments). IL-6 levels in the samples were determined by extrapolating from known standard value. The values were then analyzed and plotted, as shown in Section 3.10 **(Figure 17)**, using Microsoft Excel (Microsoft Corporation) and GraphPad Prism 8 (GraphPad) software, respectively.

2.9 Statistical Analysis

GraphPad Prism 8.0 software was used for statistical analysis. All values were represented as mean ± standard error of mean (SEM). All data excluding cardiac histology were analyzed using Two-way Analysis of Variance (ANOVA) followed by Tukey's multiple comparison test to compare between the four treatment groups. The Grubb's test was performed to determine outliers. Infarct size and cardiac rupture rate were analyzed using unpaired t-test. n, represents sample number. Data were considered significant a priori if *p value was less than 0.05.

3.0 Results

3.1 *Hsf1* Knockout results in improved survival rate and reduced cardiac rupture rate post-MI.

Male *Hsf1*$^{+/+}$ and *Hsf1*$^{-/-}$ mice, eleven to thirteen-week-old, were randomly subjected to either LAD coronary artery ligation (MI) or sham-operation to determine if knocking out *Hsf1* was beneficial or detrimental in the setting of MI. All animals that received sham operation survived throughout the study **(Figure 8A)**. Survival was 74% in *Hsf1*$^{-/-}$ mice compared to 34% in *Hsf1*$^{+/+}$ mice at 28 days post-MI, representing 40% higher survival in *Hsf1*$^{-/-}$ mice than *Hsf1*$^{+/+}$ mice **(Figure 8A)**. This was accompanied by a significant reduction in cardiac rupture rate in *Hsf1*$^{-/-}$ mice (35% ± 3.6) than *Hsf1*$^{+/+}$ mice (60% ± 3.5) post-MI **(Figure 8B)**.

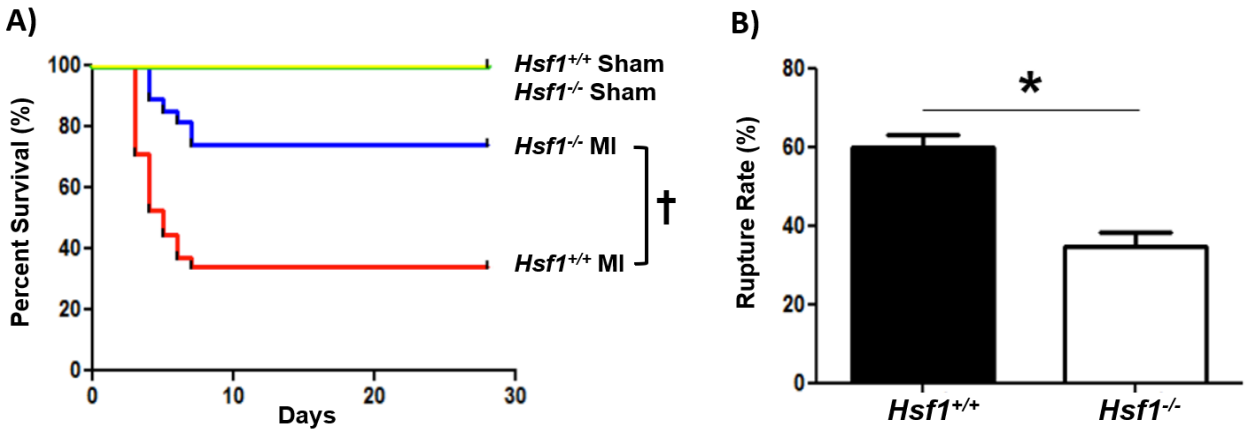

Figure 8. Percent survival and cardiac rupture rate of *Hsf1*$^{+/+}$ and *Hsf1*$^{-/-}$ mice post-MI. A) Kaplan-Meier survival analysis of *Hsf1*$^{+/+}$ and *Hsf1*$^{-/-}$ mice after sham and MI operation. n = 8 (*Hsf1*$^{+/+}$ Sham), n = 8 (*Hsf1*$^{-/-}$ Sham), n = 39 (*Hsf1*$^{+/+}$ MI), n = 27 (*Hsf1*$^{-/-}$ MI). †p<0.001. **B)** The frequency of mortality due to cardiac rupture in *Hsf1*$^{+/+}$ and *Hsf1*$^{-/-}$ mice post-MI. Statistical comparison was performed with the use of unpaired t-test. Values are mean ± SEM, *p<0.05.

3.2 Heart and lung weights of *Hsf1*$^{+/+}$ and *Hsf1*$^{-/-}$ mice on days 3, 7, & 28 post-MI.

Heart and lung weights are commonly used to assess the severity of MI[162]. Therefore, heart and lung weights were measured and normalized to tibia length, a better comparator than body weight[160,163]. The heart weight to tibia length ratio remained consistent between *Hsf1*$^{+/+}$ and *Hsf1*$^{-/-}$ sham-operated hearts **(Figures 9A-C)**. There was no significant difference in the heart weight to tibia length ratio between *Hsf1*$^{+/+}$ sham and MI hearts following 3 days of operation **(Figure 9A)**. After 7 days of operation, the heart weight to tibia length ratio of *Hsf1*$^{+/+}$ and *Hsf1*$^{-/-}$ MI hearts were significantly higher than their sham counterpart **(Figure 9B)**. There was no significant difference in the heart weight to tibia length ratio between the four treatment groups at 28 days post-MI **(Figure 9C)** and between *Hsf1*$^{+/+}$ and *Hsf1*$^{-/-}$ MI-operated hearts at each of the three time points **(Figures 9A-C)**. Therefore, Figures 9A-C suggest that there was no change in cardiac hypertrophy between *Hsf1*$^{+/+}$ and *Hsf1*$^{-/-}$ hearts post-MI. On the other hand, the lung weight to tibia length ratio remained consistent between *Hsf1*$^{+/+}$ and *Hsf1*$^{-/-}$ sham-operated hearts **(Figures 9D-F)**. Although there was no significant difference in lung weight to tibia length ratio between sham and MI hearts at 3- and 28-days post-operation **(Figures 9D & F, respectively)**, the lung weight to tibia length ratio of *Hsf1*$^{-/-}$ lungs following day 7 MI was significantly higher than the lungs from other treatment groups **(Figure 9E)**. Therefore, Figures 9D-F suggest the potential occurrence of pulmonary congestion in *Hsf1*$^{-/-}$ lungs following day 7 MI.

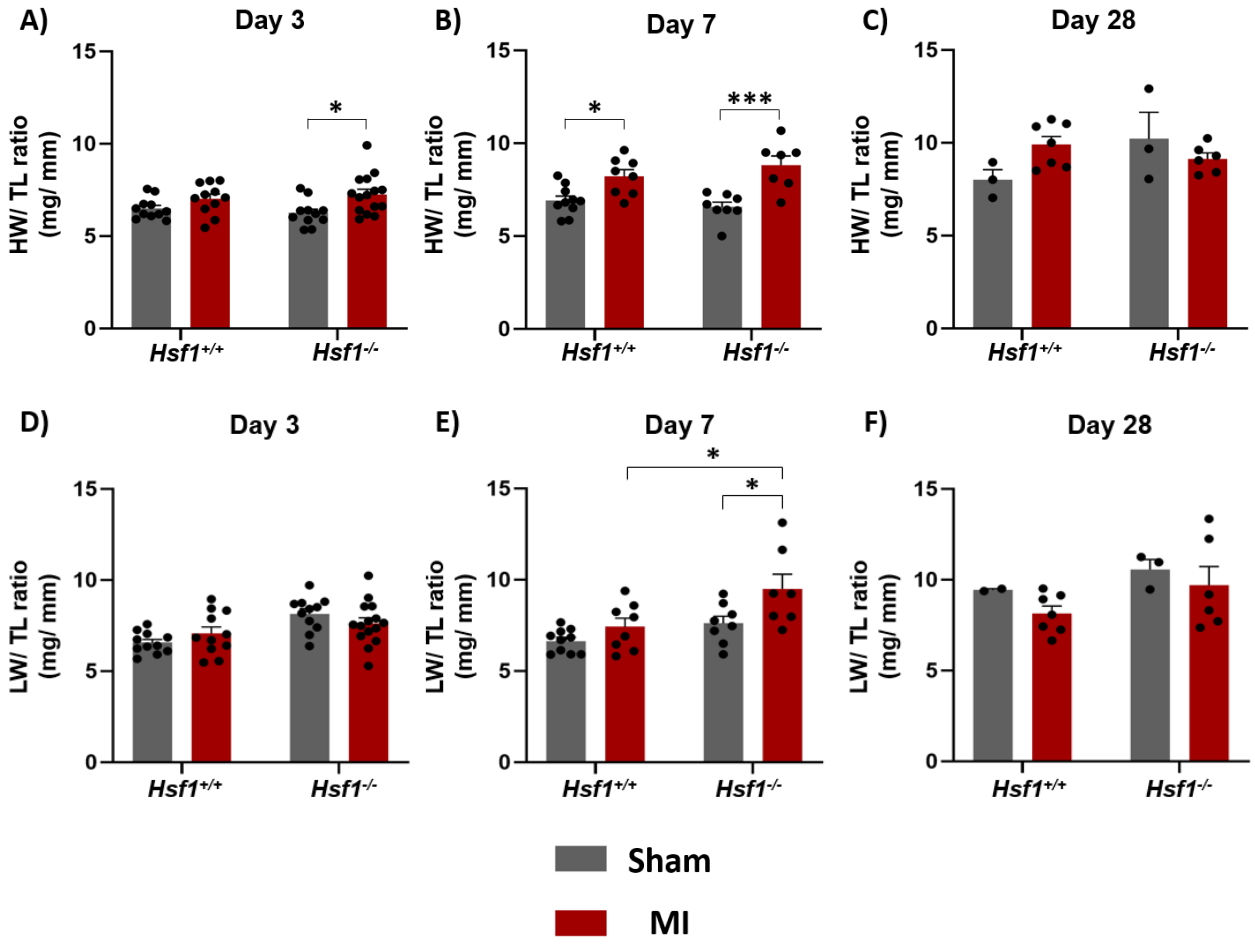

Figure 9. Time course of changes in heart and lung weights to tibia length following MI. A-C) Heart weight (HW) to Tibia length (TL) ratios of *Hsf1*$^{+/+}$ and *Hsf1*$^{-/-}$ hearts 3, 7, and 28 days post-sham and MI operation. n = 11-15 (Day 3 study), n = 7-10 (Day 7 study), and n = 3-7 (Day 28 study) (per treatment group). **D-F)** Lung weight (LW) to Tibia length (TL) ratios of *Hsf1*$^{+/+}$ and *Hsf1*$^{-/-}$ lungs 3, 7, and 28 days post-sham and MI operation. n = 11-15 (Day 3 study), n = 8-10 (Day 7 study), and n = 2-7 (Day 28 study) (per treatment group). Statistical comparison was performed with the use of Two-way ANOVA with Tukey's multiple comparison test. Values are mean ± SEM, *p<0.05, ***p<0.001.

3.3 Cardiac function of *Hsf1*$^{+/+}$ and *Hsf1*$^{-/-}$ mice post-MI.

LV dysfunction is an important consequence of MI. Many cardiac function parameters are measured by echocardiography, but most common are Left Ventricle Ejection Fraction (LVEF) and Fractional Shortening (FS)[164,165]. Therefore, echocardiography was performed to evaluate the cardiac function of *Hsf1*$^{+/+}$ and *Hsf1*$^{-/-}$ mice at 3, 7, and 28 days post-operation. It was revealed that both LVEF and FS remained consistent between *Hsf1*$^{+/+}$ and *Hsf1*$^{-/-}$ sham-operated hearts **(Figures 10A-F)**. Both *Hsf1*$^{+/+}$ and *Hsf1*$^{-/-}$ MI-operated hearts had significantly lower LVEF compared to their sham counterpart at 3, 7, and 28-days after operation **(Figures 10A-C)**. On the other hand, there was no significant difference in FS between sham- and MI-operated hearts at 3, 7, and 28 days following operation **(Figures 10D-F)**.

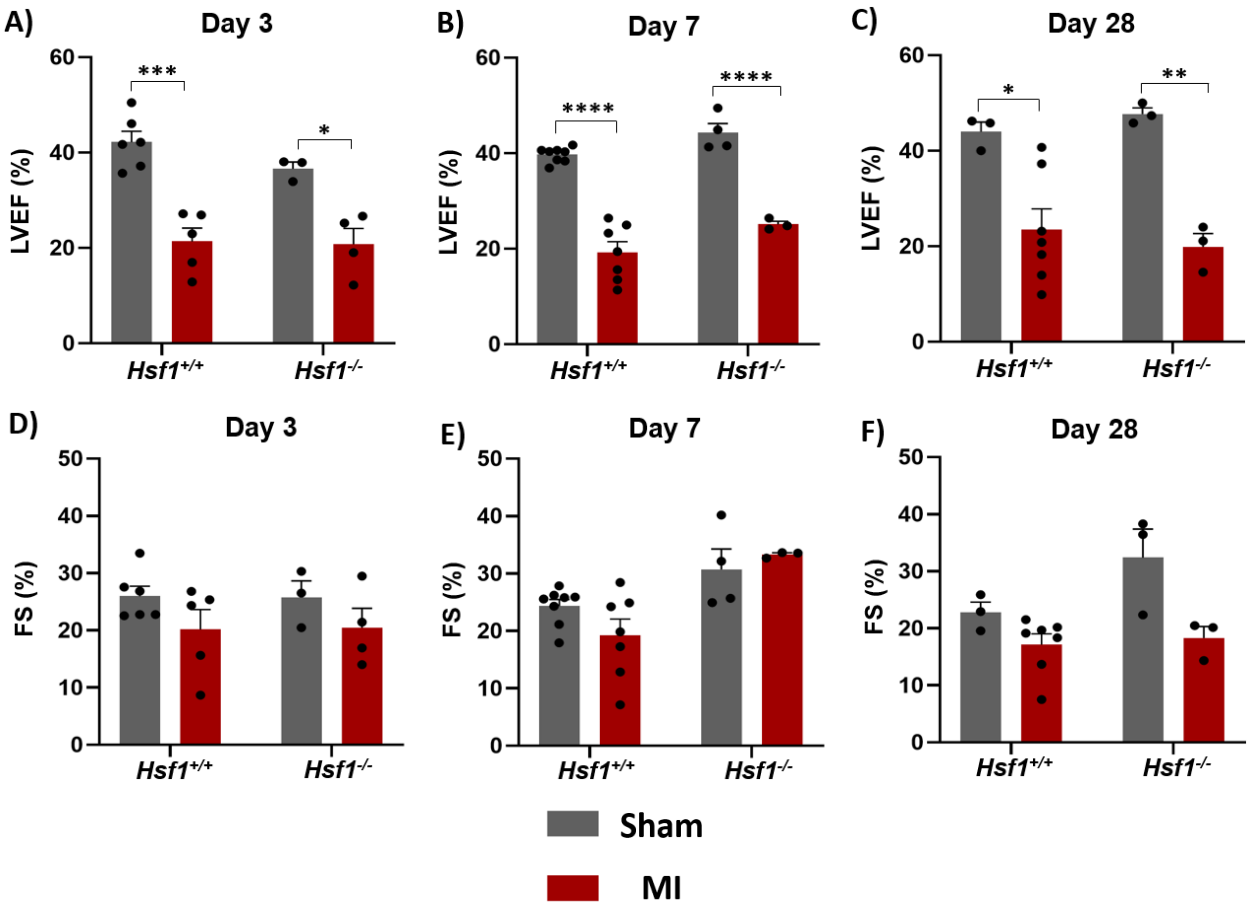

Figure 10. Echocardiography data of *Hsf1*$^{+/+}$ and *Hsf1*$^{-/-}$ mice at various time points post-MI. A-C) LVEF of *Hsf1*$^{+/+}$ and *Hsf1*$^{-/-}$ hearts 3, 7, and 28 days post-sham and MI operation. **D-F)** FS of *Hsf1*$^{+/+}$ and *Hsf1*$^{-/-}$ hearts 3, 7, and 28 days post-sham and MI operation. Statistical comparison was performed with the use of Two-way ANOVA with Tukey's multiple comparison test. n = 3-6 (Day 3 study), n = 3-8 (Day 7 study), and n = 3 (Day 28 study) (per treatment group). Values are mean ± SEM, *p<0.05, **p<0.01, ***p<0.001, **** p<0.0001.

3.4 Loss of *Hsf1* leads to smaller infarct size and less collagen deposition 7 days post-MI.

Heart injury following MI leads to myocardial cell death and subsequent replacement with collagen/ matrix deposition in the form of scar, and this indirectly reflects the magnitude of cardiac damage. LV tissue cross-sections of $Hsf1^{+/+}$ and $Hsf1^{-/-}$ hearts, collected 7 days post-operation, were stained with MTC and PSR to quantify infarct size and assess collagen deposition, respectively. Both $Hsf1^{+/+}$ and $Hsf1^{-/-}$ sham-operated LV tissue sections showed no scar **(Figures 11A, C, D, S4, S5)**. As evident in Figures 11A and B, the infarct size was reduced by 13% in $Hsf1^{-/-}$ LV tissue sections than in $Hsf1^{+/+}$ LV tissue sections post-MI **(Figures 11A, B, S5)**. This result was validated via PSR-stained sections in Figure 11C, where $Hsf1^{+/+}$ LV tissue sections had more expansive collagen deposition along its thin LV wall, suggesting that $Hsf1^{+/+}$ hearts had larger size of MI and scar formation, compared to $Hsf1^{-/-}$ LV tissue sections with smaller collagen deposition at the infarct region and thicker LV wall post-MI **(Figures 11C & S4)**. Microscopically, more collagen deposition, representing interstitial fibrosis, occurred at the infarct region than peri-infarct region of both $Hsf1^{+/+}$ and $Hsf1^{-/-}$ LV tissue sections **(Figure 11D)**. Overall, knockout of *Hsf1* leads to smaller infarct size and less collagen deposition in hearts 7 days post-MI, suggesting that $Hsf1^{-/-}$ hearts experience less cardiomyocyte necrosis post-MI.

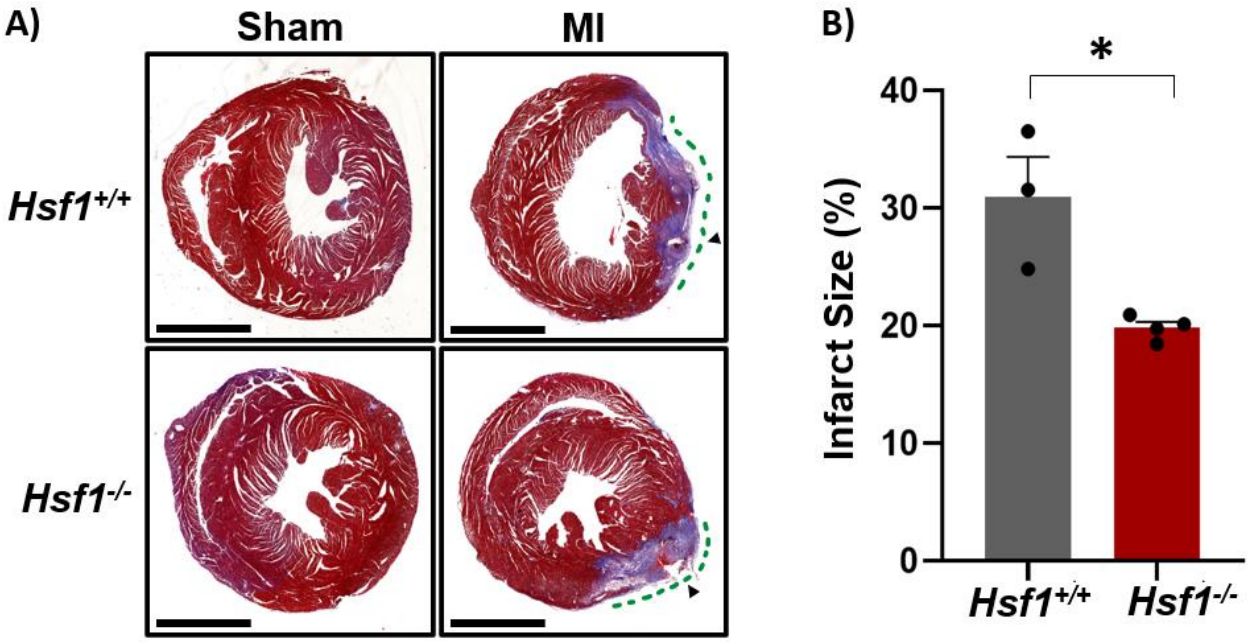

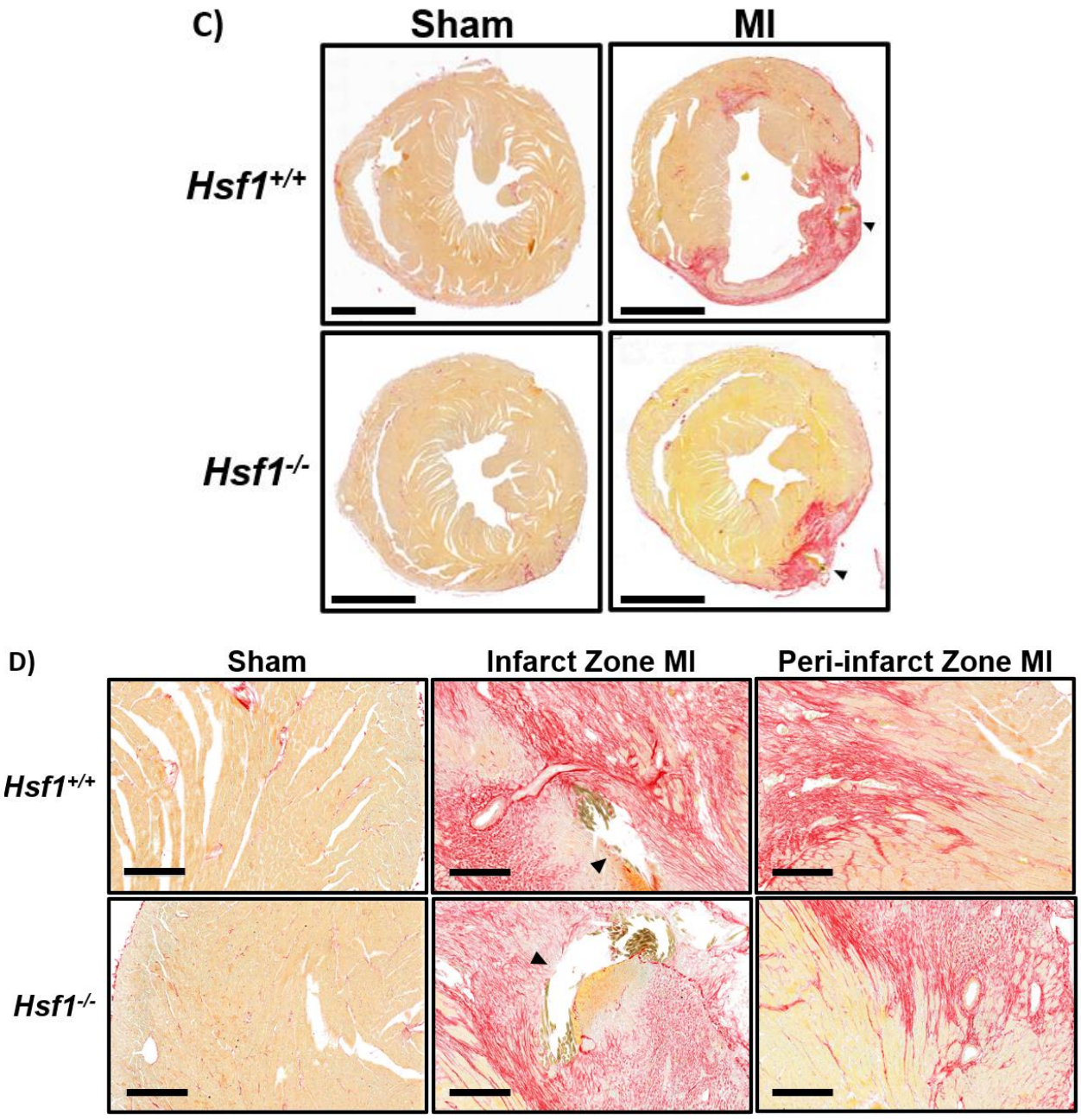

Figure 11. Assessment of infarct size and collagen deposition of *Hsf1*$^{+/+}$ and *Hsf1*$^{-/-}$ LV tissue sections after day 7 MI. A) Representative images (1.2X) of LV tissue sections from *Hsf1*$^{+/+}$ and *Hsf1*$^{-/-}$ hearts stained with MTC to illustrate infarct size in treatment groups. Scale bar = 2mm. **B)** Infarct size quantification of *Hsf1*$^{+/+}$ and *Hsf1*$^{-/-}$ LV tissue sections stained with MTC. Statistical comparison was performed with the use of unpaired t-test. n = 3-4 (per treatment group). Values are mean ± SEM, *p<0.05. **C)** 1.2X of LV tissue sections stained with PSR. Bar = 2mm. **D)** Photomicrographs (10.2X) of LV tissues sections stained with PSR. Enhanced deposition of collagen can be seen in infarct and peri-infarct regions compared with sham sections. Bar = 200µm. n = 3-4 (per treatment group). The site of LAD ligation is evident by the presence of nylon fibers within the ventricle tissue (arrows).

3.5 Heat shock gene expression levels not significantly changed at 3 days post-MI.

The next step was to assess the changes in the heat shock response (HSR) at the myocardial gene expression level in *Hsf1*$^{+/+}$ and *Hsf1*$^{-/-}$ hearts post-operation. Hence, the transcriptional changes of the genes involved in HSR, such as *Hsf1*, *Hsp90*, and *Hsp70*, were assessed in the peri-infarct region of *Hsf1*$^{+/+}$ and *Hsf1*$^{-/-}$ hearts 3 days post-MI. *Hsf1* mRNA was significantly reduced in *Hsf1*$^{-/-}$ mice **(Figure 12A)**. On the other hand, there was no significant difference in *Hsp70* and *Hsp90* gene expression between sham and MI group regardless of genotype at day 3 post-MI, indicating that heat shock gene expression level does not significantly change at day 3 post-MI **(Figures 12B & C)**.

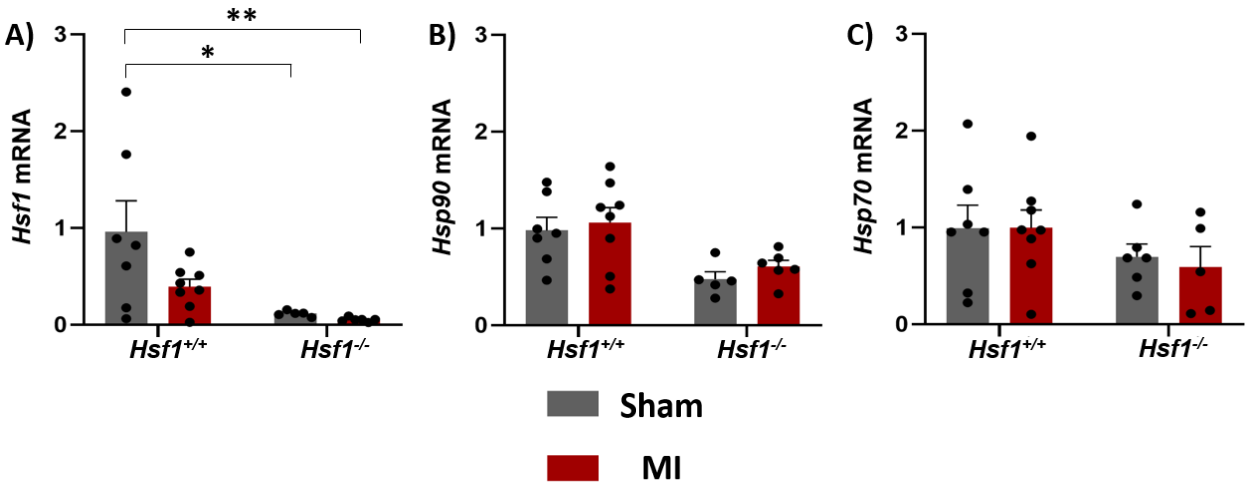

Figure 12. Changes of heat shock response at the myocardial gene level in *Hsf1*$^{+/+}$ and *Hsf1*$^{-/-}$ hearts 3 days post-MI. mRNA expression of **A)** *Hsf1*, **B)** *Hsp90* and **C)** *Hsp70* in the peri-infarct region of *Hsf1*$^{+/+}$ and *Hsf1*$^{-/-}$ hearts 3 days post-MI. mRNA expression was normalized to *Hprt1*. n = 5-8 (per treatment group). Statistical comparison was performed with use of Two-way ANOVA with Tukey's multiple comparison test. Values are mean ± SEM, *p<0.05, **p<0.01.

3.6 Loss of *Hsf1* decreases heat shock protein level 3 days post-MI.

After assessing the mRNA expression of genes involved in HSR, the next step was to assess the changes of HSR at the myocardial protein level. Hence, expression of proteins involved in HSR, such as HSF1, HSP90, HSP70, and HSP25, was assessed in the peri-infarct region of $Hsf1^{+/+}$ and $Hsf1^{-/-}$ hearts 3 days post-MI via immunoblotting. Total HSF1 antibody was validated using experimental controls **(Figure S6)**. HSF1 expression was undetectable in $Hsf1^{-/-}$ hearts in comparison to $Hsf1^{+/+}$ hearts post-sham and MI operation. However, there was no significant difference in HSF1 expression between $Hsf1^{+/+}$ sham and MI-operated hearts (**Figures 13A & B)**. Similarly, there was no significant difference in the protein expression of HSP90, HSP70, and HSP25 between $Hsf1^{+/+}$ and $Hsf1^{-/-}$ sham-operated hearts **(Figures 13A, C-E)**. Moreover, the expression of the molecular chaperones was significantly upregulated in $Hsf1^{+/+}$ hearts post-MI, but in the $Hsf1^{-/-}$ hearts, the expression was significantly downregulated post-MI **(Figures 13A, C-E)**. Therefore, Figure 13 suggests that heat shock response is significantly down-regulated at the myocardial protein level in $Hsf1^{-/-}$ hearts post- MI operation.

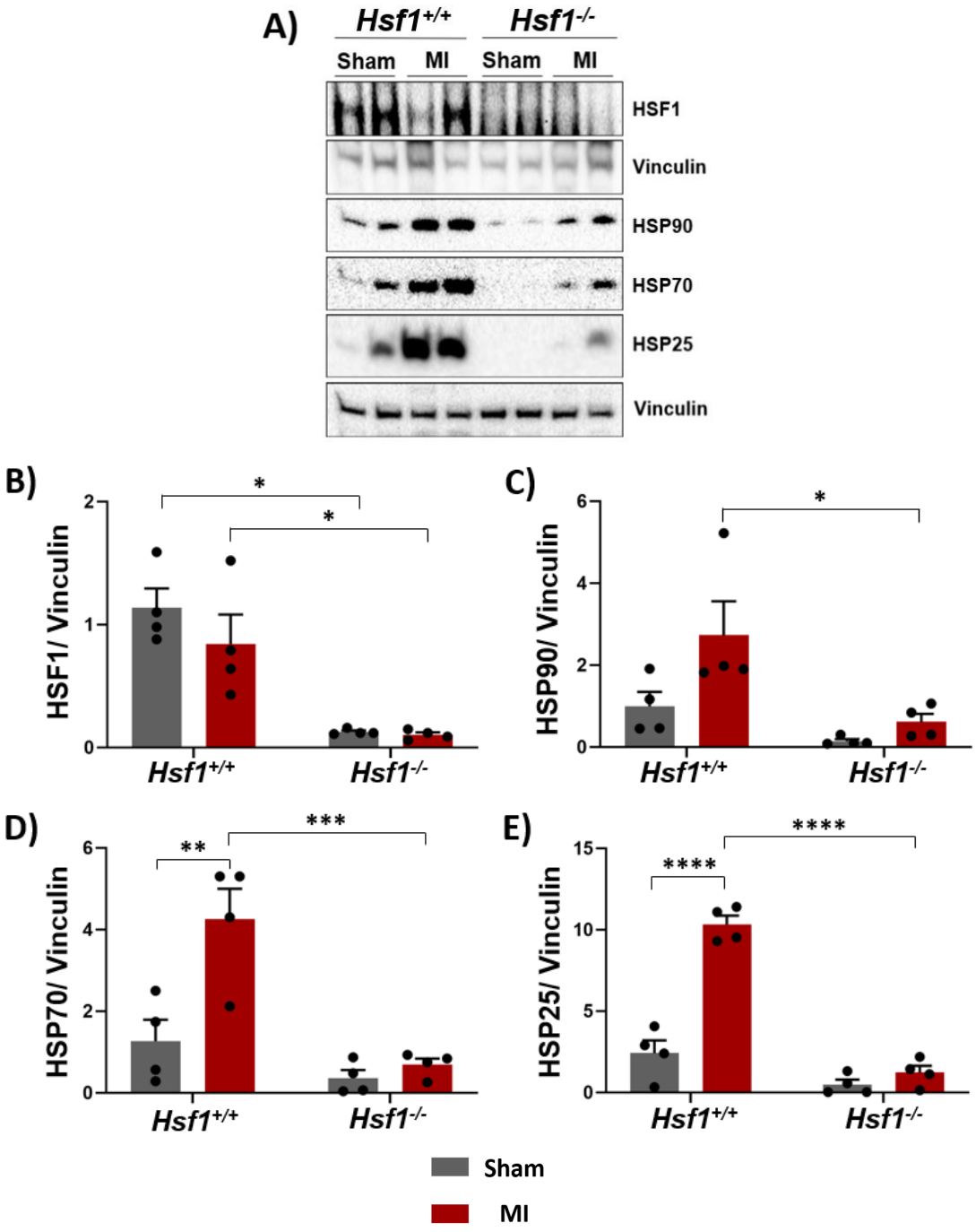

Figure 13. Changes in heat shock response at the myocardial protein level in *Hsf1*$^{+/+}$ and *Hsf1*$^{-/-}$ hearts 3 days post-MI. Protein expression of HSF1, HSP90, HSP70, and HSP25 was assessed in the peri-infarct region of *Hsf1*$^{+/+}$ and *Hsf1*$^{-/-}$ hearts following 3 days of sham and MI operation via immunoblotting. **A)** Representative immunoblots of HSF1, HSP90, HSP70, HSP25, and vinculin. Quantification of **B)** HSF1, **C)** HSP90, **D)** HSP70, and **E)** HSP25 was represented and their expression was normalized to vinculin. Statistical comparison was performed with use of Two-way ANOVA with Tukey's multiple comparison test. n = 4 (per treatment group). Values are mean ± SEM, *p<0.05, **p<0.01, ***p<0.001, **** p<0.0001.

3.7 Recruitment of neutrophils, macrophages and monocytes are consistent between the myocardium of *Hsf1*$^{+/+}$ and *Hsf1*$^{-/-}$ hearts post-MI.

Because we observed significant injury effect at acute timepoints post-MI **(Figure 8)**, we focused upon populations of known early acting immune cells, including neutrophils, macrophages, and monocytes[98,99]. Following sham- and MI-operation, there was no significant difference in the heart-trafficking neutrophils, Ly6C^{high} and Ly6C^{low} monocytes, and macrophages between *Hsf1*$^{+/+}$ and *Hsf1*$^{-/-}$ hearts **(Figures 14A-D)**. While larger group analyses may have indicated a reduced inflammatory response in *Hsf1*$^{-/-}$ hearts following MI, our available data suggest that the loss of *Hsf1* does not affect the recruitment of immune cells into the infarcted myocardium.

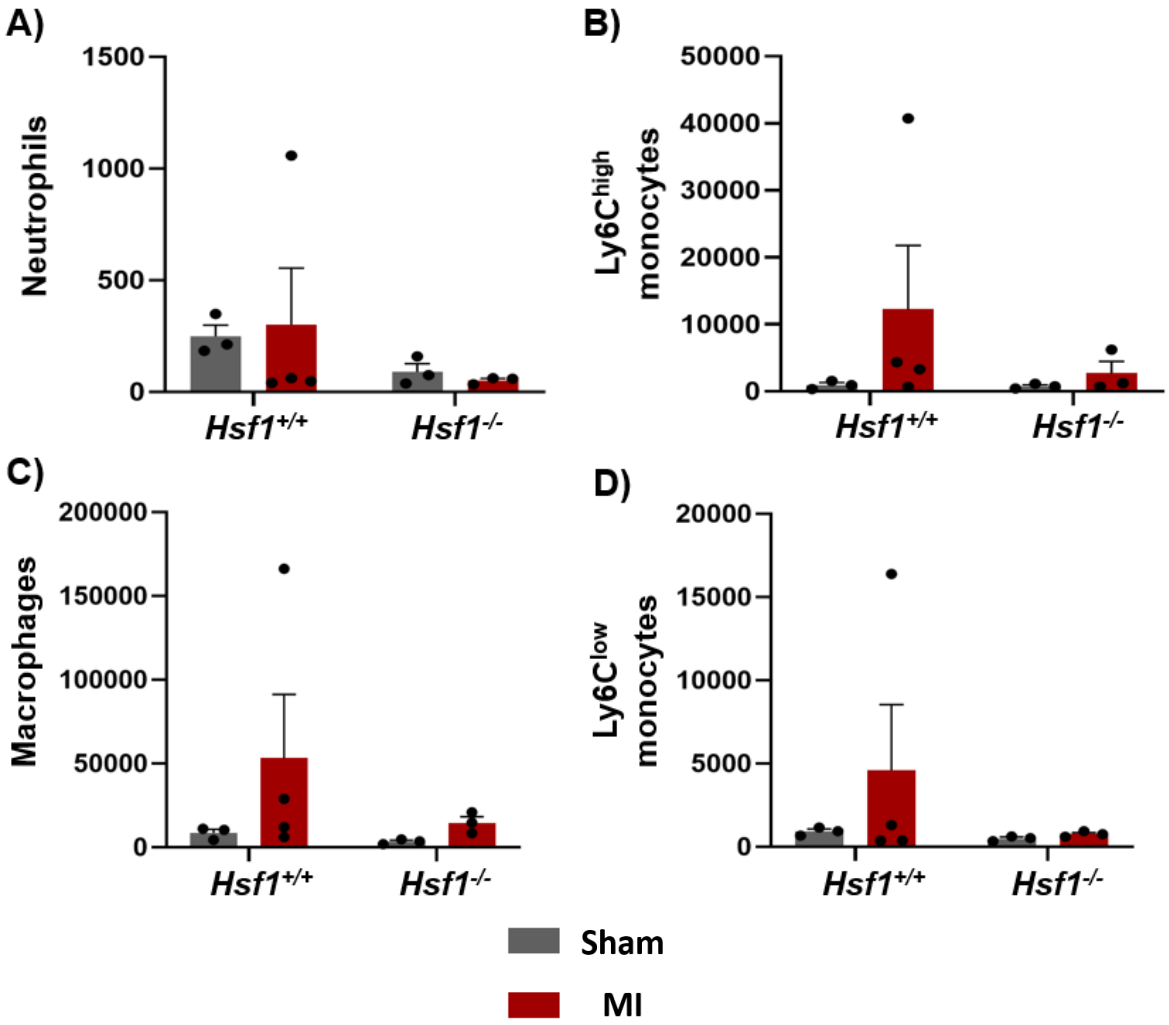

Figure 14. Quantification of neutrophils, macrophages, and monocytes in the myocardium of *Hsf1*$^{+/+}$ and *Hsf1*$^{-/-}$ hearts 3 days post-MI. Flow cytometric assessment of heart-infiltrating **A)** Neutrophils, **B)** Ly6C^{high} monocytes, **C)** Macrophages, **D)** Ly6C^{low} monocytes in *Hsf1*$^{+/+}$ and *Hsf1*$^{-/-}$ hearts post sham and MI operation. Statistical comparison was performed with use of Two-way ANOVA with Tukey's multiple comparison test. n = 3-4 (per treatment group). Values are mean ± SEM.

3.8 Myocardial gene expression of pro-inflammatory cytokines and chemokines is consistent between *Hsf1*$^{+/+}$ and *Hsf1*$^{-/-}$ mice 3 days post-MI.

Pro-inflammatory cytokines and chemokines are not constitutively present in normal hearts. Upregulation and production of pro-inflammatory cytokines and chemokines are part of the innate immune response against ischemic injury[18]. Therefore, the gene expression of pro-inflammatory cytokines (i.e. *Il6, Il1b, Tnfa*) and chemokines (i.e. *Cxcl1*, *Cxcl10*, *Ccl2*) were quantified via RT-qPCR in the peri-infarct region of *Hsf1*$^{+/+}$ and *Hsf1*$^{-/-}$ hearts 3 days post-sham and MI operation. There was no significant difference in the mRNA expression of pro-inflammatory cytokines and chemokines between *Hsf1*$^{+/+}$ and *Hsf1*$^{-/-}$ sham-operated hearts **(Figures 15A-E)**. Moreover, the gene expression of *Il6, Il1b,* and *Tnfa* was insignificant between sham- and MI-operated hearts and between *Hsf1*$^{+/+}$ and *Hsf1*$^{-/-}$ MI-operated hearts **(Figures 15A-C)**. Unlike the gene expression of pro-inflammatory cytokines, the gene expression of *Cxcl10* and *Ccl2* was significantly increased in *Hsf1*$^{+/+}$ MI-operated hearts than its sham counterparts **(Figures 15E-F)**. However, the gene expression of *Cxcl1* was not significantly upregulated in both *Hsf1*$^{+/+}$ and *Hsf1*$^{-/-}$ MI-operated hearts in comparison to *Hsf1*$^{+/+}$ sham-operated hearts **(Figure 15D)**. Lastly, there was no significant difference in the gene expression of pro-inflammatory cytokines and chemokines between *Hsf1*$^{+/+}$ and *Hsf1*$^{-/-}$ hearts post-MI **(Figures 15A-F)**. Therefore, Figure 15 suggests that when the infarction is small, loss of *Hsf1* does not affect the degree of inflammation in the infarct heart.

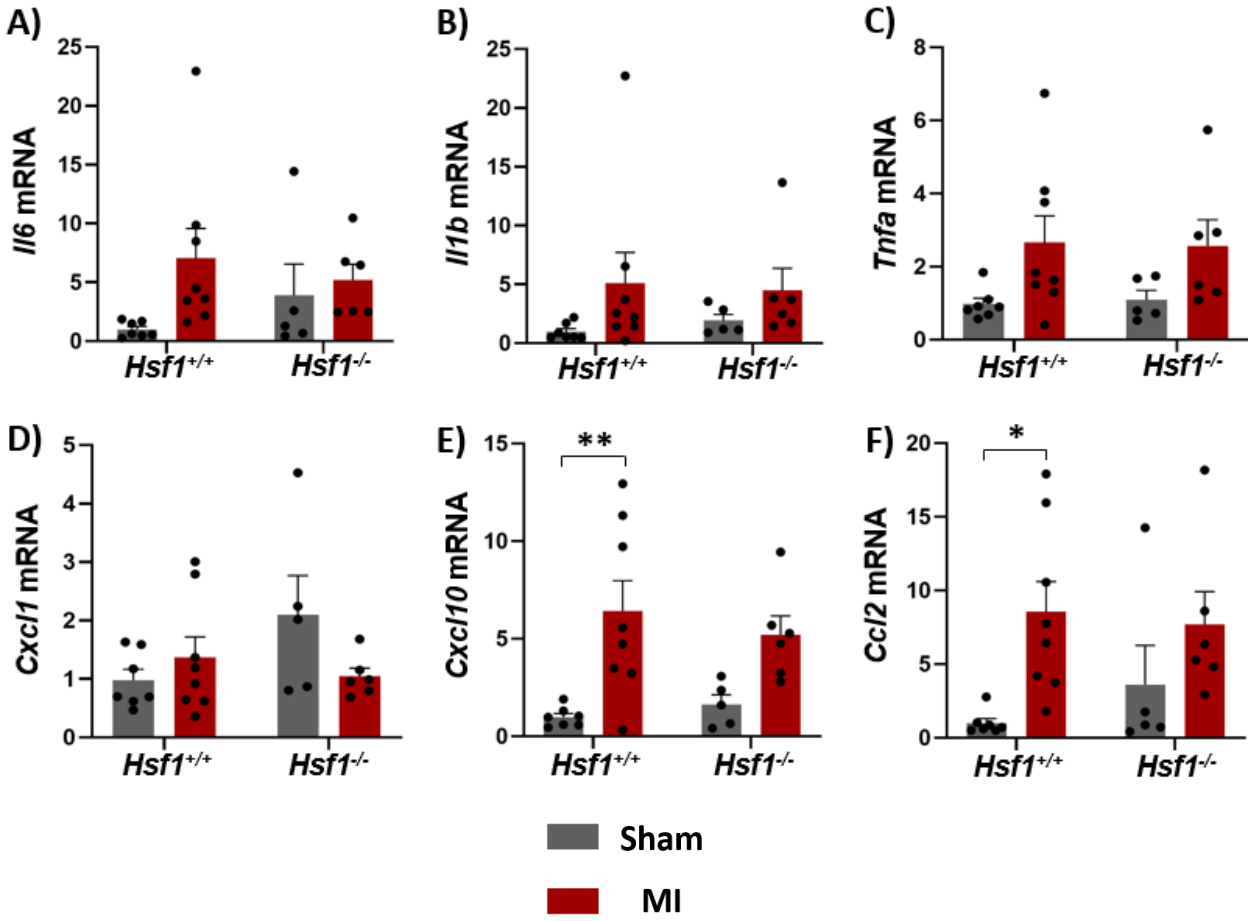

Figure 15. Myocardial gene expression of pro-inflammatory cytokines and chemokines in *Hsf1*$^{+/+}$ and *Hsf1*$^{-/-}$ mice 3 days post-MI. mRNA quantification of the following pro-inflammatory cytokines and chemokines: **A)** *Il6,* **B)** *Il1b,* **C)** *Tnfa,* **D)** *Cxcl1,* **E)** *Cxcl10,* and **F)** *Ccl2* in the peri-infarct regions of *Hsf1*$^{+/+}$ and *Hsf1*$^{-/-}$ hearts. mRNA expression was normalized to *Hprt1*. Statistical comparison was performed with use of Two-way ANOVA with Tukey's multiple comparison test. n = 5-8 (per treatment group). Values are mean ± SEM, *p<0.05; **p<0.01.

3.9 Activation NF-κB p65 and MAPK-ERK1/2 proteins did not change between *Hsf1*$^{+/+}$ and *Hsf1*$^{-/-}$ hearts 3 days post-MI.

The upregulation and production of pro-inflammatory cytokines, such as IL-6, IL-1β, TNF-α, are mediated by pro-inflammatory pathways which are activated by, but not limited to, mitogen-activated protein kinase (MAPK) and nuclear factor kappa-light-chain-enhancer of activated B cells (NF-κB)[77]. Hence, the activation of NF-κB p65 and MAPK-ERK1/2 proteins were assessed via immunoblotting in the peri-infarct region of *Hsf1*$^{+/+}$ and *Hsf1*$^{-/-}$ hearts post-operation. There was no significant difference in the phosphorylation and total expression of p44 (ERK1), p42 (ERK2), and NF-κB p65 between any of the treatment groups **(Figures 16A-G)**. Overall, Figure 16 suggests that the infarction was small and loss of *Hsf1* does not modulate the activation of pro-inflammatory signaling pathway post-MI.

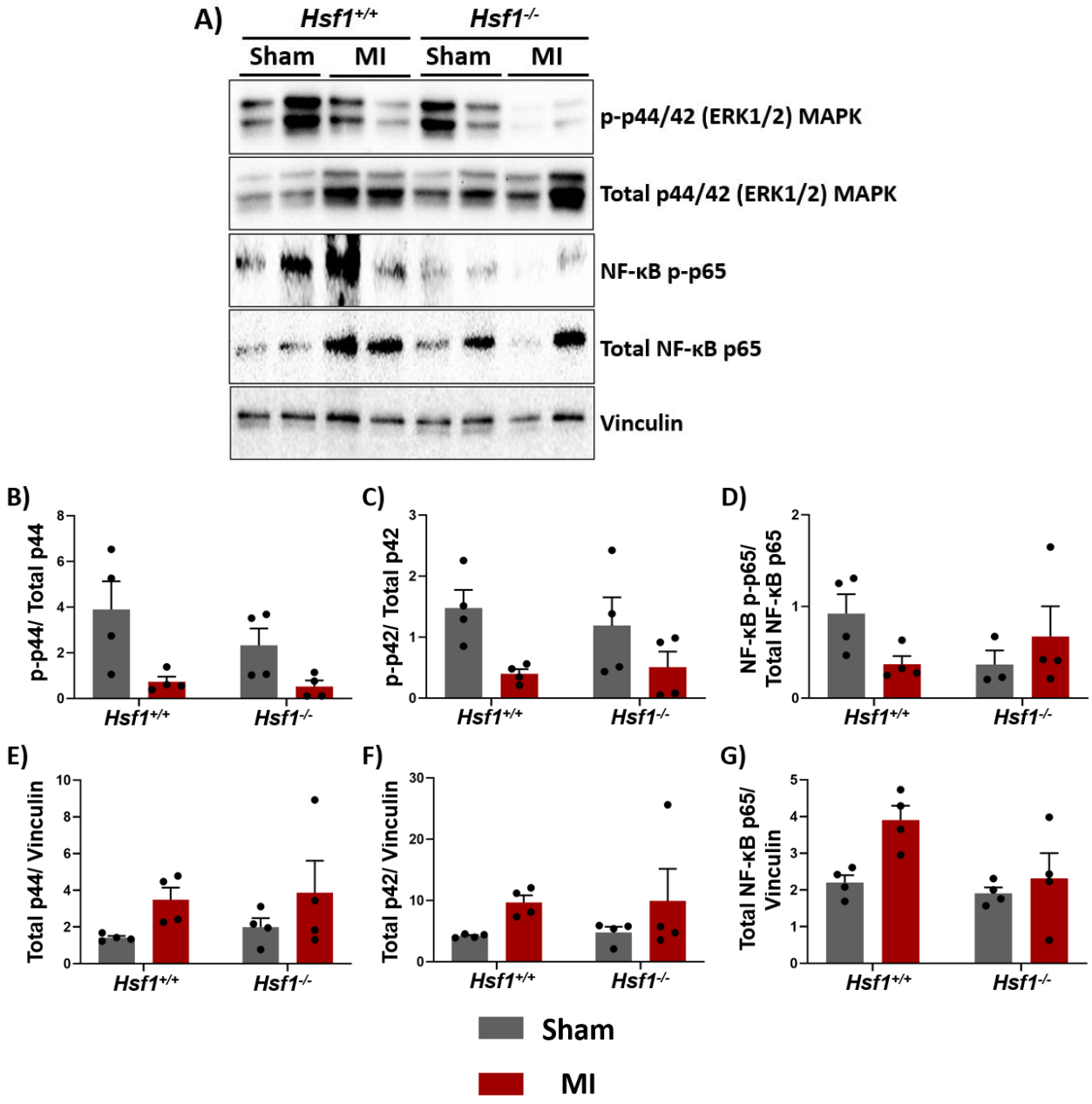

Figure 16. Immunoblotting analysis of NF-κB p65 and MAPK-ERK1/2 proteins 3 days post-MI. **A)** Representative immunoblots of p-p44 (ERK1), Total p44 (ERK1), p-p42 (ERK2), Total p42 (ERK2), NF-κB p-p65, and Total NF-κB p65. The ratio of **B)** p-p44/Total p44, **C)** p-p42/ Total p42, **D)** NF-κB p-p65/ Total NF-κB p65, **E)** Total p44/ Vinculin, **F)** Total p42/ Vinculin, **G)** Total NF-κB p65/ Vinculin. Protein levels were normalized to vinculin. Statistical comparison was performed with use of Two-Way ANOVA with Tukey's multiple comparison test. n = 4 (per treatment group). Values are mean ± SEM.

3.10 Circulating IL-6 serum concentration remained consistent between *Hsf1*$^{+/+}$ and *Hsf1*$^{-/-}$ mice 3 days post-MI.

IL-6 is a well-studied biomarker when it comes to assessing the risk of future MI[166]. Hence, serum samples from *Hsf1*$^{+/+}$ and *Hsf1*$^{-/-}$ mice 3 days post-operation were used to assess IL-6 concentration via ELISA. As evident from Figure 17, IL-6 concentration remained consistent between *Hsf1*$^{+/+}$ and *Hsf1*$^{-/-}$ sham groups. There was insignificant difference in the serum IL-6 concentration between all of the treatment groups **(Figure 17)**.

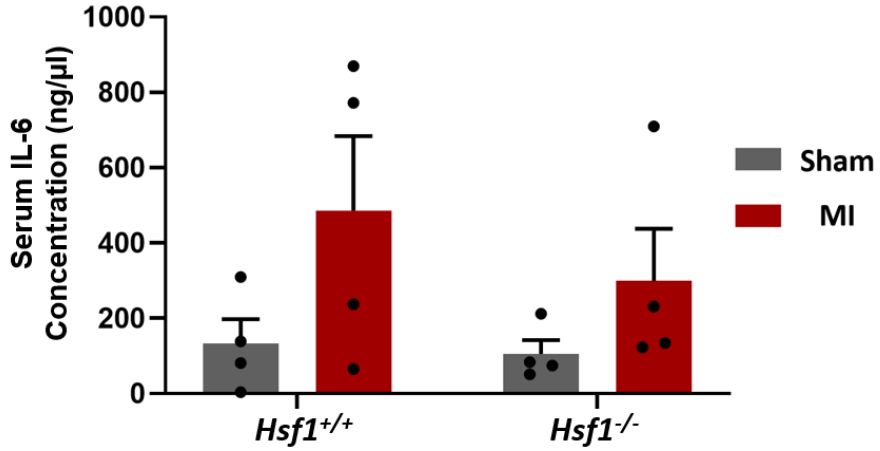

Figure 17. Serum IL-6 concentration of *Hsf1*$^{+/+}$ and *Hsf1*$^{-/-}$ mice 3 days post-MI. IL-6 ELISA kit was used to measure the concentration of IL-6 in the serum samples of *Hsf1*$^{+/+}$ and *Hsf1*$^{-/-}$ mice 3 days post-sham and MI operation. Statistical comparison was performed with the use of Two-way ANOVA with Tukey's multiple comparison test. n = 4 (per treatment group). Values are mean ± SEM.

3.11 Heat shock response remains unchanged at the myocardial gene level 7 days post-MI.

The next step was to assess the changes in the HSR at the myocardial gene expression level in *Hsf1*$^{+/+}$ and *Hsf1*$^{-/-}$ hearts 7 days post-operation. Hence, the transcriptional changes of the genes involved in HSR, such as *Hsf1*, *Hsp90*, and *Hsp70*, were assessed in the peri-infarct region of *Hsf1*$^{+/+}$ and *Hsf1*$^{-/-}$ hearts via RT-qPCR. Overall, there was no significant change in the transcriptional expression of *Hsf1*, *Hsp90*, and *Hsp70* between *Hsf1*$^{+/+}$ and *Hsf1*$^{-/-}$ post-operation**(Figures 18A-C)**.

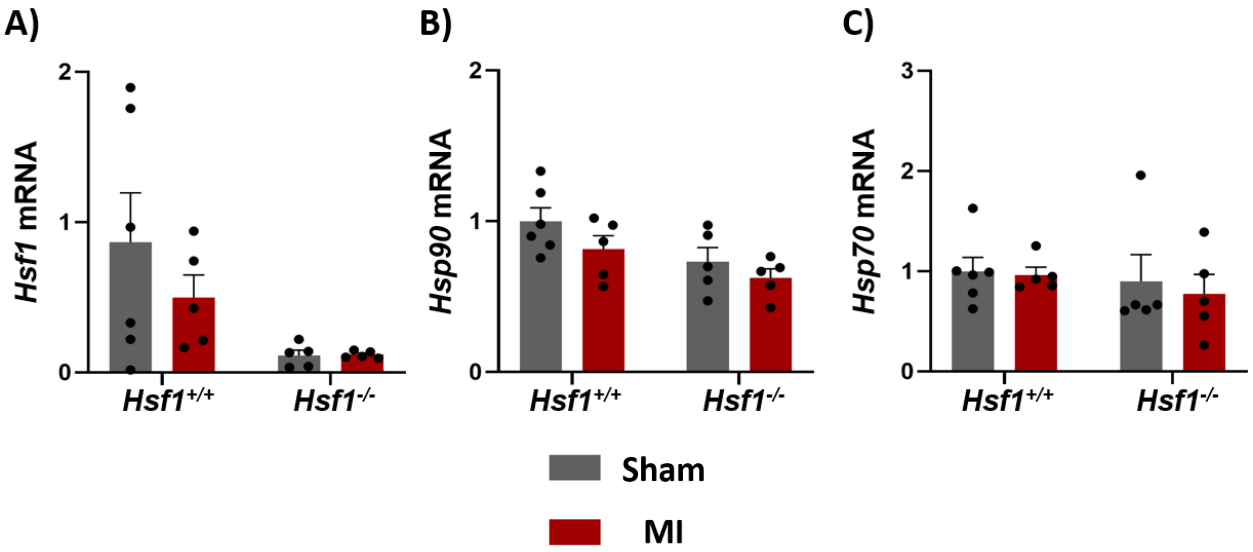

Figure 18. Changes of heat shock response at the myocardial gene level in *Hsf1*$^{+/+}$ and *Hsf1*$^{-/-}$ hearts 7 days post-MI. mRNA expression of **A)** *Hsf1*, **B)** *Hsp90* and **C)** *Hsp70* in the peri-infarct region of *Hsf1*$^{+/+}$ and *Hsf1*$^{-/-}$ hearts 7 days post-MI. mRNA expression was normalized to *Hprt1*. n = 5-6 (per treatment group). Statistical comparison was performed with use of Two-way ANOVA with Tukey's multiple comparison test. Values are mean ± SEM.

3.12 Loss of *Hsf1* decreases heat shock response at the myocardial protein level 7 days post-MI.

After assessing the mRNA expression of genes involved in HSR, the next step was to assess the changes of HSR at the myocardial protein level following 7 days of MI. Hence, expression of proteins involved in HSR, such as HSF1, HSP90, HSP70, and HSP25, was assessed in the peri-infarct region of *Hsf1*$^{+/+}$ and *Hsf1*$^{-/-}$ hearts via immunoblotting. HSF1 expression was undetectable in *Hsf1*$^{-/-}$ sham and MI-operated hearts in comparison to *Hsf1*$^{+/+}$ sham-operated hearts **(Figures 19A & B)**. Also, the expression of HSF1 was significantly reduced by 1-fold in *Hsf1*$^{+/+}$ MI-operated hearts than *Hsf1*$^{+/+}$ sham-operated hearts **(Figures 19A & B)**. Furthermore, there was no significant difference in the protein expression of HSP90, HSP70, and HSP25 between *Hsf1*$^{+/+}$ and *Hsf1*$^{-/-}$ sham-operated hearts **(Figures 19A, C-E)**. Moreover, the expression of molecular chaperones was significantly upregulated in *Hsf1*$^{+/+}$ hearts post-MI, but in the *Hsf1*$^{-/-}$ hearts, the expression was significantly downregulated post-MI **(Figures 19A, C-E)**. Therefore, Figure 19 suggests that heat shock response is significantly down-regulated at the myocardial protein level in *Hsf1*$^{-/-}$ hearts post-sham and MI operation.

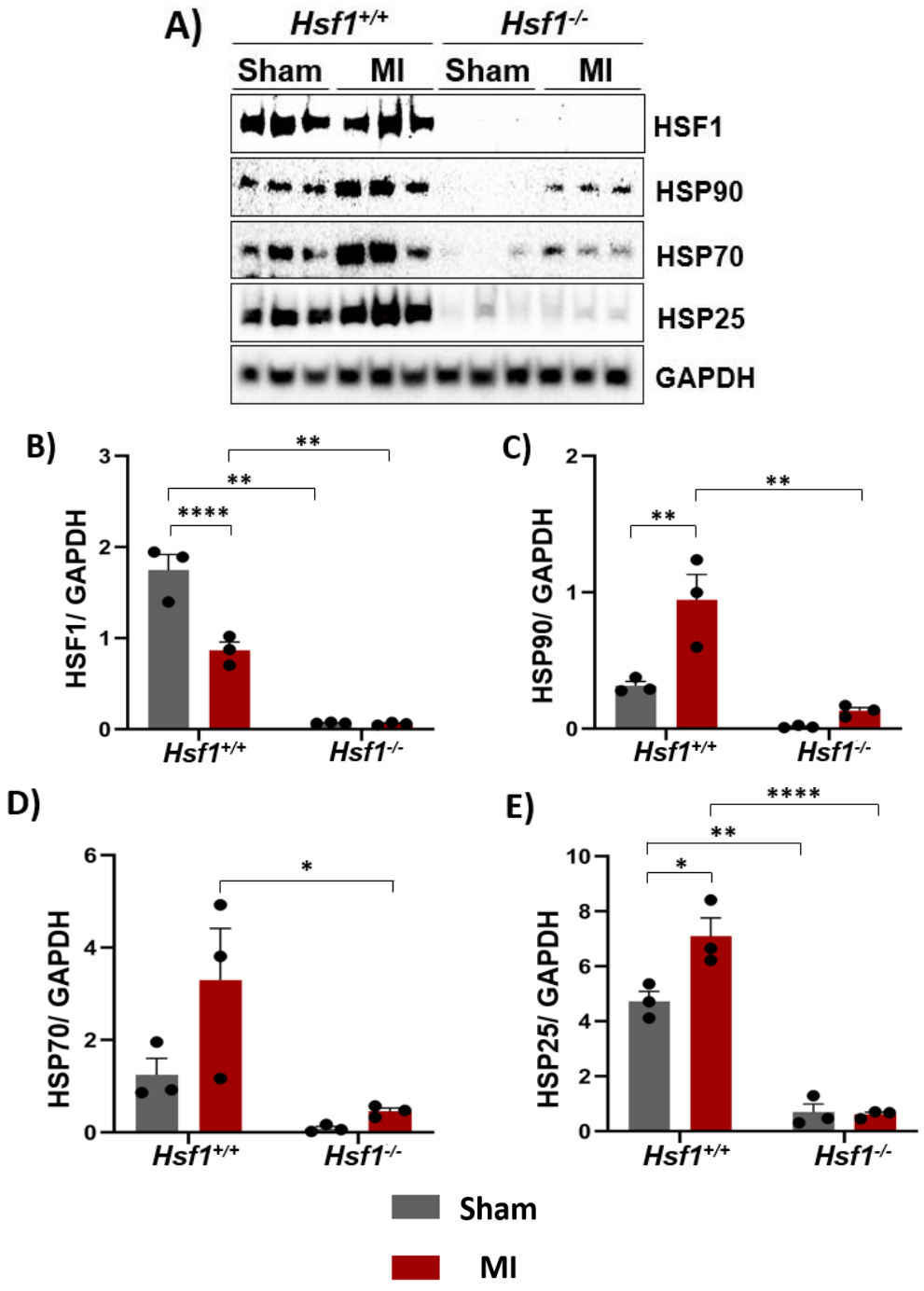

Figure 19. Changes in heat shock response at the myocardial protein level in *Hsf1*$^{+/+}$ and *Hsf1*$^{-/-}$ hearts 7 days post-MI. Protein expression of HSF1, HSP90, HSP70, and HSP25 was assessed in the peri-infarct region of *Hsf1*$^{+/+}$ and *Hsf1*$^{-/-}$ hearts following 7 days of sham and MI operation via immunoblotting. **A)** Representative immunoblots of HSF1, HSP90, HSP70, HSP25, and GAPDH. Quantification of **B)** HSF1, **C)** HSP90, **D)** HSP70, and **E)** HSP25 were represented and their expression was normalized to GAPDH. Statistical comparison was performed with use of Two-way ANOVA with Tukey's multiple comparison test. n = 3 (per treatment group). Values are mean ± SEM, *p<0.05, **p<0.01, **** p<0.0001.

3.13 Transcriptional changes of pro-inflammatory cytokines and chemokines 7 days post-MI.

Pro-inflammatory cytokines and chemokines are not constitutively present in normal hearts. Upregulation and production of pro-inflammatory cytokines and chemokines augments inflammation against ischemic injury[18]. Hence, the gene expression of pro-inflammatory cytokines (e.g. *Il6, Il1b, Tnfa*) and chemokines (e.g. *Cxcl1*, *Cxcl10*, *Ccl2*) was quantified via RT-qPCR in the peri-infarct region of *Hsf1*$^{+/+}$ and *Hsf1*$^{-/-}$ hearts 7 days post-operation. There was no significant difference in the mRNA expression of pro-inflammatory cytokines and chemokines between *Hsf1*$^{+/+}$ and *Hsf1*$^{-/-}$ sham-operated hearts **(Figures 20A-E)**. The gene expression of *Il6* and *Il1b* was significantly increased in both *Hsf1*$^{+/+}$ and *Hsf1*$^{-/-}$ MI-operated hearts than their respective sham counterpart **(Figures 20A-B)**. Moreover, there was no significant difference in the gene expression of *Tnfa* between any of the treatment groups **(Figure 20C)**. There was no significant difference in the gene expression of *Il6, Il1b,* and *Tnfa* between *Hsf1*$^{+/+}$ and *Hsf1*$^{-/-}$ hearts post-MI **(Figures 20A-C)**. Unlike the gene expression of pro-inflammatory cytokines, the gene expression of *Cxcl1* was not significant between the sham and MI-operated hearts **(Figure 20D)**. Similar to the gene expression of *Il6* and *Il1b*, the gene expression of *Cxcl10* was significantly upregulated in both *Hsf1*$^{+/+}$ and *Hsf1*$^{-/-}$ MI-operated hearts compared to their respective sham counterpart **(Figure 20E)**. Lastly, the gene expression of *Cxcl10* was not different between any treatment groups **(Figure 20E)**. Furthermore, the gene expression of pro-inflammatory chemokine, *Ccl2*, was significantly upregulated in *Hsf1*$^{-/-}$ MI-operated hearts than *Hsf1*$^{-/-}$ sham-operated hearts. The gene expression of *Ccl2* was not significantly upregulated in *Hsf1*$^{+/+}$ MI-operated hearts compared to its sham counterpart **(Figure 20F)**. Therefore, Figure 20 suggests that loss of *Hsf1* prolongs inflammation following 7 days of MI.

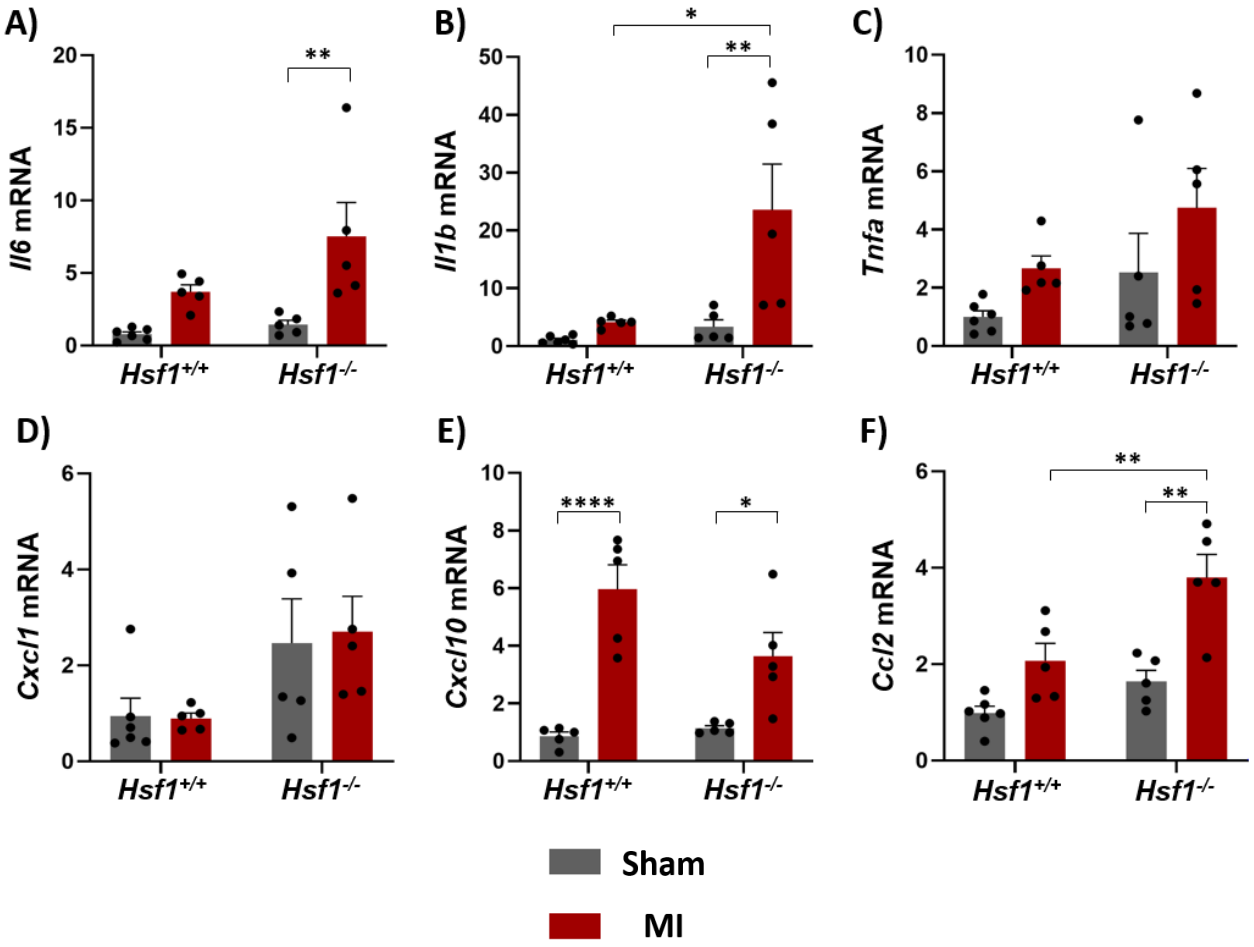

Figure 20. Myocardial gene expression of pro-inflammatory cytokines and chemokines in *Hsf1*$^{+/+}$ and *Hsf1*$^{-/-}$ mice 7 days post-MI. mRNA quantification of the following pro-inflammatory cytokines and chemokines: **A)** *Il6,* **B)** *Il1b,* **C)** *Tnfa,* **D)** *Cxcl1,* **E)** *Cxcl10,* and **F)** *Ccl2* in the peri-infarct regions of *Hsf1*$^{+/+}$ and *Hsf1*$^{-/-}$ hearts. mRNA expression was normalized to *Hprt1*. Statistical comparison was performed with use of Two-way ANOVA with Tukey's multiple comparison test. n = 5-6 (per treatment group). Values are mean ± SEM, *p<0.05, **p<0.01, ****p<0.0001.

4.0 Discussion & Future Directions

4.1 Discussion

Cardiovascular diseases, especially Myocardial Infarction (MI), are the leading causes of premature mortality worldwide, costing economies billions of dollars[1,4]. MI results from sudden occlusion of the coronary arteries, which is due to plaque rupture or erosion. The blockage of oxygen-rich blood supply leads to myocardial ischemia, which when prolongs, leads to cellular death. The release of damage-associated molecular patterns (DAMPs) by dead or injured cells in the infarct and peri-infarct regions leads to the activation of innate immune response and downstream inflammation[11]. Effective therapies are needed to mitigate the excessive inflammation associated with cardiac ischemic injury.

Recent research has shown that the release of heat shock proteins (HSPs), a classic DAMP, by severely injured cells leads to prolonged inflammation through the activation of Toll-Like receptors contributing to subsequent contractile dysfunction[56,57,62,116]. The synthesis of HSPs is regulated by its master transcription factor, Heat Shock Factor 1 (HSF1)[138]. We examined in this thesis whether the deficiency of HSF1, and consequently, the downstream target, HSPs, are beneficial or harmful following MI. We hypothesize that genetic deletion of *Hsf1* can lead to improved survival and LV remodeling via the attenuation of HSPs expression and the subsequent reduction of pro-inflammatory pathway activation following MI. For the first time, we show that deletion of *Hsf1* results in higher survival percentage and smaller infarct size following MI in a murine model of coronary ligation. However, cardiac function remained consistent at each time point between $Hsf1^{+/+}$ and $Hsf1^{-/-}$ mice as well as inflammatory processes until 7 days following MI.

Following sham or MI operation, the Kaplan-Meier survival analysis revealed that survival at 28 days was 74% in $Hsf1^{-/-}$ mice, compared to 34% in $Hsf1^{+/+}$ mice, representing significant 40% higher survival in $Hsf1^{-/-}$ mice than $Hsf1^{+/+}$ mice, $p<0.001$ **(Figure 8A)**. The earliest difference in survival, quantitatively by 20%, was seen in $Hsf1^{+/+}$ mice compared to $Hsf1^{-/-}$ mice following 3 days of MI, which was primarily due to decreased cardiac rupture in $Hsf1^{-/-}$ mice **(Figures 8A &**

B). Rupture of the LV wall is due to excessive inflammatory response leading to activation of matrix metalloproteinases (MMPs) in prolonged ischemia[20]. As indicated in Figure 8B, cardiac rupture rate was 60% in *Hsf1*$^{+/+}$ mice compared to 35% in *Hsf1*$^{-/-}$ mice, representing 25% less in *Hsf1*$^{-/-}$ mice than *Hsf1*$^{+/+}$ mice following MI **(Figure 8B)**. This survival study was performed with larger MI generation with ligature in LAD located "under the tip of the left atrial appendage". However, for the *in vivo* studies in this thesis, the model was conducted with smaller MI, with ligature located 1-1.5mm below the atrial appendage, to avoid excessive mortality, thus generating a survival bias in tissue harvesting and analysis[159]. For this reason, the latter studies found 7 in 26 *Hsf1*$^{+/+}$ and 1 in 28 *Hsf1*$^{-/-}$ mice died following the smaller MI protocol in this study **(Section 2.2)**. These results are consistent with other studies done by our lab team and others in the field, showing that knocking out inflammatory signal mediators, such as TNF-α, TLR4, and IRAK4, mediates cardioprotection following MI[27,68,83].

To assess the severity of MI, heart and lung weights were evaluated at 3, 7, and 28 days post-MI and normalized to tibia length[162]. According to Yang et al., the total heart weight significantly increased after 1 week of MI compared to sham hearts, indicating the occurrence of myocardial hypertrophy over time[167]. Consistent with this finding, there was no difference in heart weight to tibia length ratio between *Hsf1*$^{+/+}$ sham and MI-operated hearts at 3 days following operation, but a significant increase in heart weight was observed following day 7 MI **(Figures 9A & B)**. Unlike *Hsf1*$^{+/+}$ hearts, the heart weight to tibia length ratio was significantly increased in *Hsf1*$^{-/-}$ MI-operated mice than sham-operated mice at day 3 and 7 post-operation, indicating a significant upregulation in myocardial hypertrophy **(Figures 9A & B)**. Structural differences and cardiac hypertrophy were not detected between *Hsf1*$^{+/+}$ and *Hsf1*$^{-/-}$ sham-operated LV sections when stained with HE and PSR following 3 and 7 days of sham-operation **(Figures S2-S4)**, indicating that myocardial hypertrophy is induced by MI, especially in *Hsf1*$^{-/-}$ mice. On the other hand, pulmonary congestion, which is a useful marker in predicting the development of heart failure, can result from the increased filling pressures in the heart following acute MI. Hence, many pre-clinical studies have indicated that the lung weight increases following 1 week of MI[38,68,167,168]. Consistent with this finding, the lung weight to tibia length ratio remained consistent between sham and MI groups of *Hsf1*$^{+/+}$ and *Hsf1*$^{-/-}$ mice at day 3, but at day

7, the lung weight to tibia length ratio was significantly higher in *Hsf1*$^{-/-}$ MI-operated mice compared to *Hsf1*$^{-/-}$ sham-operated mice and *Hsf1*$^{+/+}$ MI-operated mice **(Figures 9D & E)**. This suggests the potential occurrence of pulmonary congestion in *Hsf1*$^{-/-}$ hearts following day 7 MI. However, the heart weight to tibia length ratio and the lung weight to tibia length ratio following 28 days of surgery remained consistent between MI and sham-operated hearts **(Figures 9C & F)**. This result is inconsistent with other pre-clinical studies that show heart and lung weight to gradually increase after 7 days of MI. This inconsistency may be due to smaller sample number for the day 28 observations, and residual survivor effect difference despite our best countermeasure efforts.

One of the major consequences of MI is LV dysfunction. LVEF and FS are two of the most commonly used measurement to assess cardiac function. LVEF is the percentage of blood ejected from the LV while FS is the percent change in LV diameter. These are measurements of cardiac remodeling incorporating some measures of cardiac contractile function[169]. As evident from Figures 10A-C, the LVEF was significantly reduced in the MI-operated hearts than sham-operated hearts for both *Hsf1*$^{+/+}$ and *Hsf1*$^{-/-}$ mice at each time point **(Figures 10A-C)**, indicating that volume changes are consistent following MI. On the other hand, there was no significant difference in FS between both groups at each study point **(Figures 10D-F)**. Hence, loss of *Hsf1* does not improve cardiac function following MI in our smaller MI model procedure.

Four days following MI, the infarct heart transitions into proliferative phase, where there is an attenuation of the expression of pro-inflammatory markers and an upregulation in the expression of anti-inflammatory markers and collagen deposition[14]. Assessment of infarct size and collagen deposition determines the magnitude of cardiac damage; hence, heart tissue sections were stained with MTC and PSR. According to Figures 11A and B, the infarct size was 32% in *Hsf1*$^{+/+}$ MI-operated hearts while it was 19% in *Hsf1*$^{-/-}$ MI-operated hearts, representing a significant 13% ($p<0.05$) reduction in *Hsf1*$^{-/-}$ hearts compared to *Hsf1*$^{+/+}$ hearts **(Figures 11A, B, & S5)**. Similar to infarct size, the collagen deposition in *Hsf1*$^{+/+}$ MI-operated hearts were more expansive along its thin LV wall than *Hsf1*$^{-/-}$ MI-operated hearts **(Figures 11C, D & S4)**. Therefore,

Hsf1$^{-/-}$ leads to smaller infarct size and collagen deposition following MI. As scar is an indicator of cell loss, our results suggest that MI-operated *Hsf1*$^{-/-}$ hearts experience less cardiomyocyte death.

Following the evaluation of survival, functional, and structural parameters, we next assess molecular parameters to better understand the underlying biological mechanisms. Therefore, the transcriptional and protein expression of genes involved in Heat Shock Response (HSR), such as HSF1, HSP90, HSP70, and HSP25, was evaluated with RT-qPCR and immunoblotting, respectively, in the peri-infarct region of *Hsf1*$^{+/+}$ and *Hsf1*$^{-/-}$ hearts following 3 and 7 days of MI. As expected, the *Hsf1* mRNA and HSF1 protein expression was significantly downregulated in *Hsf1*$^{-/-}$ hearts following 3 and 7 days of operation, confirming that *Hsf1* gene deletion was effective in these *Hsf1*$^{-/-}$ homozygous mice (**Figures 12A, 13A & B, 18A, 19A & B)**. HSP90 and HSP70 and/ or HSP70 and its co-chaperone, HSP40, can negatively regulate HSF1 via negative feedback loop[140]. Therefore, the lack of change in *Hsf1* mRNA and HSF1 protein expression between *Hsf1*$^{+/+}$ sham and MI-operated hearts could be due to the negative feedback loop caused by an increase of HSP90 and HSP70 protein expression as evident in Figures 13A, 13C, 13D, 19A, 19C, 19D. Unlike *Hsf1* mRNA and protein expression, *Hsp90* and *Hsp70* mRNA expression remained consistent between the four treatment groups while the protein expression of HSP90, HSP70 and HSP25 was significantly increased in *Hsf1*$^{+/+}$ hearts following MI and then significantly decreased in *Hsf1*$^{-/-}$ hearts following MI **(Figures 13A, 13C, 13D, 13E, 19A, 19C, 19D, & 19E)**. The discrepancy between HSPs mRNA and protein expression suggests that the regulation of HSPs could be controlled via post-transcriptional modifications, protein turnover rate, and/or by other transcription factors, such as Heat shock factor (HSF) 2 and Hypoxia-inducible factor (HIF) 1-α[145,170]. Therefore, loss of *Hsf1* decreases the synthesis of HSPs, which are a classic DAMP in the context of MI.

After confirming that deletion of *Hsf1* significantly decreases the expression of HSPs, the next critical question was whether these results were associated with changes in myocardial inflammation in *Hsf1*$^{+/+}$ and *Hsf1*$^{-/-}$ hearts following day 3 MI. In this early phase, the first cells to be recruited into the infarcted myocardium are neutrophils, which engulf dead cells and tissue debris, and then Ly6C^{high} monocytes that give rise to pro-inflammatory macrophages, which clear

cellular debris via phagocytosis or secreting proteolytic enzymes, and finally Ly6C^{low} monocytes, which resolve inflammation and initiate proliferative phase[11,98,99]. As evident from Figure 14, there was no significant difference between the number of neutrophils, macrophages, Ly6C^{high} and Ly6C^{low} monocytes, which is mostly likely due to small sample size. While larger sample number and larger MI may have allowed us to observe a reduction in inflammatory response in *Hsf1*$^{-/-}$ hearts following MI, our current data show that loss of *Hsf1* does not affect the recruitment of immune cells. However, we could not assess activation status of cells in the respective treatment groups; therefore, further experimental work employing immunostaining for cellular expression of inflammatory factors could address this question.

Cytokines, released by injured and immune cells, play an essential role in augmenting inflammation and recruiting more immune cells to the infarcted myocardium for the clearance of cellular debris. Some of the well-studied cytokines in the context of MI are IL-6, IL-1β, and TNF-α, which according to Deten et al. is upregulated approximately 5-fold in MI-operated hearts following day 3 MI[78]. Consistent with Deten et al., the mRNA expression of *Il6*, *Il1b*, and *Tnfa* was upregulated 5-fold, but there was no statistical difference between treatment groups **(Figures 15A-C)**. Hence, this result may be due to small sample size, which leads to high variance in the data. Lastly but not the least, there was no difference in the mRNA expression of these cytokines between *Hsf1*$^{+/+}$ and *Hsf1*$^{-/-}$ MI-operated hearts **(Figures 15A-C),** suggesting that loss of *Hsf1* does not affect the synthesis of pro-inflammatory cytokines.

Chemokines function by recruiting immune cells, such as neutrophils, monocytes, and lymphocytes, into the injury site. Among the family of chemokines, CXCL1, CXCL10, and CCL2 are some chemokines that are well-studied in the context of MI[95,172]. According to Figures 15D and E, the gene expression of *Cxcl1* was not significantly changed between the treatment groups following 3 days of operation **(Figure 15D)**. Furthermore, *Hsf1*$^{+/+}$ MI-operated hearts demonstrated significant upregulation of *Cxcl10* and *Ccl2* gene expression compared to sham operation **(Figures 15E-F)**. According to literature, the mRNA expression of pro-inflammatory chemokines can increase to 40-fold following 3 days of MI, which is much higher in compared to *Cxcl1, Cxcl10,* and *Ccl2* mRNA expression in Figures 15D-F[173,174]. This, again, suggests that the size

of the MI in our model is quite small, which may explain why there was no change in the infiltration of immune cells in the peri-infarct region of *Hsf1*$^{+/+}$ and *Hsf1*$^{-/-}$ hearts following MI.

In the context of MI, the activation of MAPK-ERK signaling pathway leads to cardioprotection while the activation of NF-κB signaling pathway can be detrimental if prolonged[76,175]. Therefore, the protein expression of p44 (ERK1)/ p42 (ERK2) and NF-κB p65, which are the key components in the MAPK-ERK and NF-κB signaling pathways, respectively, was assessed via immunoblotting in the peri-infarct region of *Hsf1*$^{+/+}$ and *Hsf1*$^{-/-}$ hearts following 3 days of sham and MI operation. According to Mutlak et al., the total and phosphorylation expression of p44 (ERK1) and p42 (ERK2) was increased in MI-operated hearts compared to sham-operated hearts[176]. There was no significant difference in the phosphorylation and total expression of p44 (ERK1) and p42 (ERK2) **(Figures 16A, B, C, E, & F).** Hence, the result by Mutlak et al. was not consistent with Figures 16A, B, C, E and F, which may be due to variance caused by smaller sample size. Furthermore, various pre-clinical studies have indicated that both total and phosphorylation of NF-κB p65 protein expression was upregulated in MI-operated hearts relative to sham-operated hearts[72,153]. However, there was no significant difference in the phosphorylation and total expression of NF-κB **(Figures 16A, D, G)**. Therefore, consistent with Figures 14 (the number of immune cells) and 15 (the gene expression of pro-inflammatory cytokines and chemokines), our current data show that the loss of *Hsf1* does not affect the inflammatory signaling pathways in our model of relatively small sized MI.

Activation of pro-inflammatory pathways and transcription factors leads to the synthesis of pro-inflammatory cytokines and chemokines, but in the setting of MI, it can result in the release of IL-6 into the serum by injured cells. Recent research has shown circulating IL-6 to be an accurate biomarker in assessing the risk of future MI[166]. Consistent with Figure 17 data, the serum IL-6 concentration was not significantly different between the treatment groups, most likely due to both smaller MI size and sample size. While larger group analyses might have indicated a reduction in serum IL-6 concentration in *Hsf1*$^{-/-}$ mice following MI, the current data suggest that loss of *Hsf1* does not affect the release of IL-6 following 3 days of MI.

Following 7 days of MI, the heart has entered proliferative phase where the clearance of cellular debris and immune cell leads to the downregulation of pro-inflammatory cytokines and chemokines expression as well as the upregulation of anti-inflammatory cytokines, pro-fibrotic and angiogenic factors[11,20,41]. Deten et al. have demonstrated that gene expression of pro-inflammatory cytokines, such as IL-6, IL-1, and TNF-α, is increased in heart failure[78]. Inconsistent with this result, the transcriptional expression of *Il6* and *Il1b* was significantly upregulated in *Hsf1*$^{-/-}$ hearts than *Hsf1*$^{+/+}$ hearts following MI **(Figures 20A & B)**. Unlike Figures 20A & B, the gene expression of *Tnfa* was not significantly changed between treatment groups **(Figure 20C)**. While there was no change in the mRNA expression of *Cxcl1* between the treatment groups, the mRNA expression of *Cxcl10* was significantly increased in the MI-operated hearts than their sham counterparts. Furthermore, *Ccl2* mRNA expression was significantly upregulated in the *Hsf1*$^{-/-}$ MI-operated hearts compared to *Hsf1*$^{-/-}$ sham- and *Hsf1*$^{+/+}$ MI-operated hearts **(Figures 20D-F)**. Taken together, Figure 20 may suggest that *Hsf1*$^{-/-}$ hearts were becoming hypertrophied following 7 days of MI. This may explain why the LV wall of *Hsf1*$^{-/-}$ hearts was consistently thicker than *Hsf1*$^{+/+}$ hearts following day 7 MI **(Figures 11A, C, D, S3, S4, & S5)**. Further molecular analyses, such as flow cytometry and immunoblotting of various proteins of the MAPK-ERK pathway, are required to verify that *Hsf1*$^{-/-}$ hearts are becoming hypertrophied following MI.

In conclusion, the loss of *Hsf1* improves survival and reduces infarct size following MI but does not improve cardiac function. However, *Hsf1* deletion does not affect the recruitment of immune cells, activation of inflammatory signalling pathways, and gene expression of pro-inflammatory cytokines and chemokines or serum IL-6 concentration following 3 days of MI.

4.2 Limitations

One of the major limitations of this study is the generation of *Hsf1*$^{-/-}$ mice. Traditionally, a knockout male and female mice are mated to generate more knockout mice. Since H*sf1*$^{-/-}$ females are sterile, various mating pairs, as indicated in **Table 2**, are used to generate *Hsf1*$^{+/+}$ *and Hsf1*$^{-/-}$ mice. Still, one cannot expect to receive mendelian ratio because as explained by Xiao et al., the *Hsf1*$^{-/-}$ mice exhibit prenatal lethality[149]. As a result, one is uncertain how many mice one will receive from a breeding pair and always needs a larger cohort each time to run an

experiment, so that there is minimal variance. Due to this limitation, investigators in the field have used *Hsf1*-heterozygyte (*Hsf1*$^{+/-}$) mice instead of *Hsf1*-knockout (*Hsf1*$^{-/-}$) mice because *Hsf1*$^{+/-}$ mice are generated in abundance and considered them as not only haploinsufficient, but fully functioning as a homozygous *Hsf1*-knockout mice. This, in retrospect, is a major error made by the researchers in the field to date, because as explained by Xiao et al., the phenotype of *Hsf1*$^{+/-}$ mice is more similar to wildtype controls and very different than *Hsf1*$^{-/-}$ mice. For example, unlike *Hsf1*$^{-/-}$ mice, *Hsf1*-heterozygoyte mice are not affected by pre-natal lethality, fertilization, and post-natal growth retardation as well as the heat shock response (HSR) is not abolished[149].

The smaller generation of *Hsf1*$^{-/-}$ mice also led to smaller sample size achieved in multiple parameters in this study. Initially, more samples were planned, but due to COVID-19 interruption, it was recommended to proceed to thesis completion with more limited data rather than waiting for the reopening of the lab. In addition, we thought that smaller MI would still show the molecular and functional differences between *Hsf1*$^{+/+}$ and *Hsf1*$^{-/-}$ animals while maintaining more survivors. However, this led to many situations where no differences were found between multiple parameters. Therefore, in retrospect, the MI size was likely too small and missed the opportunity to observe the difference between *Hsf1*$^{+/+}$ and *Hsf1*$^{-/-}$ hearts post-MI.

4.3 Future Directions

As explained in Section 1.4.4, false assumption and imprecise scientific tool used, such as the usage of *Hsf1*$^{+/-}$ mice in the place of *Hsf1*$^{-/-}$ mice, in the field generates a big gap in the understanding of HSF1's role in the setting of MI[87,157,177]. Therefore, we, for the first time, used actual homozygous *Hsf1*-knockout mice and age-matched wildtype controls to study the role of HSF1 in MI. Moreover, there are many pre-clinical studies that have studied the role of individual HSP in MI, but no one has studied the consequences of the deletion of *Hsf1* following MI[63,116,129,130,132,178–180]. Therefore, we have shown for the first time that the loss of *Hsf1* and consequently, the downregulation of HSPs, results in improved survival and reduced infarct size following MI. However, there are more critical and intriguing questions that should be answered to build upon this thesis.

1. Does the loss of *Hsf1* lead to hypertrophied hearts following 28 days of MI?

The structural and molecular changes of *Hsf1*$^{+/+}$ and *Hsf1*$^{-/-}$ hearts were not extensively studied at day 28 following MI in this thesis. Therefore, MTC and PSR staining should be performed on the MI-operated heart sections to assess infarct size and collagen deposition, respectively. The significant upregulation of pro-inflammatory cytokines in *Hsf1*$^{-/-}$ hearts at day 7 post-MI indicate that *Hsf1*$^{-/-}$ hearts may be developing hypertrophy **(Figures 20A-C)**. But further molecular analysis, such as the changes in MAPK-ERK pathway and fibrosis-related genes (e.g. connective tissue growth factor (CTGF) and TGFβ-1), and other hypertrophy related pathways, should be assessed at day 28 via immunoblotting and RT-qPCR, respectively.

2. Which cellular death mechanisms are accountable for the difference in infarct size and mortality in *Hsf1*$^{-/-}$ hearts following MI?

Even though we did not observe a significant change in inflammatory processes between *Hsf1*$^{+/+}$ and *Hsf1*$^{-/-}$ hearts following MI, cell death mechanism, such as apoptosis, necrosis or necroptosis, may be reduced to mediate cardioprotection in *Hsf1*$^{-/-}$ hearts post-MI. Preliminary data from our lab suggests that the intrinsic apoptotic pathway (caspase 9 dependent) is less activated in *Hsf1*$^{-/-}$ hearts than *Hsf1*$^{+/+}$ hearts following 3 days of MI **(Figure S7)**. Extensive molecular analyses are needed to further study the role of apoptosis and other cell death mechanisms, such as necrosis and necroptosis, in the *Hsf1*$^{-/-}$ hearts following MI. Some molecular analyses that can be performed are TUNEL assay, electron microscopy to assess mitochondria swelling, and immunoblotting of RIP1, RIP3 and MLKL protein expression following 1 and 3 days of MI.

3. Does HSF2 or HIF-1α compensate for the loss of HSF1 following MI?

Literature has identified various transcription factors and proteins to regulate the function of HSF1 and its downstream targets, HSPs. Two transcription factors, HSF2 and HIF-1α, are known to regulate the synthesis of HSPs in the absence of *Hsf1* during heme and hypoxia treatment,

respectively[145,181]. Both publications have performed *in vitro* studies using cancer cell-line but not cardiomyocytes. Hence, there is no evidence in the scientific literature showing the role of HSF2 or HIF-1α in regulating the synthesis of HSPs in the absence of *Hsf1* in cardiomyocytes. Therefore, with the use of *Hsf1*$^{-/-}$, *Hsf2*$^{-/-}$, *Hifa1*$^{-/-}$ mice and their respective double-knockout mice (e.g. *Hsf1*$^{-/-}$*Hsf2*$^{-/-}$and *Hsf1*$^{-/-}$*Hif1a*$^{-/-}$), one could study the link between HSF1 and HSF2 or HSF1 and HIF-1α and whether the modulation of both factors is beneficial or detrimental in the setting of MI. One would do so by assessing survival, functional, structural, and molecular parameters.

References

1. Roth, G. A. *et al.* Global, regional, and national age-sex-specific mortality for 282 causes of death in 195 countries and territories, 1980–2017: a systematic analysis for the Global Burden of Disease Study 2017. *Lancet* **392**, 1736–1788 (2018).
2. Kaptoge, S. *et al.* World Health Organization cardiovascular disease risk charts: revised models to estimate risk in 21 global regions. *Lancet Glob. Heal.* **7**, e1332–e1345 (2019).
3. CCO and Ontario Agency for Health Protection and Promotion (Public Health Ontario). *The burden of chronic diseases in Ontario: key estimates to support efforts in prevention*. *Toronto: Queen's Printer for Ontario* (2019). doi:10.1016/j.ics.2005.01.021.
4. Foundation, H. and S. *2019 Report on Heart, Stroke and Vascular Cognitive Impairment*. (2019).
5. Hennessy, D. A. *et al.* Population health impact of statin treatment in Canada. *Heal. Reports* **27**, 20–28 (2016).
6. Public Health Agency of Canada. *Report from the Canadian Chronic Disease Surveillance System: Heart Disease in Canada, 2018*. https://www.canada.ca/content/dam/phac-aspc/documents/services/publications/diseases-conditions/report-heart-disease-canada-2018/pub1-eng.pdf (Archived by WebCite® at http://www.webcitation.org/75UuX4oGO)%0Ahttps://www.canada.ca/content/dam/phac-aspc/docu (2018).
7. Anderson, Jeffrey L; Morrow, D. A. Acute Myocardial Infarction. *N. Engl. J. Med.* (2017) doi:10.1056/NEJMra1606915.
8. Kübler, W. & Spieckermann, P. G. Regulation of glycolysis in the ischemic and the anoxic myocardium. *J. Mol. Cell. Cardiol.* **1**, 351–377 (1970).
9. Wildenthal, K., Mierzwiak, D. S., Myers, R. W. & Mitchell, J. H. Effects of acute lactic acidosis on left ventricular performance. *Am. J. Physiol.* **214**, 1352–1359 (1968).
10. Nisbet, A. M. *et al.* Acidosis slows electrical conduction through the atrio-ventricular node. *Front. Physiol.* **5 JUN**, 1–8 (2014).
11. Frangogiannis, N. G. Pathophysiology of myocardial infarction. *Compr. Physiol.* **5**, 1841–1875 (2015).

12. Bloom, M. W. *et al.* Heart failure with reduced ejection fraction. *Nat. Rev. Dis. Prim.* **3**, 1–20 (2017).
13. Mcmurray, J. J. V. *et al.* ESC Guidelines for the diagnosis and treatment of acute and chronic heart failure 2012. *Eur. J. Heart Fail.* **14**, 803–869 (2012).
14. Nah, D. Y. & Rhee, M. Y. The inflammatory response and cardiac repair after myocardial infarction. *Korean Circ. J.* **39**, 393–398 (2009).
15. Dobaczewski, M., Gonzalez-Quesada, C. & Frangogiannis, N. G. The extracellular matrix as a modulator of the inflammatory and reparative response following myocardial infarction. *J. Mol. Cell. Cardiol.* **48**, 504–511 (2010).
16. Epelman, S., Liu, P. P. & Mann, D. L. Role of innate and adaptive immune mechanisms in cardiac injury and repair. *Nature Reviews Immunology* vol. 15 117–129 (2015).
17. Saparov, A. *et al.* Role of the immune system in cardiac tissue damage and repair following myocardial infarction. *Inflamm. Res.* **66**, 739–751 (2017).
18. Nian, M., Lee, P., Khaper, N. & Liu, P. Inflammatory cytokines and postmyocardial infarction remodeling. *Circ. Res.* **94**, 1543–1553 (2004).
19. Christia, P. & Frangogiannis, N. G. Targeting inflammatory pathways in MI. *Eur. J. Clin. Invest.* **23**, 1–7 (2013).
20. Liehn, E. A., Postea, O., Curaj, A. & Marx, N. Repair after myocardial infarction, between fantasy and reality: The role of chemokines. *J. Am. Coll. Cardiol.* **58**, 2357–2362 (2011).
21. Abbate, A. *et al.* Alterations in the interleukin-1/interleukin-1 receptor antagonist balance modulate cardiac remodeling following myocardial infarction in the mouse. *PLoS One* **6**, (2011).
22. Bujak, M. *et al.* Interleukin-1 receptor type I signaling critically regulates infarct healing and cardiac remodeling. *Am. J. Pathol.* **173**, 57–67 (2008).
23. Li, X. *et al.* NOD2 deficiency protects against cardiac remodeling after myocardial infarction in mice. *Cell. Physiol. Biochem.* **32**, 1857–1866 (2013).
24. Liao, Y. H. *et al.* Interleukin-17A contributes to myocardial ischemia/reperfusion injury by regulating cardiomyocyte apoptosis and neutrophil infiltration. *J. Am. Coll. Cardiol.* **59**, 420–429 (2012).

25. Liehn, E. A. *et al.* Ccr1 deficiency reduces inflammatory remodelling and preserves left ventricular function after myocardial infarction: In Focus: Heart. *J. Cell. Mol. Med.* **12**, 496–506 (2008).
26. Onai, Y. *et al.* Inhibition of NF-κB improves left ventricular remodeling and cardiac dysfunction after myocardial infarction. *Am. J. Physiol. - Hear. Circ. Physiol.* **292**, 1–5 (2007).
27. Riad, A. *et al.* Toll-Like Receptor-4 Modulates Survival by Induction of Left Ventricular Remodeling after Myocardial Infarction in Mice. *J. Immunol.* **180**, 6954–6961 (2008).
28. Savvatis, K. *et al.* Interleukin-23 deficiency leads to impaired wound healing and adverse prognosis after myocardial infarction. *Circ. Hear. Fail.* **7**, 161–171 (2014).
29. Shishido, T. *et al.* Toll-Like Receptor-2 Modulates Ventricular Remodeling after Myocardial Infarction. *Circulation* **108**, 2905–2910 (2003).
30. Toldo, S. *et al.* Interleukin-1β blockade improves cardiac remodelling after myocardial infarction without interrupting the inflammasome in the mouse. *Exp. Physiol.* **98**, 734–745 (2013).
31. Wang, Y. *et al.* C-X-C Motif Chemokine Receptor 4 Blockade Promotes Tissue Repair after Myocardial Infarction by Enhancing Regulatory T Cell Mobilization and Immune-Regulatory Function. *Circulation* **139**, 1798–1812 (2019).
32. Zhang, J. *et al.* CXCR7 suppression modulates macrophage phenotype and function to ameliorate post-myocardial infarction injury. *Inflamm. Res.* **69**, 523–532 (2020).
33. Chen, W. *et al.* Endogenous IRAK-M attenuates postinfarction remodeling through effects on macrophages and fibroblasts. *Arterioscler. Thromb. Vasc. Biol.* **32**, 2598–2608 (2012).
34. Hendrik B. Sager, MD*; Timo Heidt, MD*; Maarten Hulsmans, PhD; Partha Dutta, DVM, PhD; Gabriel Courties, PhD; Matthew Sebas, BA; Gregory R. Wojtkiewicz, Ms. & Benoit Tricot, MSc; Yoshiko Iwamoto, BS; Yuan Sun, MD, PhD; Ralph Weissleder, MD, PhD; Peter Libby, MD; Filip K. Swirski, PhD; Matthias Nahrendorf, MD, P. Targeting Interleukin-1β Reduces Leukocyte Production After Acute Myocardial Infarction. *Circ. J.* **15**, 2674–2676 (2015).

35. De Kleijn, D. P. V. *et al.* Toll-like receptor 7 deficiency promotes survival and reduces adverse left ventricular remodelling after myocardial infarction. *Cardiovasc. Res.* **115**, 1791–1803 (2019).
36. Fallach, R. *et al.* Cardiomyocyte Toll-like receptor 4 is involved in heart dysfunction following septic shock or myocardial ischemia. *J. Mol. Cell. Cardiol.* **48**, 1236–1244 (2010).
37. Jing, R., Long, T. Y., Pan, W., Li, F. & Xie, Q. Y. IL-6 knockout ameliorates myocardial remodeling after myocardial infarction by regulating activation of M2 macrophages and fibroblast cells. *Eur. Rev. Med. Pharmacol. Sci.* **23**, 6283–6291 (2019).
38. Kawano, S. *et al.* Blockade of NF-κB improves cardiac function and survival after myocardial infarction. *Am. J. Physiol. - Hear. Circ. Physiol.* **291**, 1337–1344 (2006).
39. King, K. R. *et al.* IRF3 and type i interferons fuel a fatal response to myocardial infarction. *Nat. Med.* **23**, 1481–1487 (2017).
40. Li, J. *et al.* CD226 deletion improves post-infarction healing via modulating macrophage polarization in mice. *Theranostics* **10**, 2422–2435 (2020).
41. Prabhu, S. D. & Frangogiannis, N. G. The biological basis for cardiac repair after myocardial infarction. *Circulation Research* vol. 119 91–112 (2016).
42. Eschenhagen, T. A new concepts of fibroblast dynamics in post-myocardial infarction remodeling. *J. Clin. Invest.* **128**, 1731–1733 (2018).
43. Acute Myocardial Infarction (MI) - Cardiovascular Disorders - Merck Manuals Professional Edition. https://www.merckmanuals.com/en-ca/professional/cardiovascular-disorders/coronary-artery-disease/acute-myocardial-infarction-mi.
44. Percutaneous coronary intervention | Heart and Stroke Foundation. https://www.heartandstroke.ca/heart/treatments/surgery-and-other-procedures/percutaneous-coronary-intervention.
45. O'Gara, P. T. *et al.* 2013 ACCF/AHA guideline for the management of st-elevation myocardial infarction: A report of the American college of cardiology foundation/american heart association task force on practice guidelines. *J. Am. Coll. Cardiol.* **61**, 78–140 (2013).

46. Amsterdam, E. A. *et al.* 2014 AHA/acc guideline for the management of patients with Non-ST-Elevation acute coronary syndromes: A report of the American College of Cardiology/American Heart Association Task Force on Practice Guidelines. *J. Am. Coll. Cardiol.* **64**, e139–e228 (2014).
47. Ong, S. B. *et al.* Inflammation following acute myocardial infarction: Multiple players, dynamic roles, and novel therapeutic opportunities. *Pharmacol. Ther.* **186**, 73–87 (2018).
48. Burnet, M. Clonal Selection Theory of Acquired Immunity. *American Journal of Public Health and the Nations Health* vol. 51 488–488 (1961).
49. Matzinger, P. The danger model: A renewed sense of self. *Science (80-.).* **296**, 301–305 (2002).
50. Matzinger, P. TOLERANCE , DANGER , DANGER , AND AND THE THE EXTENDED FAMILY * F AMIL y * EXTENDED. *Annu. Rev.lmmunol* **12**, 991–1045 (1994).
51. Matzinger, P. Essay 1: The danger model in its historical context. *Scand. J. Immunol.* **54**, 4–9 (2001).
52. Pradeu, T. & Cooper, E. L. The danger theory: 20 years later. *Front. Immunol.* **3**, 1–9 (2012).
53. Schaefer, L. Complexity of danger: The diverse nature of damage-associated molecular patterns. *J. Biol. Chem.* **289**, 35237–35245 (2014).
54. Bianchi, M. E. DAMPs, PAMPs and alarmins: all we need to know about danger. *J. Leukoc. Biol.* **81**, 1–5 (2007).
55. Oppenheim, J. J. & Yang, D. Alarmins: Chemotactic activators of immune responses. *Curr. Opin. Immunol.* **17**, 359–365 (2005).
56. Tian, J. *et al.* Extracellular HSP60 induces inflammation through activating and up-regulating TLRs in cardiomyocytes. *Cardiovasc. Res.* **98**, 391–401 (2013).
57. Satoh, M. *et al.* Activated toll-like receptor 4 in monocytes is associated with heart failure after acute myocardial infarction. *Int. J. Cardiol.* **109**, 226–234 (2006).
58. Baiersdörfer, M. *et al.* Toll-like receptor 3 mediates expression of clusterin/apolipoprotein J in vascular smooth muscle cells stimulated with RNA released from necrotic cells. *Exp. Cell Res.* **316**, 3489–3500 (2010).

59. Zhang, W. *et al.* Necrotic myocardial cells release Damage-Associated Molecular Patterns that provoke fibroblast activation in vitro and trigger myocardial inflammation and fibrosis in vivo. *J. Am. Heart Assoc.* **4**, 1–19 (2015).
60. Chen, G.-Y., Tang, J., Zheng, P. & Liu, Y. CD24 and Siglec-10 Selectively Repress Tissue Damage-Induced Immune Responses. **323**, 1722–1725 (2009).
61. Liu, F. Y. *et al.* TLR9 is essential for HMGB1-mediated post-myocardial infarction tissue repair through affecting apoptosis, cardiac healing, and angiogenesis. *Cell Death Dis.* **10**, (2019).
62. Heiserman, J. P. *et al.* TLR4 mutation and HSP60-induced cell death in adult mouse cardiac myocytes. *Cell Stress Chaperones* **20**, 527–535 (2015).
63. Li, Y. *et al.* Myocardial ischemia activates an injurious innate immune signaling via cardiac heat shock protein 60 and toll-like receptor 4. *J. Biol. Chem.* **286**, 31308–31319 (2011).
64. De Haan, J. J., Smeets, M. B., Pasterkamp, G. & Arslan, F. Danger signals in the initiation of the inflammatory response after myocardial infarction. *Mediators Inflamm.* **2013**, (2013).
65. Chao, W. Toll-like receptor signaling: A critical modulator of cell survival and ischemic injury in the heart. *Am. J. Physiol. - Hear. Circ. Physiol.* **296**, (2009).
66. Botos, I., David M., S. & Davies, D. R. Structural biology of TLRs. *HHS public acces* **19**, 447–459 (2011).
67. O'Neill, L. A. J. & Bowie, A. G. The Family of Five - TIR domain-containing adaptors in TLR signaling. 353–364 (2007).
68. Maekawa, Y. *et al.* Survival and cardiac remodeling after myocardial infarction are critically dependent on the host innate immune interleukin-1 receptor-associated kinase-4 signaling: A regulator of bone marrow-derived dendritic cells. *Circulation* **120**, 1401–1414 (2009).
69. Arslan, F. *et al.* Myocardial ischemia/reperfusion injury is mediated by leukocytic toll-like receptor-2 and reduced by systemic administration of a novel anti-toll-like receptor-2 antibody. *Circulation* **121**, 80–90 (2010).
70. Liu, T., Zhang, L., Joo, D. & Sun, S. C. NF-κB signaling in inflammation. *Signal Transduct.*

Target. Ther. **2**, (2017).

71. Christian, F., Smith, E. & Carmody, R. The Regulation of NF-κB Subunits by Phosphorylation. *Cells* **5**, 12 (2016).
72. Misra, A. *et al.* Nuclear Factor-κB Protects the Adult Cardiac Myocyte Against Ischemia-Induced Apoptosis in a Murine Model of Acute Myocardial Infarction. *Circulation* **108**, 3075–3078 (2003).
73. Moss, N. C., Stansfield, W. E., Willis, M. S., Tang, R. H. & Selzman, C. H. IKKβ inhibition attenuates myocardial injury and dysfunction following acute ischemia-reperfusion injury. *Am. J. Physiol. - Hear. Circ. Physiol.* **293**, 2248–2253 (2007).
74. Kawai, T. & Akira, S. Signaling to NF-κB by Toll-like receptors. *Trends Mol. Med.* **13**, 460–469 (2007).
75. Lips, D. J. *et al.* MEK1-ERK2 Signaling Pathway Protects Myocardium from Ischemic Injury In Vivo. *Circulation* **109**, 1938–1941 (2004).
76. Gallo, S., Vitacolonna, A., Bonzano, A., Comoglio, P. & Crepaldi, T. ERK: A key player in the pathophysiology of cardiac hypertrophy. *Int. J. Mol. Sci.* **20**, 1–21 (2019).
77. Shimizu, N. *et al.* Activation of mitogen-activated protein kinases and activator protein- 1 in myocardial infarction in rats. *Cardiovasc. Res.* **38**, 116–124 (1998).
78. Deten, A., Volz, H. C., Driest, W. & Zimmer, H. G. Cardiac cytokine expression is upregulated in the acute phase after myocardial infarction. Experimental studies in rats. *Cardiovasc. Res.* **55**, 329–340 (2002).
79. Irwin, M. W. *et al.* Tissue expression and immunolocalization of tumor necrosis factor-α in postinfarction dysfunctional myocardium. *Circulation* **99**, 1492–1498 (1999).
80. Beg, A. A. & Baltimore, D. An essential role for NF-κB in preventing TNF-α-induced cell death. *Science (80-.).* **274**, 782–784 (1996).
81. Huang, S. & Frangogiannis, N. G. Anti-inflammatory therapies in myocardial infarction: failures, hopes and challenges. *Br. J. Pharmacol.* **175**, 1377–1400 (2018).
82. Krishnamurthy, P. *et al.* IL-10 inhibits inflammation and attenuates left ventricular remodeling after myocardial infarction via activation of STAT3 and suppression of HuR. *Circ. Res.* **104**, 9–18 (2009).

83. Maekawa, N. *et al.* Improved myocardial ischemia/reperfusion injury in mice lacking tumor necrosis factor-α. *J. Am. Coll. Cardiol.* **39**, 1229–1235 (2002).
84. Ridker, P. M. *et al.* Antiinflammatory therapy with canakinumab for atherosclerotic disease. *N. Engl. J. Med.* **377**, 1119–1131 (2017).
85. ASSessing the Effect of Anti-IL-6 Treatment in Myocardial Infarction: The ASSAIL-MI Trial - Full Text View - ClinicalTrials.gov. https://clinicaltrials.gov/ct2/show/NCT03004703.
86. Cavalera, M. & Frangogiannis, N. G. Targeting the chemokines in cardiac repair. *Curr. Pharm. Des.* **20**, 1971–9 (2014).
87. Wang, S. *et al.* HSF1 deficiency accelerates the transition from pressure overload-induced cardiac hypertrophy to heart failure through endothelial miR-195a-3p-mediated impairment of cardiac angiogenesis. *J. Mol. Cell. Cardiol.* **118**, 193–207 (2018).
88. Hayasaki, T. *et al.* CC Chemokine Receptor-2 Deficiency Attenuates Oxidative Stress and Infarct Size Caused by Myocardial Ischemia-Reperfusion. *Circ. J.* **70**, 342–351 (2006).
89. Day, R. B. & Link, D. C. Regulation of neutrophil trafficking from the bone marrow. *Cell. Mol. Life Sci.* **69**, 1415–1423 (2012).
90. Borregaard, N., Theilgaard-Mönch, K., Cowland, J. B., Ståhle, M. & Sørensen, O. E. Neutrophils and keratinocytes in innate immunity-cooperative actions to provide antimicrobial defense at the right time and place. *J. Leukoc. Biol.* **77**, 439–443 (2005).
91. Semerad, C. L., Liu, F., Gregory, A. D., Stumpf, K. & Link, D. C. G-CSF is an essential regulator of neutrophil trafficking from the bone marrow to the blood. *Immunity* **17**, 413–423 (2002).
92. Chia, S. *et al.* Association of Leukocyte and Neutrophil Counts With Infarct Size, Left Ventricular Function and Outcomes After Percutaneous Coronary Intervention for ST-Elevation Myocardial Infarction. *Am. J. Cardiol.* **103**, 333–337 (2009).
93. Bratton, D. L. & Henson, P. M. Neutrophil clearance: When the party is over, clean-up begins. *Trends Immunol.* **32**, 350–357 (2011).
94. Frangogiannis, N. G. Regulation of the inflammatory response in cardiac repair. *Handb. Neurochem. Mol. Neurobiol.* **110**, 159–173 (2012).
95. Ma, Y., Yabluchanskiy, A. & Lindsey, M. L. Neutrophil roles in left ventricular remodeling

following myocardial infarction. *Fibrogenes. Tissue Repair* **6**, 1 (2013).

96. Shinagawa, H. & Frantz, S. Cellular Immunity and Cardiac Remodeling After Myocardial Infarction: Role of Neutrophils, Monocytes, and Macrophages. *Curr. Heart Fail. Rep.* **12**, 247–254 (2015).
97. Nahrendorf, M. *et al.* The healing myocardium sequentially mobilizes two monocyte subsets with divergent and complementary functions. *J. Exp. Med.* **204**, 3037–3047 (2007).
98. Peet, C., Ivetic, A., Bromage, D. I. & Shah, A. M. Cardiac monocytes and macrophages after myocardial infarction. *Cardiovasc. Res.* **116**, 1101–1112 (2020).
99. Nahrendorf, M. Myeloid cells in cardiovascular organs. *J. Intern. Med.* **285**, 491–502 (2019).
100. Akodad, M. *et al.* Interest of colchicine in the treatment of acute myocardial infarct responsible for heart failure in a mouse model. *Int. J. Cardiol.* **240**, 347–353 (2017).
101. Bakhta, O. *et al.* Cardioprotective Role of Colchicine Against Inflammatory Injury in a Rat Model of Acute Myocardial Infarction. *J. Cardiovasc. Pharmacol. Ther.* **23**, 446–455 (2018).
102. Tardif, J. C. *et al.* Efficacy and safety of low-dose colchicine after myocardial infarction. *N. Engl. J. Med.* **381**, 2497–2505 (2019).
103. Jenei, Z. M. *et al.* Elevated extracellular HSP70 (HSPA1A) level as an independent prognostic marker of mortality in patients with heart failure. *Cell Stress Chaperones* **18**, 809–813 (2013).
104. Zhang, X. *et al.* Elevated heat shock protein 60 levels are associated with higher risk of coronary heart disease in Chinese. *Circulation* **118**, 2687–2693 (2008).
105. Willis, M. S. & Patterson, C. Hold me tight: Role of the heat shock protein family of chaperones in cardiac disease. *Circulation* **122**, 1740–1751 (2010).
106. De Maio, A., Gabriella Santoro, M., Tanguay, R. M. & Hightower, L. E. Ferruccio Ritossa's scientific legacy 50 years after his discovery of the heat shock response: A new view of biology, a new society, and a new journal. *Cell Stress Chaperones* **17**, 139–143 (2012).
107. Ritossa, F. M. Experimental activation of specific loci in polytene chromosomes of

Drosophila. *Exp. Cell Res.* **35**, 601–607 (1964).

108. Ritossa, F. A new puffing pattern induced by temperature shock and DNP in Drosophila. *Experientia* **18**, 571–573 (1962).
109. Tissiéres, A., Mitchell, H. K. & Tracy, U. M. Protein synthesis in salivary glands of Drosophila melanogaster: Relation to chromosome puffs. *J. Mol. Biol.* **84**, (1974).
110. Åkerfelt, M., Morimoto, R. I. & Sistonen, L. Heat shock factors: Integrators of cell stress, development and lifespan. *Nat. Rev. Mol. Cell Biol.* **11**, 545–555 (2010).
111. Hartl, F. U., Bracher, A. & Hayer-Hartl, M. Molecular chaperones in protein folding and proteostasis. *Nature* **475**, 324–332 (2011).
112. Wu, C. HEAT SHOCK TRANSCRIPTION FACTORS : Structure and Regulation translocation , higher order assembly , and protein degradation (Gething &. *Annu. Rev. Cell Dev. Biol.* **11**, 441–469 (1995).
113. Golenhofen, N., Perng, M. Der, Quinlan, R. A. & Drenckhahn, D. Comparison of the small heat shock proteins αb-crystallin, MKBP, HSP25, HSP20, and cvHSP in heart and skeletal muscle. *Histochem. Cell Biol.* **122**, 415–425 (2000).
114. Kampinga, H. H. *et al.* Guidelines for the nomenclature of the human heat shock proteins. *Cell Stress and Chaperones* vol. 14 105–111 (2009).
115. Srivastava, P. Roles of heat-shock proteins in innate and adaptive immunity. *Nature Reviews Immunology* vol. 2 185–194 (2002).
116. Mathur, S., Walley, K. R., Wang, Y., Indrambarya, T. & Boyd, J. H. Extracellular heat shock protein 70 induces cardiomyocyte inflammation and contractile dysfunction via TLR2. *Circ. J.* **75**, 2445–2452 (2011).
117. Satoh, M. *et al.* Elevated circulating levels of heat shock protein 70 are related to systemic inflammatory reaction through monocyte Toll signal in patients with heart failure after acute myocardial infarction. *Eur. J. Heart Fail.* **8**, 810–815 (2006).
118. Chen, Y., Voegeli, T. S., Liu, P. P., Noble, E. G. & Curie, R. W. Heat stock paradox and a new role of heat shock proteins and their receptors as anti-inflammation targets. *Inflamm. Allergy - Drug Targets* **6**, 91–100 (2007).
119. Rosenfeld, G. E., Mercer, E. J., Mason, C. E. & Evans Todd. Small heat shock proteins

Hspb7 and Hspb12 regulate early steps of cardiac morphogenesis. *Dev. Biol.* **381**, 389–400 (2013).

120. Cuerrier, C. M. *et al.* Chronic Over-Expression of Heat Shock Protein 27 Attenuates Atherogenesis and Enhances Plaque Remodeling: A Combined Histological and Mechanical Assessment of Aortic Lesions. *PLoS One* **8**, (2013).
121. Vander Heide, R. S. Increased expression of HSP27 protects canine myocytes from simulated ischemia-reperfusion injury. *Am. J. Physiol. - Hear. Circ. Physiol.* **282**, 935–941 (2002).
122. Marunouchi, T. *et al.* Changes in small heat shock proteins HSPB1, HSPB5 and HSPB8 in mitochondria of the failing heart following myocardial infarction in rats. *Biol. Pharm. Bull.* **36**, 529–539 (2013).
123. Li, J. *et al.* HSPA12B attenuates cardiac dysfunction and remodelling after myocardial infarction through an eNOS-dependent mechanism. *Cardiovasc. Res.* **99**, 674–684 (2013).
124. Raizman, J. E. *et al.* Biochimica et Biophysica Acta Heat shock protein-27 attenuates foam cell formation and atherogenesis by down-regulating scavenger receptor-A expression via NF- κ B signaling. *BBA - Mol. Cell Biol. Lipids* **1831**, 1721–1728 (2013).
125. Fan, F. *et al.* Deletion of heat shock protein 60 in adult mouse cardiomyocytes perturbs mitochondrial protein homeostasis and causes heart failure. *Cell Death Differ.* **27**, 587–600 (2020).
126. Benjamin, I. J. & McMillan, D. R. Stress (heat shock) proteins molecular chaperones in cardiovascular biology and disease. *Circ. Res.* **83**, 117–132 (1998).
127. Marber, M. S. *et al.* Overexpression of the Rat Inducible 70-kD Heat Stress Protein in Mouse Increases the Resistance of the Heart to Ischemic Injury Transgenic. **95**, 1446–1456 (1995).
128. Plumier, J. C. L. *et al.* Transgenic mice expressing the human heat shock protein 70 have improved post-ischemic myocardial recovery. *J. Clin. Invest.* **95**, 1854–1860 (1995).
129. Trost, S. U. *et al.* Protection Against Myocardial Dysfunction After a Brief Ischemic Period in Transgenic Mice Expressing Inducible Heat Shock Protein 70. *J. Clin. Invest.* **101**, 855–862 (1998).

130. Song, N. *et al.* Heat Shock Protein 70 Protects the Heart from Ischemia / Reperfusion Injury through Inhibition of p38 MAPK Signaling. *Oxid. Med. Cell. Longev.* **2020**, (2020).
131. Kim, Y. K. *et al.* Deletion of the inducible 70-kDa heat shock protein genes in mice impairs cardiac contractile function and calcium handling associated with hypertrophy. *Circulation* **113**, 2589–2597 (2006).
132. Zhao, Y., Wang, W. & Qian, L. Hsp70 may protect cardiomyocytes from stress-induced injury by inhibiting Fas-mediated apoptosis. *Cell Stress Chaperones* **12**, 83–95 (2007).
133. Tanonaka, K. *et al.* Hsp70 attenuates hypoxia/reoxygenation-induced activation of poly(ADP-ribose) synthetase in the nucleus of adult rat cardiomyocytes. *Mol. Cell. Biochem.* **248**, 149–155 (2003).
134. Zhang, X. *et al.* Plasma levels of Hsp70 and anti-Hsp70 antibody predict risk of acute coronary syndrome. *Cell Stress Chaperones* **15**, 675–686 (2010).
135. Krepuska, M. *et al.* Serum level of soluble Hsp70 is associated with vascular calcification. *Cell Stress Chaperones* **16**, 257–265 (2011).
136. Liu, P. *et al.* Targeting Extracellular Heat Shock Protein 70 Ameliorates Doxorubicin-Induced Heart Failure Through Resolution of Toll-Like Receptor 2–Mediated Myocardial Inflammation. *J. Am. Heart Assoc.* **8**, 1–11 (2019).
137. Fujimoto, M. & Nakai, A. The heat shock factor family and adaptation to proteotoxic stress. *FEBS J.* **277**, 4112–4125 (2010).
138. Zou, J., Guo, Y., Guettouche, T., Smith, D. F. & Voellmy, R. Repression of heat shock transcription factor HSF1 activation by HSP90 (HSP90 complex) that forms a stress-sensitive complex with HSF1. *Cell* **94**, 471–480 (1998).
139. Vihervaara, A. & Sistonen, L. HSF1 at a glance. *J. Cell Sci.* **127**, 261–266 (2014).
140. Westerheide, S. D., Anckar, J., Stevens, S. M., Sistonen, L. & Morimoto, R. I. Stress-inducible regulation of heat shock factor 1 by the deacetylase SIRT. *Science (80-.).* **323**, 1063–1066 (2009).
141. Wales, C. T. K., Taylor, F. R., Higa, A. T., McAllister, H. A. & Jacobs, A. T. ERK-dependent phosphorylation of HSF1 mediates chemotherapeutic resistance to benzimidazole carbamates in colorectal cancer cells. *Anticancer. Drugs* **26**, 657–666 (2015).

142. Wang, X., Grammatikakis, N., Siganou, A., Stevenson, M. A. & Calderwood, S. K. Interactions between extracellular signal-regulated protein kinase 1, 14-3-3ε, and heat shock factor 1 during stress. *J. Biol. Chem.* **279**, 49460–49469 (2004).

143. Knauf, U., Newton, E. M., Kyriakis, J. & Kingston, R. E. Repression of human heat shock factor 1 activity at control temperature by phosphorylation. *Genes Dev.* **10**, 2782–2793 (1996).

144. Chu, B., Zhong, R., Soncin, F., Stevenson, M. A. & Calderwood, S. K. *Transcriptional Activity of Heat Shock Factor 1 at 37 o C Is Repressed through Phosphorylation on Two Distinct Serine Residues by Glycogen Synthase Kinase 3 and Protein Kinases C and C **. http://www.jbc.org/ (1998).

145. Baird, N. A., Turnbull, D. W. & Johnson, E. A. Induction of the heat shock pathway during hypoxia requires regulation of heat shock factor by hypoxia-inducible factor-1. *J. Biol. Chem.* **281**, 38675–38681 (2006).

146. Gabai, V. L. *et al.* Heat Shock Transcription Factor Hsf1 Is Involved in Tumor Progression via Regulation of Hypoxia-Inducible Factor 1 and RNA-Binding Protein HuR. *Mol. Cell. Biol.* **32**, 929–940 (2012).

147. Tian, X. *et al.* Heat shock transcription factor 1 regulates exercise-induced myocardial angiogenesis after pressure overload via HIF-1α/VEGF pathway. *J. Cell. Mol. Med.* **24**, 2178–2188 (2020).

148. McMillan, D. R., Xiao, X., Shao, L., Graves, K. & Benjamin, I. J. Targeted disruption of heat shock transcription factor 1 abolishes thermotolerance and protection against heat-inducible apoptosis. *J. Biol. Chem.* **273**, 7523–7528 (1998).

149. Xiao, X. Z. *et al.* HSF1 is required for extra-embryonic development, postnatal growth and protection during inflammatory responses in mice. *EMBO J.* **18**, 5943–5952 (1999).

150. Schett, G., Steiner, C. W., Xu, Q., Smolen, J. S. & Steiner, G. TNFα mediates susceptibility to heat-induced apoptosis by protein phosphatase-mediated inhibition of the HSF1/hsp70 stress response. *Cell Death Differ.* **10**, 1126–1136 (2003).

151. Wu, L. *et al.* Heat shock transcription factor 1 attenuates TNFα-induced cardiomyocyte death through suppression of NFκB pathway. *Gene* **527**, 89–94 (2013).

152. Xie, Y., Chen, C., Stevenson, M. A., Auron, P. E. & Calderwood, S. K. Heat shock factor 1 represses transcription of the IL-1β gene through physical interaction with the nuclear factor of interleukin 6. *J. Biol. Chem.* **277**, 11802–11810 (2002).

153. Chen, Y. & Currie, R. W. Small interfering RNA knocks down heat shock factor-1 (HSF-1) and exacerbates pro-inflammatory activation of NF-κB and AP-1 in vascular smooth muscle cells. *Cardiovasc. Res.* **69**, 66–75 (2006).

154. Wirth, D., Bureau, F., Melotte, D., Christians, E. & Gustin, P. Evidence for a role of heat shock factor 1 in inhibition of NF-κB pathway during heat shock response-mediated lung protection. *Am. J. Physiol. - Lung Cell. Mol. Physiol.* **287**, 953–961 (2004).

155. Zou, Y. *et al.* Heat Shock Transcription Factor 1 Protects Cardiomyocytes from Ischemia/Reperfusion Injury. *Circulation* **108**, 3024–3030 (2003).

156. Yin, C., Xi, L., Wang, X., Eapen, M. & Kukreja, R. C. Silencing heat shock factor 1 by small interfering RNA abrogates heat shock-induced cardioprotection against ischemia-reperfusion injury in mice. *J. Mol. Cell. Cardiol.* **39**, 681–689 (2005).

157. Ma, H. *et al.* Association of Stat3 with HSF1 plays a critical role in G-CSF-induced cardio-protection against ischemia/reperfusion injury. *J. Mol. Cell. Cardiol.* **52**, 1282–1290 (2012).

158. Vedam, K. *et al.* Role of heat shock factor-1 activation in the doxorubicin-induced heart failure in mice. *Am. J. Physiol. - Hear. Circ. Physiol.* **298**, 1832–1841 (2010).

159. Orenstein, T. L. *et al.* Favorable left ventricular remodeling following large myocardial infarction by exercise training: Effect on ventricular morphology and gene expression. *J. Clin. Invest.* **96**, 858–866 (1995).

160. Yin, F. C. P., Spurgeon, H. A. & Rakusan, K. Use of tibial length to quantify cardiac hypertrophy: Application in the aging rat. *Am. J. Physiol. - Hear. Circ. Physiol.* **12**, (1982).

161. Takagawa, J. *et al.* Myocardial infarct size measurement in the mouse chronic infarction model: Comparison of area- and length-based approaches. *J. Appl. Physiol.* **102**, 2104–2111 (2007).

162. Jasmin, J. F., Calderone, A., Leung, T. K., Villeneuve, L. & Dupuis, J. Lung structural remodeling and pulmonary hypertension after myocardial infarction: Complete reversal

with irbesartan. *Cardiovasc. Res.* **58**, 621–631 (2003).

163. McLaughlin, S. *et al.* Injectable human recombinant collagen matrices limit adverse remodeling and improve cardiac function after myocardial infarction. *Nat. Commun.* **10**, (2019).
164. Ahnve, S. *et al.* Limitations and advantages of the ejection fraction for defining high risk after acute myocardial infarction. *Am. J. Cardiol.* **58**, 872–878 (1986).
165. Lindsey, M. L., Kassiri, Z., Virag, J. A. I., De Castro Brás, L. E. & Scherrer-Crosbie, M. Guidelines for measuring cardiac physiology in mice. *Am. J. Physiol. - Hear. Circ. Physiol.* **314**, H733–H752 (2018).
166. Ridker, P. M., Rifai, N., Stampfer, M. J. & Hennekens, C. H. Plasma Concentration of Interleukin-6 and the Risk of. **101**, 1767–1772 (2000).
167. Yang, F. *et al.* Myocardial infarction and cardiac remodelling in mice. *Exp. Physiol. Transl. Integr.* **87**, 547–555 (2002).
168. Mutlak, D. *et al.* Utility of pulmonary hypertension for the prediction of heart failure following acute myocardial infarction. *Am. J. Cardiol.* **109**, 1254–1259 (2012).
169. Lindsey, M. L. *et al.* Guidelines for experimental models of myocardial ischemia and infarction. *Am. J. Physiol. - Hear. Circ. Physiol.* **314**, H812–H838 (2018).
170. Östling, P., Björk, J. K., Roos-Mattjus, P., Mezger, V. & Sistonen, L. Heat Shock Factor 2 (HSF2) contributes to inducible expression of hsp genes through interplay with HSF1. *J. Biol. Chem.* **282**, 7077–7086 (2007).
171. Takii, R. *et al.* Heat Shock Transcription Factor 1 Inhibits Expression of IL-6 through Activating Transcription Factor 3. *J. Immunol.* **184**, 1041–1048 (2010).
172. Szentes, V., Gazdag, M., Szokodi, I. & Dézsi, C. A. The Role of CXCR3 and Associated Chemokines in the Development of Atherosclerosis and During Myocardial Infarction. *Front. Immunol.* **9**, 1932 (2018).
173. Hayashidani, S. *et al.* Anti-Monocyte Chemoattractant Protein-1 Gene Therapy Attenuates Left Ventricular Remodeling and Failure After Experimental Myocardial Infarction. *Circulation* **108**, 2134–2140 (2003).
174. Huang, J. *et al.* Genetic modification of mesenchymal stem cells overexpressing ccr1

increases cell viability, migration, engraftment, and capillary density in the injured myocardium. *Circ. Res.* **106**, 1753–1762 (2010).

175. Gordon, J. W., Shaw, J. A. & Kirshenbaum, L. A. Multiple facets of NF-κB in the heart: To be or not to NF-κB. *Circ. Res.* **108**, 1122–1132 (2011).
176. Mutlak, M. & Kehat, I. Extracellular signal-regulated kinases 1/2 as regulators of cardiac hypertrophy. *Front. Pharmacol.* **6**, 1–8 (2015).
177. Zou, Y. *et al.* Heat shock transcription factor 1 protects heart after pressure overload through promoting myocardial angiogenesis in male mice. *J. Mol. Cell. Cardiol.* **51**, 821–829 (2011).
178. Kupatt, C. *et al.* Heat shock protein 90 transfection reduces ischemia-reperfusion - Induced myocardial dysfunction via reciprocal endothelial NO synthase serine 1177 phosphorylation and threonine 495 dephosphorylation. *Arterioscler. Thromb. Vasc. Biol.* **24**, 1435–1441 (2004).
179. Iwaki, K., Chi, S. H., Dillmann, W. H. & Mestril, R. Induction of HSP70 in cultured rat neonatal cardiomyocytes by hypoxia and metabolic stress. *Circulation* **87**, 2023–2032 (1993).
180. Efthymiou, C. A. *et al.* Heat shock protein 27 protects the heart against myocardial infarction. *Basic Res. Cardiol.* **99**, 392–394 (2004).
181. Sistonen, L., Sarge, K. D. & Morimoto, R. I. Human heat shock factors 1 and 2 are differentially activated and can synergistically induce hsp70 gene transcription. *Mol. Cell. Biol.* **14**, 2087–2099 (1994).

Appendix: Supplementary Figures

Figure S1. Morphology of 12-week-old male *Hsf1*$^{+/+}$ and *Hsf1*$^{-/-}$ mice. At baseline, *Hsf1*$^{-/-}$ mouse is smaller and leaner than *Hsf1*$^{+/+}$ mouse.

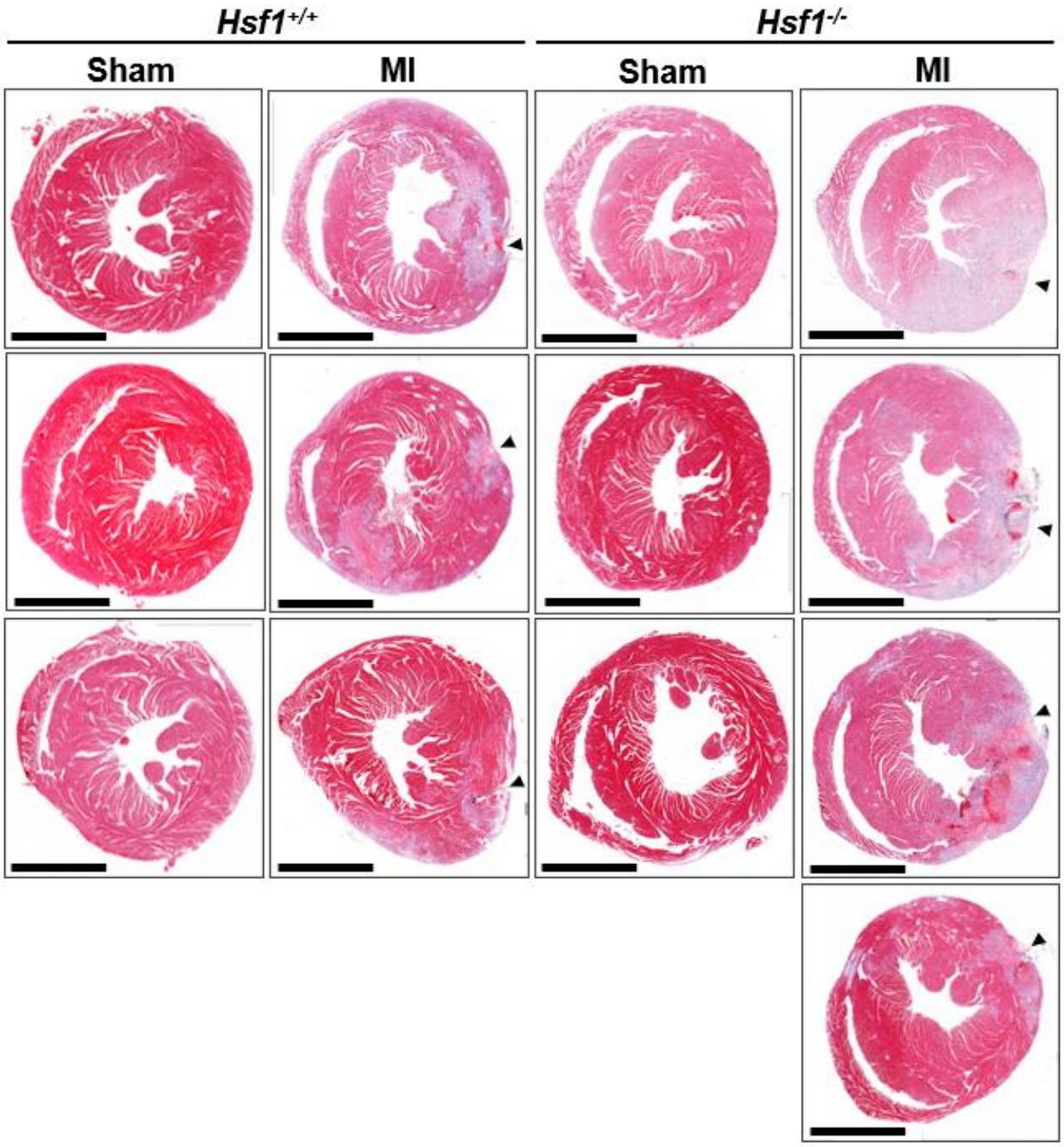

Figure S2. Hematoxylin & Eosin staining of *Hsf1*$^{+/+}$ and *Hsf1*$^{-/-}$ LV tissue sections after 3 days of sham and MI operation. LV of *Hsf1*$^{+/+}$ and *Hsf1*$^{-/-}$ hearts, harvested 3-days post-operation, were embedded in paraffin, and sectioned serially. The replicates of LV tissue sections from *Hsf1*$^{+/+}$ and *Hsf1*$^{-/-}$ hearts were stained with HE to illustrate immune cell recruitment. Bar = 2mm. The site of LAD ligation is evident by the presence of nylon fibers within the ventricle tissue (arrows).

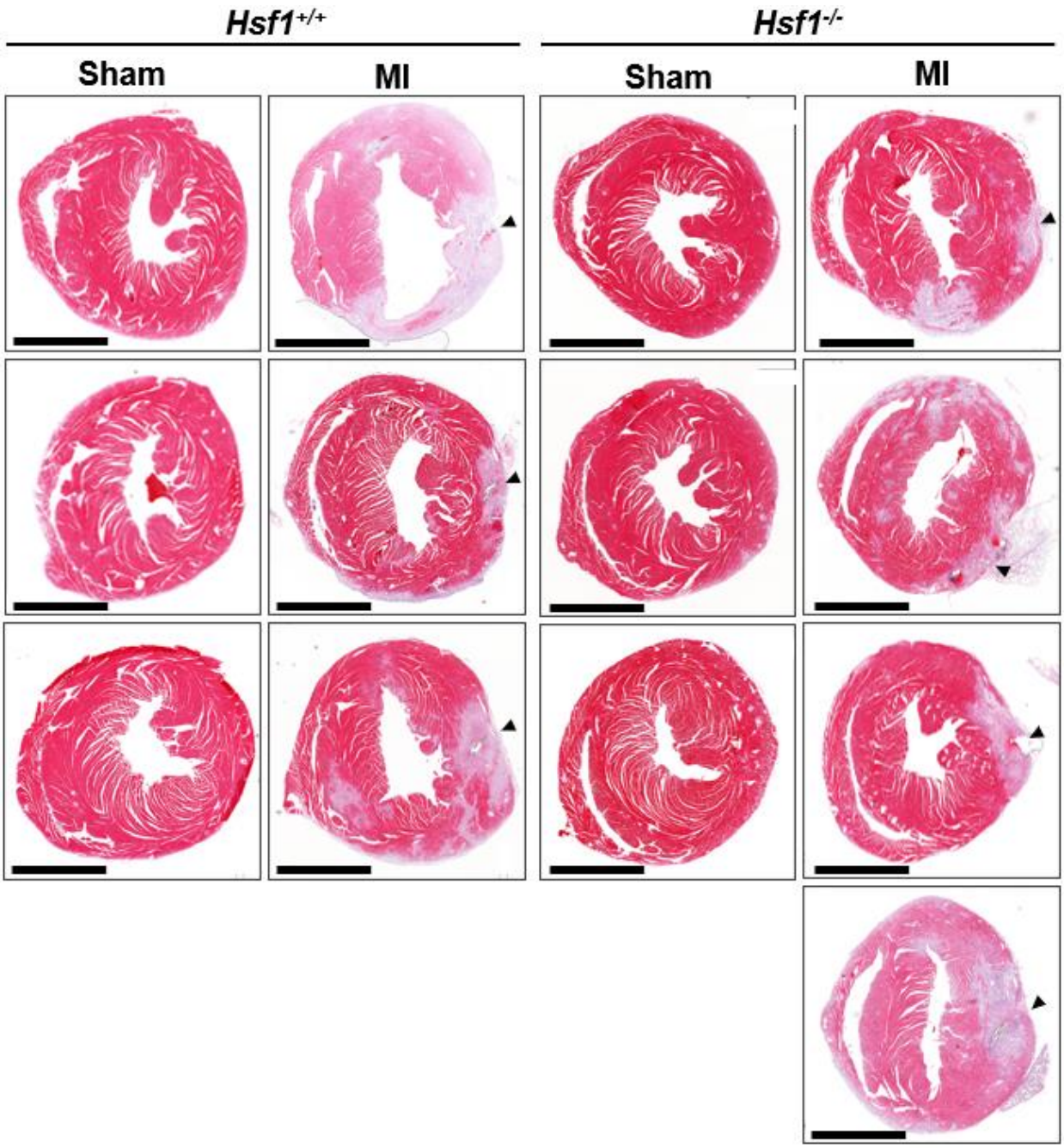

Figure S3. Hematoxylin & Eosin staining of *Hsf1*$^{+/+}$ and *Hsf1*$^{-/-}$ LV tissue sections after 7 days of sham and MI operation. LV of *Hsf1*$^{+/+}$ and *Hsf1*$^{-/-}$ hearts, harvested 7-days post-operation, were embedded in paraffin, and sectioned serially. The replicates of LV tissue sections from *Hsf1*$^{+/+}$ and *Hsf1*$^{-/-}$ hearts were stained with HE to illustrate immune cell recruitment. Bar = 2mm. The site of LAD ligation is evident by the presence of nylon fibers within the ventricle tissue (arrows).

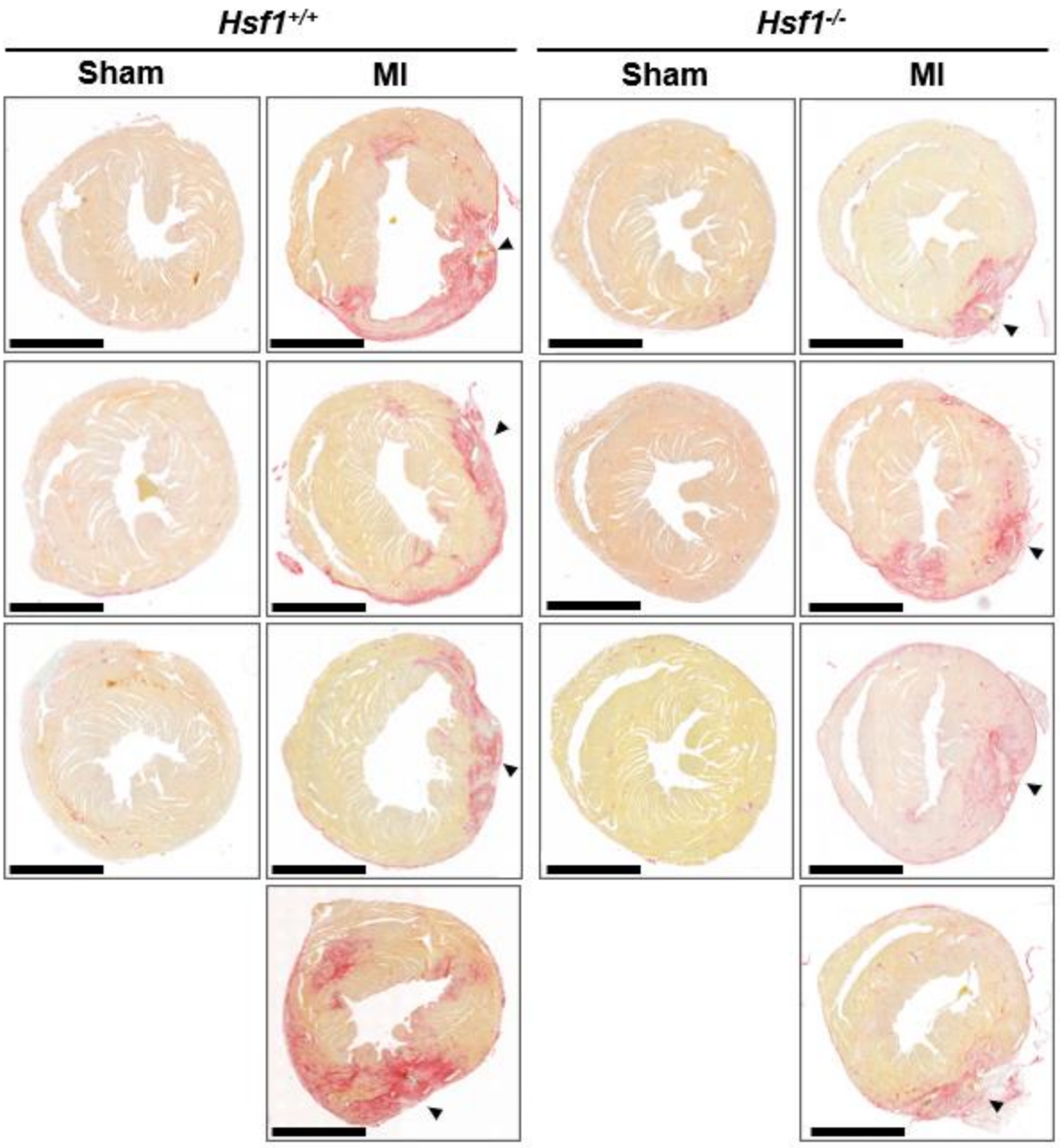

Figure S4. Picro-Sirius Red staining of *Hsf1*$^{+/+}$ and *Hsf1*$^{-/-}$ LV tissue sections after 7 days of sham and MI operation. LV of *Hsf1*$^{+/+}$ and *Hsf1*$^{-/-}$ hearts, harvested 7-days post-operation, were embedded in paraffin, and sectioned serially. The replicates of LV tissue sections from *Hsf1*$^{+/+}$ and *Hsf1*$^{-/-}$ hearts were stained with PSR to illustrate collagen deposition in treatment groups. Bar = 2mm. The site of LAD ligation is evident by the presence of nylon fibers within the ventricle tissue (arrows).

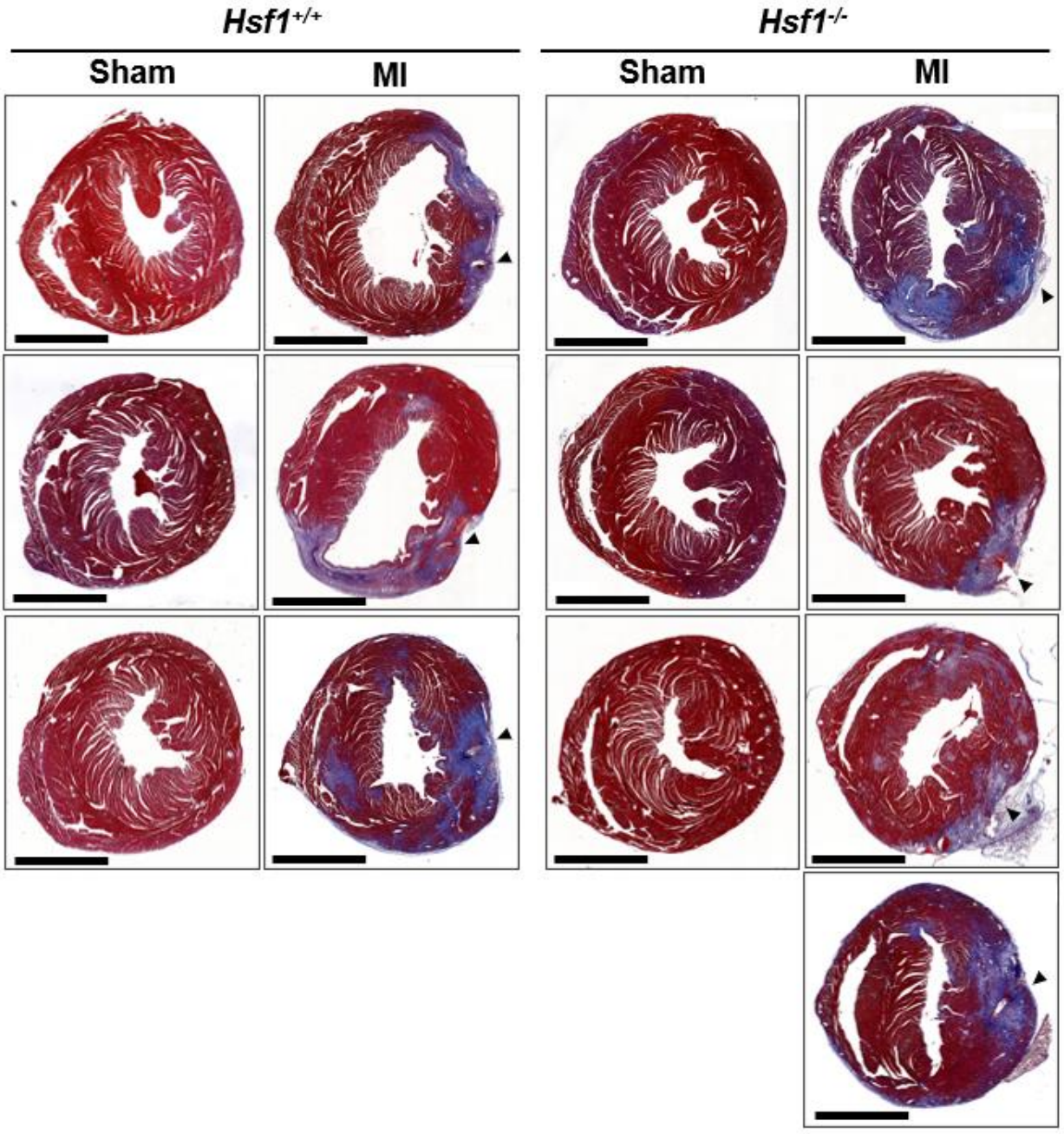

Figure S5. Masson Trichrome staining of *Hsf1*$^{+/+}$ and *Hsf1*$^{-/-}$ LV tissue sections after day 7 sham and MI operation. LV of *Hsf1*$^{+/+}$ and *Hsf1*$^{-/-}$ hearts, harvested 7-days post-operation, were embedded in paraffin, and sectioned serially. The replicates of LV tissue sections from *Hsf1*$^{+/+}$ and *Hsf1*$^{-/-}$ hearts were stained with Masson Trichrome to illustrate infarct size in treatment groups. Scale bar = 2mm. The site of LAD ligation is evident by the presence of nylon fibers within the ventricle tissue (arrows).

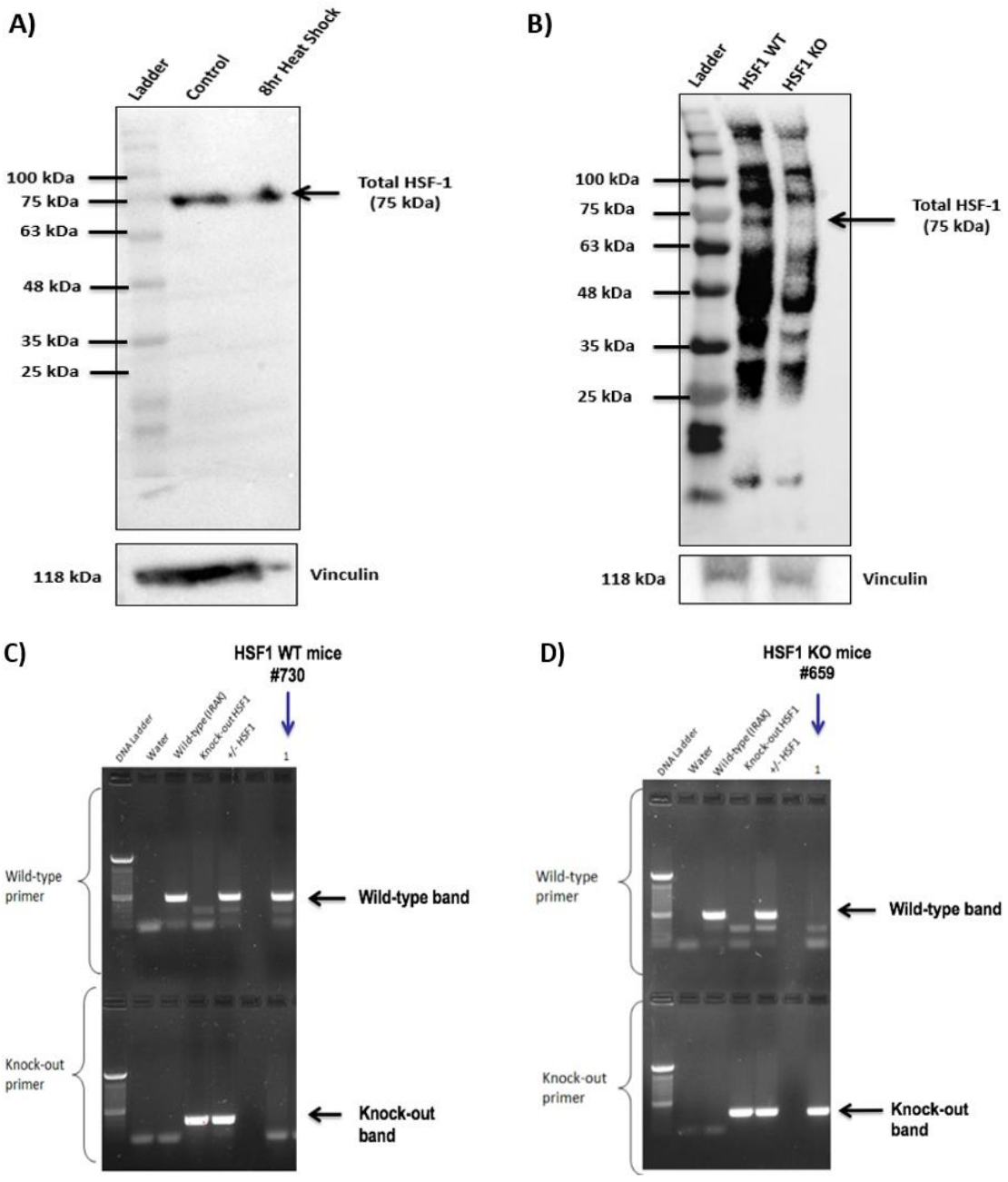

Figure S6. Validation of Total HSF1 antibody using Heat Shock Treated H9C2 rat cardiomyocyte cell line and *Hsf1* Wildtype (*Hsf1*$^{+/+}$) and Knockout (*Hsf1*$^{-/-}$) mice. A) H9C2 rat cardiomyocytes were incubated at 37°C (Control) and 42°C (Heat Shock) for eight hours. After treatment, protein was extracted from cell pellet and the protein lysates were used to probe with antibody against Total HSF1 Rabbit Monoclonal antibody from Cell Signaling Technology. Vinculin was used as a loading control. **B)** Protein lysates from heart tissue of *Hsf1*$^{+/+}$ and *Hsf1*$^{-/-}$ mice were used to probed for Total HSF1 Rabbit Monoclonal antibody from Cell Signaling Technology. Vinculin was used as a loading control. **C)** and **D)** The genotype validation of *Hsf1*$^{+/+}$ and *Hsf1*$^{-/-}$mice used in this experiment.

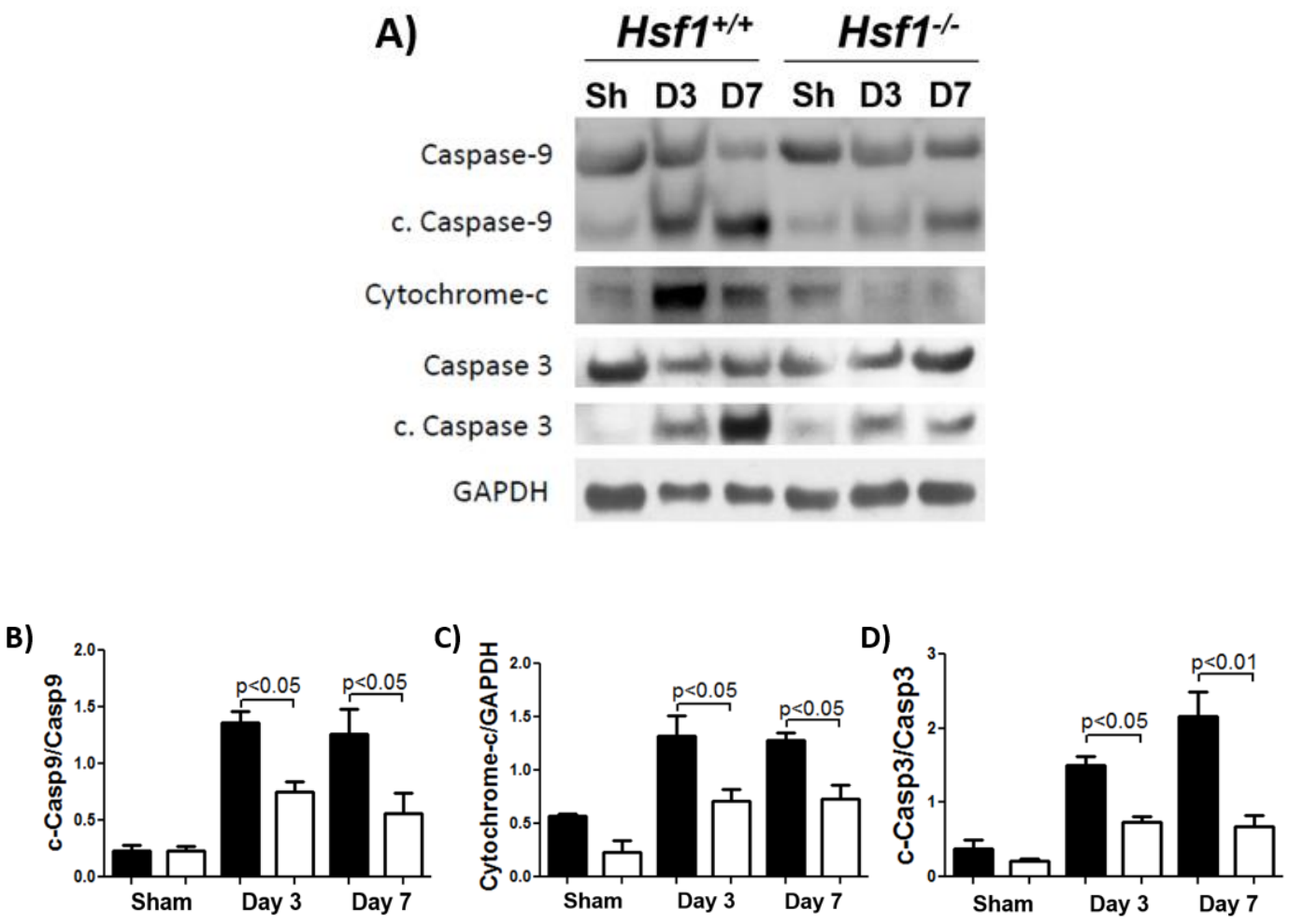

Figure S7. Immunoblotting analysis of apoptotic markers identify decrease in activation of caspases 3 and 9 and cytoplasmic cytochrome c-level in *Hsf1*$^{-/-}$ heart tissue. A) Representative immunoblots of cleaved and total expression of caspase 9 and 3 and cytochrome-c. The ratio of **B)** cleaved caspase 9/ total caspase 9, **C)** cytochrome-c/ GAPDH, **D)** cleaved caspase 3/ total caspase 3. Statistical comparison was performed with use of Two-Way ANOVA with Tukey's multiple comparison test. n = 6 (per treatment group). Values are mean ± SEM.